MASTER IN BIOCHEMISTRY AND MOLECULAR AND CELL BIOLOGY RESEARCH FOCUS

Study of the mechanisms leading to a hypoxic-like response during the infection by B. abortus

Fayt, Youri

Award date:
2022

Awarding institution:
University of Namur

Faculté des Sciences

Etude des mécanismes menant à l'induction d'une réponse hypoxique lors de l'infection par *Brucella abortus*

Mémoire présenté pour l'obtention

du grade académique de master 120 en biochimie et biologie moléculaire et cellulaire

Youri FAYT

Janvier 2022

Université de Namur
FACULTE DES SCIENCES
Secrétariat du Département de Biologie
Rue de Bruxelles 61 - 5000 NAMUR
Téléphone: + 32(0)81.72.44.18 - Téléfax: + 32(0)81.72.44.20
E-mail: joelle.jonet@unamur.be - http://www.unamur.be

Etude des mécanismes menant à une réponse hypoxique lors de l'infection par *Brucella abortus*

FAYT Youri

Résumé

Brucella abortus est un pathogène du bétail responsable de cas de zoonoses suite à sa transmission à l'homme, ce qui induit une maladie chronique appelée brucellose. La virulence de *B. abortus* dépend de sa capacité à éviter la reconnaissance par le système immunitaire, ce qui passe notamment par sa capacité à envahir et prospérer au sein des sentinelles du système immunitaire, les macrophages. La bactérie s'est révélée capable de moduler de nombreux processus cellulaires afin d'établir sa niche réplicative qui se situe au niveau du réticulum endoplasmique de la cellule infectée. Néanmoins, les facteurs responsables de la production ainsi que de la maintenance de cette niche réplicative ne sont pas encore totalement élucidés.

La mitochondrie est un organite essentiel au fonctionnement des cellules mammaliennes qui est la cible de différents pathogènes bactériens qui en tirent différents avantages. Cela passe par la modulation des aspects dynamiques de fusion et de fission du réseau mitochondrial et sa dégradation par autophagie spécifique (mitophagie).

Des résultats préliminaires obtenus par notre équipe ont montré que *B. abortus* induit une fragmentation du réseau mitochondrial qui semble associée à une induction de la mitophagie au sein de macrophages et de cellules épithéliales (HeLa) infectées. Ces phénotypes mitochondriaux sont accompagnés de l'activation d'un axe de mitophagie bien décrit dans la littérature qui comprend le facteur de transcription HIF-1α et un de ses gènes cibles : BNIP-3L/Nix, décrit comme un récepteur important de la mitophagie.

Les objectifs de ce mémoire étaient donc de (i) déterminer les acteurs moléculaires responsables de la stabilisation de HIF-1α dans des cellules épithéliales et myéloïdes infectées par *B. abortus*, (ii) d'établir un lien éventuel entre la stabilisation de HIF-1α et la fragmentation mitochondriale et/ou la mitophagie induite par *B. abortus* et (iii) de remettre ces découvertes dans un contexte de relation hôte-pathogène.

Les résultats les plus importants de ce travail ont mis à jour un rôle capital du fer dans la stabilisation de HIF-1α induite par *B. abortus* et termine sur des résultats encourageant élargissant le rôle du fer à l'apparition de la fragmentation mitochondriale. Si ces résultats se confirment, ils impliquent la déplétion d'un métabolite normalement impliqué dans l'import de fer dans la mitochondrie, vestige de son lien de parenté avec *Brucella,* dans l'apparition des phénotypes mitochondriaux induits lors de l'infection avec *B. abortus*.

Mémoire de master 120 en biochimie et biologie moléculaire et cellulaire

Janvier 2022

Promoteur: A. Thierry

Co-promoteur: X. De Bolle

Université de Namur
FACULTE DES SCIENCES
Secrétariat du Département de Biologie
Rue de Bruxelles 61 - 5000 NAMUR
Téléphone: + 32(0)81.72.44.18 - Téléfax: + 32(0)81.72.44.20
E-mail: joelle.jonet@unamur.be - http://www.unamur.be

Study of the mechanisms leading to a hypoxic-like response during the infection by *B. abortus*

FAYT Youri

Abstract

B. abortus is a pathogen of the cattle responsible for cases of zoonosis from cattle to humans leading to the onset of a chronic disease called brucellosis. The virulence of *B. abortus* depends on its ability to avoid recognition by the immune system, which includes its ability to invade and thrive within the sentinels of the immune system: the macrophages. The bacterium modulates differents aspect of the host cell biology in order to establish its replicative niche inside the ER of the infected host cell. However, the factors responsible for the establishment as well as the maintenance of the replicative niche are not fully understood, notably at the level of the host cell's biology.

The mitochondrion is an essential organelle for mammalian cell function that has been shown, in recent research, to constitute a prime target for many bacterial pathogens. This involves the modulation of the dynamic aspects of fusion and fission of the mitochondrial network as well as their degradation by specific autophagy (mitophagy) to their advantage.

Previously, our team has shown that *B. abortus* induces the fragmentation of the mitochondrial network that appears to be associated with the induction of mitophagy in infected macrophages and epithelial (HeLa) cells. These mitochondrial aspects are accompanied by the activation of a mitophagy axis well described in the literature dependent on the transcription factor HIF-1α and its target gene BNIP-3L/Nix, described as a mitophagy receptor.

The objectives of this master's thesis were therefore to (i) determine the molecular actors responsible for the stabilisation of HIF-1α in epithelial and myeloid cells infected with *B. abortus*, (ii) to establish whether there is a link between HIF-1α stabilisation and *B. abortus*-induced mitochondrial fragmentation and/or mitophagy and (iii) to put these findings into a host-pathogen context.

The major outcome/results of this work revealed a crucial role for iron in the stabilisation of HIF-1α induced by *B. abortus* and concludes with encouraging results expanding the role of iron in the occurrence of the mitochondrial fragmentation. If confirmed, these results indicate that the depletion of a metabolite implicated in mitochondrial iron import, derived from the distant evolutionary relationship between *Brucella* and the mitochondria, is involved in the mitochondrial fragmentation induced by *B. abortus*.

Thesis of master 120 in biochemistry and molecular and cellular biology

January 2022

Promoter: A. Thierry

Co-promoter: X. De Bolle

Remerciements

En premier lieu, merci aux membres du jury de prendre le temps de lire mon mémoire. J'espère que vous y prendrez un peu de plaisir quand même à parcourir ce manuscrit.

Ensuite, vient le tour de mon promoteur, Mr. Arnould. Merci de m'avoir donné l'opportunité de prendre part à ce projet passionnant. Merci aussi pour l'enthousiasme dont vous avez pu faire preuve pour ce projet. Malgré nos points de désaccord et débats parfois animés, vous m'avez challengé, et aussi corrigé, quand il le fallait.

Après, je ne pouvais pas manquer de remercier Jeremy, qui a fait preuve d'un engagement à toute épreuve pour Lisa et moi. Merci d'avoir été derrière nous et d'avoir toujours été disponibles lorsqu'on avait des questions ou que l'on doutait. Tu as été un encadrant exemplaire et j'espère avoir pu un peu t'aider dans ton projet. Je te souhaite tout le meilleur pour la suite, et un chouette papier !

Bien sûr, je remercie tous les membres de l'équipe DYSO et Patricia Renard pour les conseils qu'ils ont pu me prodiguer au cours de ce projet. Je remercie également les membres de l'URBC pour m'avoir accueilli. Merci aux techniciens, Antoine, Catherine, Marc, Sophie et bien entendu Dorian pour le travail qu'ils ont fourni pour le labo (et merci aussi pour les lifts en voitures Catherine).

Enfin, merci à tous les autres mémorants et à Dorian, sans qui cette aventure aurait été beaucoup moins épicée. Merci pour ces soupers de thèses et autres soirées mémorables. Merci aussi pour votre ouverture d'esprit et l'esprit bon enfant que vous avez fait régner au cours de ces 10 mois. Ce fut vraiment une chance d'avoir été en URBC au cours de l'année 2021. Bien entendu, merci particulièrement à ma collègue Brucelliste Lisa, ce fut un plaisir de faire ce chemin avec toi. Tu es une personne super attentionnée, il en faut plus des comme toi. Bonne chance au pays des caribous.

Table of contents

List of abbreviation

2,5(or 3)-DHBA = 2,5(or 3)-dihydroxybenzoic acid

2-OG/α-KG = 2-oxoglutarate/α-ketoglutarate

AIM2 = absent in melanoma 2

ALAS 1/2 = 5-aminolevulinate synthase 1 (non-specific)/2 (erythroid-specific)

AMPK = AMP-activated protein kinase

AR = aspect ratio

ATP = adenosine triphosphate

ATPs-β = ATP synthase subunit β

e/r/aBCV = endosomal/replicative/autophagic *Brucella*-containing vacuole

Bcl-2-L-13 = Bcl-2-like protein 13

Bdh2 = 3-hydroxybutyrate dehydrogenase type 2

BMDM = Bone Marrow-derived macrophages

BNIP3 = BCL2 Interacting protein 3

BNIP-3L = BCL2 Interacting Protein 3 Like

BSA = bovine serum albumin

Ca = calcium

CAD = *cis*-aconitate decarboxylase

CDN = cyclic dinucleotide

c-di-GMP = cyclic-diguanylate monophosphate

CFU = colony-forming unit

CISD1/2/3 = CDGSH iron-sulfur domain protein 1/2/3

CLR = C-type lectin receptor

$CoCl_2$ = cobalt chloride

CTCF = corrected total cell fluorescence

CTRL = control cells

DAMP = damage-associated molecular pattern

DC = dendritic cells

DFO = desferrioxamine

DFP = deferiprone

DMT1 = Divalent Metal (Ion) Transporter 1

DNA = deoxyribonucleic acid

DRP1 = dynamin-related protein 1

EDTA = ethylenediaminetetraacetic acid

EF5 = (2-(2-Nitro-1H-imidazol-1- yl)-N-(2,2,3,3,3-pentafluoropropyl) acetamide

EP/BP = end point/branch point ratio

ER = endoplasmic reticulum

ERK1/2 = extracellular signal -regulated kinase 1/2

ETC = electron transport chain

FACS = fluorescence-activated cell sorting

$FADH_2$ = flavine adenine dinucleotide (reduced form)

FBS = Fetal Bovine Serum

FCCP = carbonyl cyanide-p-trifluoromethoxyphenylhydrazone

Fe-S cluster = iron-sulfur cluster

FKBP8 = FK506 binding protein 8

FPN = ferroportin

FUNDC1 = FUN14 domain containing 1

FXN = Frataxin

GFP = green fluorescent protein

GSH = reduced glutathione

HIF-1α = hypoxia-inducible factor 1α

HRE = hypoxia response element

IFN-β = interferon-beta

IFN-γ = interferon-gamma

IL-1β = interleukin-1 beta

IMM = inner mitochondrial membrane

IMS = intermembrane space

IRF = interferon-regulatory factor

IRE1 = inositol-requiring enzyme 1

IRP1/2 = iron regulatory protein ½

ISC = iron-sulfur cluster

ISCU = iron-sulfur cluster assembly enzyme, mitochondrial

LAMP1 = lysosome-associated membrane glycoprotein 1

LC3(B) = microtubule-associated protein 1A/1B-light chain 3 (B)

Lcn2 = lipocalin 2

LIP = labile iron pool

LPS = lipopolysaccharide

KD = knock-down

KO = knock-out

MAPK = mitogen-activated protein kinase

MAMs = mitochondria-associated ER membranes

MAVS = mitochondrial antiviral signalling protein

MFN1/2 = mitofusin 1/2

MFR1/2 = mitoferrin 1/2

MMP = mitochondrial membrane potential

mRNA = messenger ribonucleic acid

mtDNA/RNA = mitochondrial DNA/RNA

(mt)ROS: (mitochondrial) reactive oxygen species

mTORC1 = mammalian target of rapamycin complex 1

Mt-Tpl = Mito-TEMPOL

MyD88 = myeloid differentiation primary response 88

NAC = *N*-acetylcysteine

NAD^+/NADH = oxidised/reduced nicotinamide adenine dinucleotide

$NAPD^+$/NADPH = oxidised/reduced nicotinamide adenine dinucleotide phosphate

NDP52 = nuclear dot protein 52 kDa

NF-κB = nuclear factor-kappa B

NFS1 = cysteine desulfurase, mitochondrial

NI = non-infected cells

NLR = NOD-like receptor

NLRC4 = nucleotide-binding domain, leucine-rich repeat containing family caspase recruitment domain containing 4

NLRP3 = NLR family pyrin domaing containing 3

NO = nitric oxide

NOS2/iNOS = nitric oxide synthase 2/ inducible nitric oxide synthase

NOX2 = NADPH oxidase 2

OMM = outer mitochondrial membrane

OPA1 = optic atrophy 1

OXPHOS = oxidative phosphorylation

PAMP = pathogen-associated molecular pattern

PBS = Phosphate-buffered saline

PHD = HIF prolyl hydroxylases

p.i. = post-infection

PRR = pattern recognition receptor

Prdx 5/6 = peroxiredoxin 5/6

RLR = Rig1-like receptor

RNA = ribonucleic acid

SD = standard deviation

siRNA = small-interfering RNA

SOD1/2 = superoxide dismutase cytosolic (1)/mitochondrial (2) isoform

STING = stimulator of interferon genes

STX17 = syntaxin 17

TBC1D15 = TBC1 Domain Family Member 15

TCA = tricarboxylic acid

TfR1 = transferrin receptor 1

TLR = Toll-like receptor

TNF-α = Tumor necrosis factor α

TOM20 = translocase of the outer mitochondrial membrane 20

TRIF = TIR-domain-containing adapter-inducing interferon-β

TXNIP = Thioredoxin-interacting protein

ULK1 = Unc-51 like autophagy activating kinase 1

UPR = unfolded protein response

1. Introduction

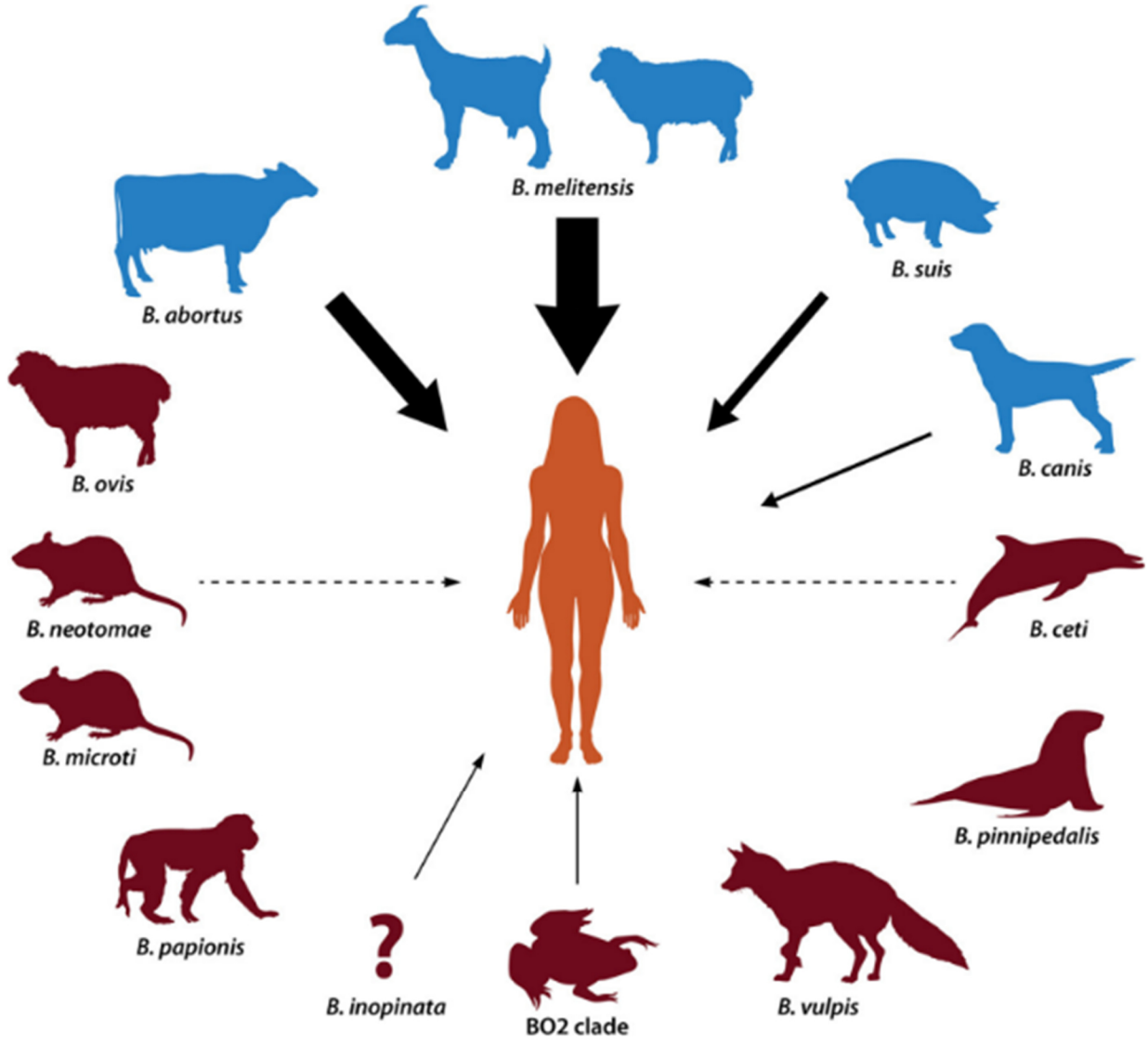

Figure 1: Zoonotic potential of different *Brucella* species that are associated with their natural hosts. The thickness of the arrows represent the relative frequencies of zoonosis cases between the different *Brucella* species. Dashed arrow indicate that the specie has been isolated from brucellosis patients but transmission cases have not been documented. The natural host of *B. inopinata* is not known (symbolised by a question mark). Picture from ref 339.

1.1. Brucellosis

1.1.1. In humans

Brucellosis, also called Malta fever or Mediterranean fever, is a worldwide zoonosis caused by the intracellular pathogens of the bacterial genus *Brucella*, responsible for 500 000 new cases annually making it one of the most common zoonosis[1]. In humans, brucellosis manifests itself as a chronic inflammatory disease translating in the following symptoms: low grade relapsing fever, weight loss, joint and back pain but it can also cause more severe outcomes like splenomegaly, hepatomegaly (in around 25 % of cases), epididymo-orchitis (inflammation of male genital tract) or even neuropsychiatric complications (4/100 patients) and endocarditis (1/100 patients) which can be lethal for the latter in some individuals [2,3]. This disease is mainly present in Middle-East and developing countries (sub-Saharian Africa, Latin America, Central Asia, Mediterranean coast)[2]. This is linked to a greater consumption of unpasteurised milk[4] with more than 60% of brucellosis cases linked to dairy consumption in Turkey or Kuweit[5]. Additionally, brucellosis can be transmitted by direct contact with fluids and tissue of infected animals putting veterinarians, butchers and farmers at higher risk[2]. Transmission between humans has rarely been observed leading experts to think that humans represents accidental, unnatural, host for *Brucella* species (*Brucella* spp.) and an "evolutionary dead-end"[2]. Whatever, human brucellosis is a highly debilitating disease impairing the infected individuals to pursue their working life. Currently, no effective human-edible vaccine or treatment exist[2]. Traditionally, a long antibiotic therapy is prescribed but it is not completely efficient[2]. There is thus a need to study in depth the infection by *Brucella* spp. in order to discover new therapeutic targets.

1.1.2. In natural hosts

Brucella spp. are facultative intracellular bacteria, facultative meaning that bacteria able to survive outside of its host for extended period of times. *Brucella* spp. belongs to Rhizobiales order of the α-proteobacteria class[6] and are, more specifically, closely related to the soil-living bacterium *Ochrobactrum*[7]. The *Brucella* genus contain 6 classical species and 7 novel species each named following the preferred host it infects[6] but the species are very similar to each other with 97% of sequence identity between their genomes[7]. Four species can infect humans with, by order of importance, *B. melitensis*, *B. abortus*, *B. suis* and *B canis* the causative agents of ovine, cattle, swine and canine brucellosis, respectively (**Figure 1**)[2]. In their natural host, in addition to spleen, liver or mammary gland colonisation, *Brucellae* have a particular tropism for genital organs in both males and females associated with the infection of uterus and placentas in gravid females[6]. Placental throphoblasts represent a very permissive cell type for *Brucella* replication which is followed by the induction of necrotic cell death causing inflammation in the surrounding tissue (placentitis) and opening the door for foetal infection[8]. As a consequence, brucellosis is linked to abortion in pregnant females (30 at 80 % of cases in cattle) or birth of weak offspring which are commonly the sole symptoms along with reduced milk production and fertility[6]. This can cause enormous economic burden in livestock farming. Currently, the use of different vaccination strains such as *B. abortus* S19 and RB51 and *B. melitensis* Rev1 were shown to be effective to prevent disease outbreaks in natural hosts and associated economic losses but their use can still be problematic in weak or pregnant individuals[6]. The transmission in the natural host can occur vertically (from mother to offspring) through the milk or horizontally (between individuals of the same generation) by direct contact

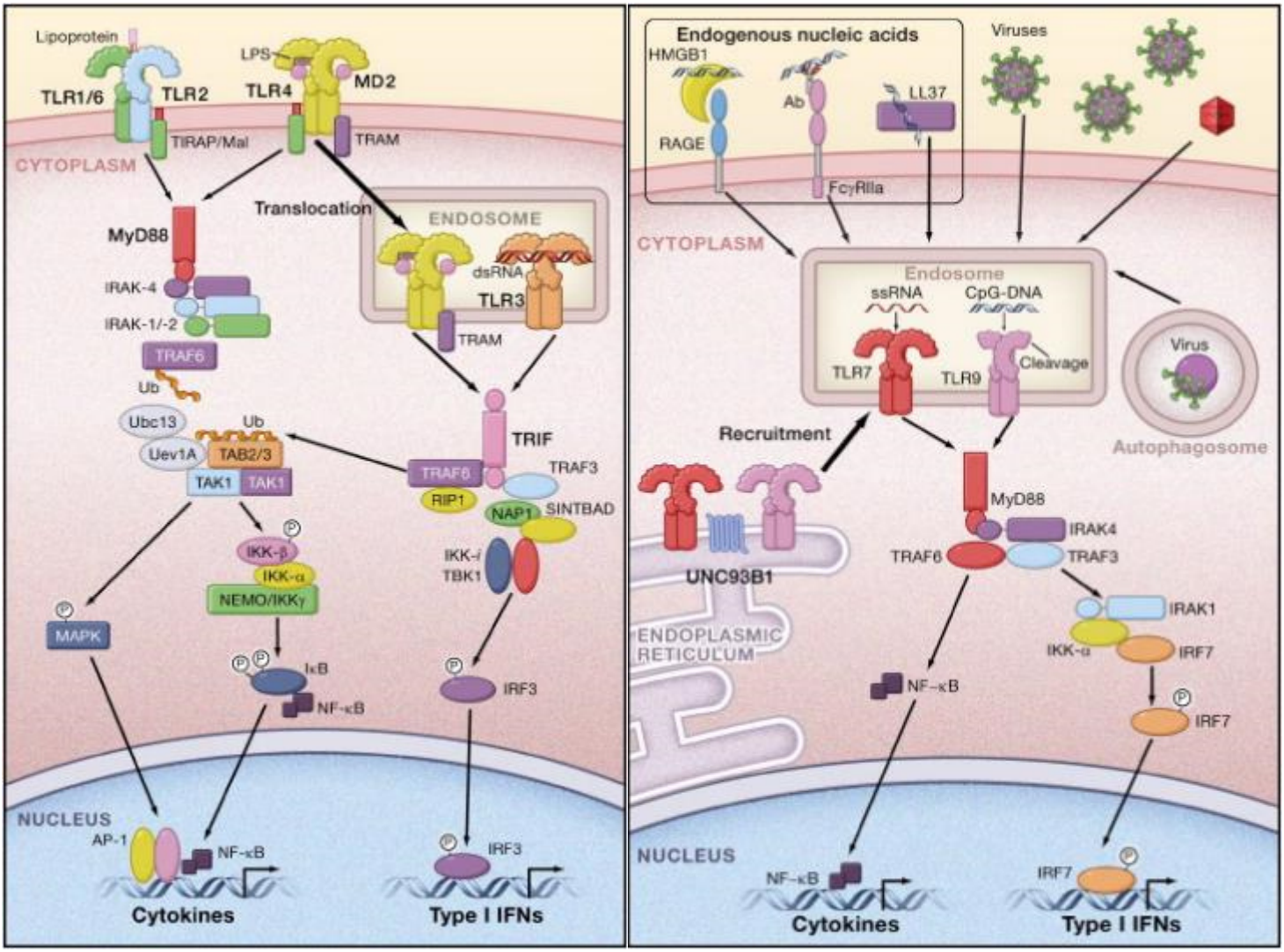

Figure 2: **Innate immune recognition by TLRs and downstream signalling.**

Left: bacterial lipoproteins or lipopolysaccharide (LPS) bind to the TLR1/6-TLR2 heterodimer or to TLR4-MD2 complex expressed in the plasma membrane. This leads to the recruitment of MyD88 adaptor which culminates in the activation of the AP-1 and NF-κB transcription through activation of the MAPK pathway and the IKK complex, respectively, triggering the expression of pro-inflammatory genes. TLR4 stimulation by LPS leads to its translocation to endosomes where it recruits the TRIF adaptor leading to IRF3 activation and type 1 IFN production.

Right: Infection triggers TLR7 and TLR9 trafficking from the ER to the endosomes and TLR9 cleavage where they can sense viral (or bacterial) nucleic acids delivered by endocytosis or autophagy. TLR7 or TLR9 stimulation leads to MyD88 recruitment and culminates in NF-κB and IRF7 activation and pro-inflammatory gene transcription. Pictures taken from ref 335.

with aborted foetus or by aerosols, sexual contact and ingestion of food or water that has been in contact with bodily fluids[6].

1.1.3. In the laboratory

Experimentally, the main model used to study brucellosis is the intraperitoneal or intranasal infection of mice[2]. The bacteria produce a chronic infection of the spleen and quite well reflects human brucellosis but does not reproduce the acute placental infection found in natural hosts[8]. Following intranasal infection, bacteria were showed to be transported into the lymph nodes, probably by dentritic cells (DC), before entering the bloodstream and disseminating in other organs, particularly those of the reticulo-endothelial system such as the spleen, lymph nodes and bone-marrow[9]. Importantly, the infection route does heavily modulate the evolution of the infection[10]. These organs are heavily populated with macrophages, the main reservoir of *Brucella* in humans and mice[11]. However, a lot of other cell types are permissive to *Brucella* replication such as, of course, placental trophoblasts from their natural host[12] or human[13], but also fibroblasts, endothelial cells and various epithelial cells[11]. At the cellular level, the success of the infection largely depends on the reaching of a particular microenvironment termed the "replication niche" in which *Brucella* is protected from immune recognition[14]. In the case of Brucellae, this niche is a particular compartment with several features of the endoplasmic reticulum (ER) termed the replicative *Brucella* Containing Vacuole (rBCV). *Brucella* must absolutely attain this rBCV in order to proliferate inside macrophages [15] and to maintain chronic infection in the spleen of infected mice[14]. Before diving into the intracellular lifestyle of *Brucella*, let's acknowledge the characteristics and functions of a macrophage.

1.2. Focus on the host cell: the macrophage

Macrophages are composed of heterogeneous cell sub-populations that act as guardians of tissue homeostasis by detecting signs of damage or infection and mounting the appropriate response[16]. The particularly high expression of pattern recognition receptors (PRRs) allows them to detect either "non-self" molecules, called pathogen-associated molecular patterns (PAMPs), in order to elicit an inflammatory response[17]. Trans-membrane PRRs are called toll-like receptors (TLR) with each member recognising a particular PAMPs: lipoproteins (TLR1, TLR2 and TLR6), double-stranded (ds) RNA (TLR3), lipopolysaccharide (LPS, TLR4), flagellin (TLR5), single-stranded (ss) RNA (TLR7 and TLR8) and DNA containing hypo-methylated CpG sequences (TLR9)[18]. Other PRR include trans membrane C-type lectin receptors (CLRs) that bind microbial carbohydrates, RIG-1-like receptors (RLRs) that trigger anti-viral programs in response to RNAs and the cytosolic receptors called NOD-like receptors (NLRs)[18]. The stimulation of PRRs converge in the activation of pro-inflammatory gene expression through activation of NF-κB and/or mitogen-activated protein kinases (MAPKs) and/or interferon (IFN)-regulatory factors (IRFs) (**Figure 2**)[19]. Some PRR, including members of the NLR family such as NLR family pyrin domain containing 3 (NLRP3) or NLR family CARD domain-containing protein 4 (NLRC4), differ because they activate the caspase 1 protease which maturate different proteins such as the pro-inflammatory cytokines interleukin (IL)-1β and IL-18[18]. Many PRR can also react to endogenous ligands called damage-associated molecular patterns (DAMPs) such as mitochondrial DNA (mtDNA) or the presence of ATP in the extracellular space to elicit inflammation in response to cellular or tissue damage[20].

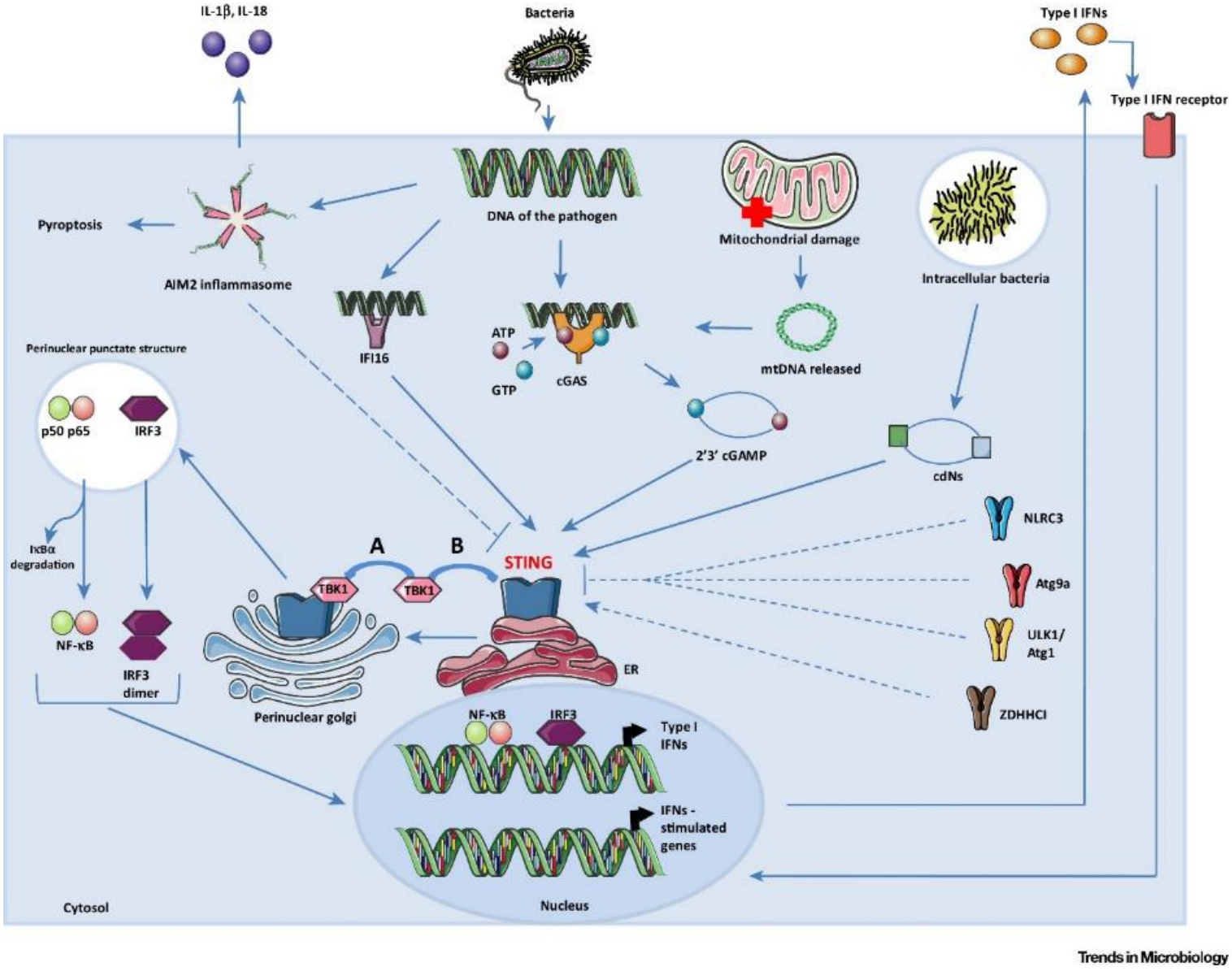

Figure 3: **Sensing of bacterial pathogens by the cGAS-STING pathway.**

Following the classical pathway of STING activation, intracellular DNA is sensed by cGAS which in turn produces 2', 3' cyclic GMP-AMP (cGAMP) which is a STING agonist. Both pathogenic and endogenous DNA, such as the mtDNA, can activate cGAS. Alternatively, STING can directly bind cyclic dinucleotides (CDNs) such as c-di-GMP, produced by *Brucella* spp., that acts as second messenger in bacterial signalling. Then, STING could translocate in the Golgi and interact with Tank-binding-kinase 1 (TBK1) which will phosphorylate STING to allow its complete activation. This is followed by the activation of NF-κB and IRF3 which induce the expression of pro-inflammatory gene. Such as type I IFNs (IFN-β) that can activate type I IFN receptor (IFNAR). STING activation is regulated by NLRP3, ULK1, Atg9a and possibly the AIM2 inflammasome. Picture taken from ref 331.

Besides the induction of inflammation, macrophages are also an important part of the effector branch of the immune system as they are able to phagocyte microbial invaders that are subsequently digested by hydrolases after fusion of phagosomes with macrophage's lysosomes[21]. In addition, when exposed to pro-infammatory stimuli, macrophages produce a lot of different anti-microbials such as nitric oxide (NO) and reactive oxygen species (ROS) through the inducible nitric oxide synthase (iNOS/NOS2) and the NADPH oxidase 2 (NOX2), respectively[22]. In consequence, the immune response is also a damaging process for the surrounding tissue and the macrophage plays a fundamental role in the switch from the acute, damaging, phase of inflammation to the phase of tissue repair, also referred to as the "resolution phase"[23]. Macrophages are thus dynamic cells that respond to environmental stimuli to change their phenotype in a process called "macrophage polarisation". Pro-inflammatory and microbicidal macrophages called M1 or classically-activated macrophages (CAM) are usually obtained *in vitro* in response to LPS + interferon (IFN)-γ stimuli while IL-4/IL-13 stimuli induce the polarisation into anti-inflammatory/repair macrophages called M2 or alternatively-activated macrophages (AAM)[24].

1.3. *Brucella*'s host-pathogen relationship

1.3.1. A stealthy pathogen

One of the main characteristics of *Brucella* species is their ability to evade the recognition by the immune system. Indeed, the main cell type infected by *Brucella* during chronic infections is the bactericidal macrophage that possess, as we have discussed, a wide range of anti-bacterial effectors[22]. Several virulence determinants of *Brucella* are thus meant to avoid macrophage activation by active and passive mechanisms giving rise to the term "stealthy pathogen" when referring to *Brucella* species[25]. For example, the LPS molecule present at the surface of the outer-membrane of smooth *Brucella* strains (in opposition to rough *Brucella* strains) possess specific structural features that distinguishes it from other Gram-negative bacteria. As a result, it reduces its binding to innate immune receptors such as TLR4 or the complement pathway and thus the induction of inflammatory responses. The rough *Brucella* strains were shown to induce extracellular signal -regulated kinase (ERK) 1/2 and p38 MAPK pathways and downstream expression of NOS2 that was detrimental for its survival in comparison to smooth *Brucella* strains[26]. Furthermore, this "stealthy" strategy is the best demonstrated by the fact that the presence of large amounts of intracellular bacteria does not impair cell cycle progression and mitosis in infected HeLa cells[27].

Important studies using mice deleted for the genes encoding IFN-γ or the downstream transcription factors IRF1 or IFN consensus sequence binding protein (ICSBP) highlighted the critical role of these immunity actors to fight *Brucella* as the mice were not able to clear the infection which even become lethal[28,29]. Macrophages activated by a IFN-γ/LPS (from *Escherichia Coli*) showed that *B. abortus* was sensitive to the anti-bacterial effect of NO[30]. Myeloid differentiation primary response 88 (MyD88) activation through TLR signalling is essential for the containment of *Brucella* infection[31,32] by inducing IFN-γ and subsequent NOS2 expression in macrophages[33] but the exact TLRs implicated is controversial with, sometimes contrasting reports, implicating TLR9, TLR2 and TLR4[31,34–36]. In the case of NLRs, *Brucella* spp. flagellin, which escapes TLR5 recognition, and *Brucella* DNA were shown to activate the NLRC4 and absent in melanoma (AIM) 2 inflammasomes, respectively, and to drive IL-1β and IL-18 production[37,38]. These cytokines promotes the containment of the infection in the spleen of infected mice[37].

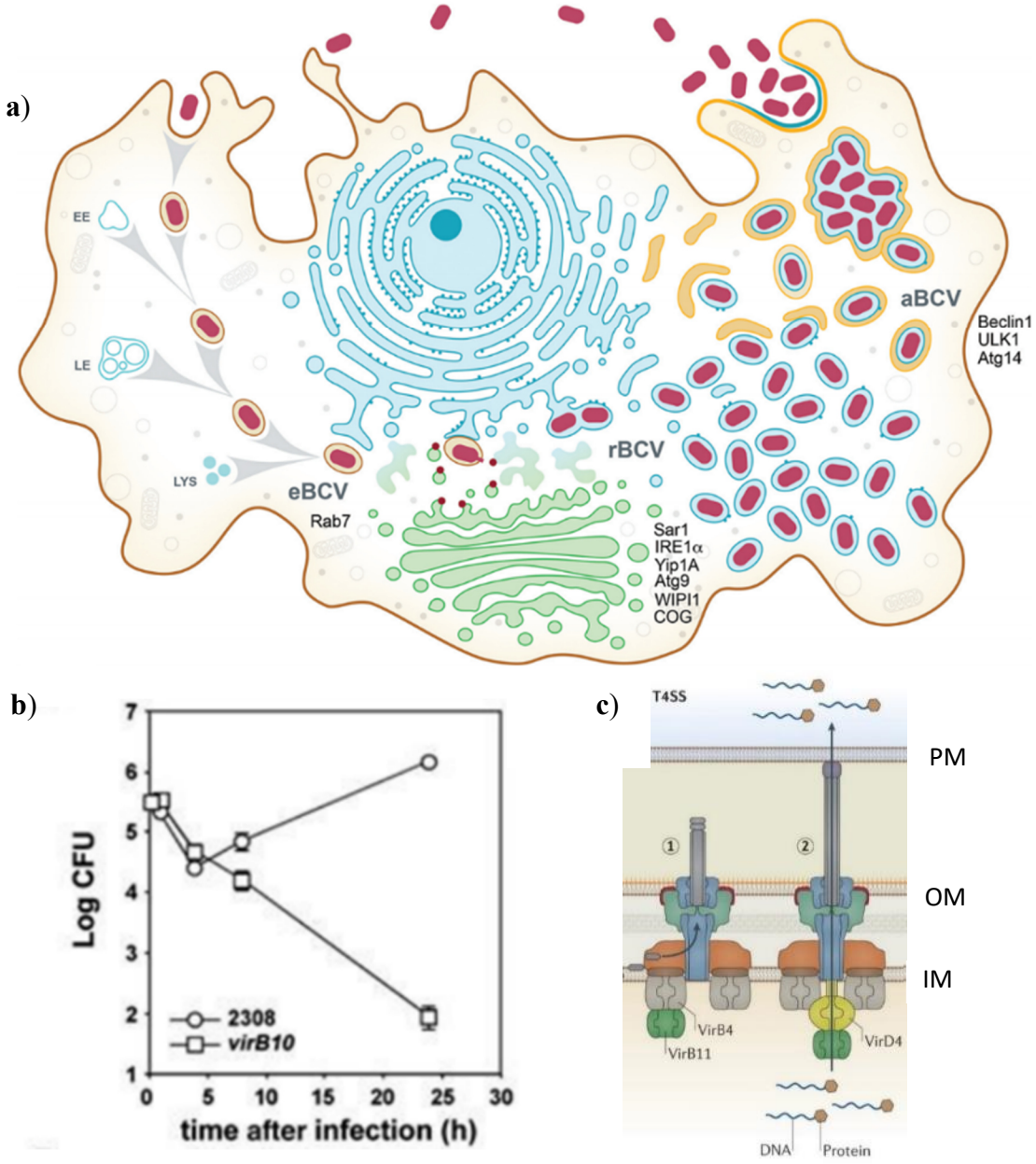

Figure 4: Intracellular trafficking and replication of *B. abortus*

a) The bacteria are first internalized by a particular form of endocytosis involving cholesterol rich membrane regions (lipid rafts). *Brucella* is present in a membrane closed compartment (the endosomal *Brucella* containing vacuole = eBCV) that go through endocytic maturation: it interacts with early endosomes (EE), it becomes acidified (pH of approximately 4.5) and acquires the late endosomal marker LAMP1 by interacting with late endosomes (LE) and finally with lysosomes (LYS) thanks to host Rab7 protein, a small GTPase. Acidification and Rab7 are even required for the expression of the virulence factor type IV secretion system (T4SS). The T4SS secrete proteins ('effectors') modulating immune function and host vesicular trafficking. Effectors are necessary to initiate the conversion of the eBVC to the replicative *Brucella* containing vacuole (rBCV) (from 8 to 12 h p.i.) in which the bacteria massively replicate (from 12 to 48 h p.i). Sar1, IRE1α, Yip1A, Atg9, WIPI1 and COG from the host contribute to rBCV biogenesis. The rBCV harbours several markers of the endoplasmic reticulum (ER) including calreticulin, calnexin and Sec61β and even harbours structural and functional ER features. After 48h p.i. the rBCV becomes engulfed by autophagosome-like structures in a T4SS-dependent manner giving rise to the autophagic *Brucella* containing vacuole (aBCV). Surprisingly, aBCV formation requires the autophagic nucleation complex (such as Beclin1, ULK1, Atg14) but not downstream effectors such as LC3-II. The aBCV is necessary for bacterial escape and infection of adjacent cells. Picture taken from ref 15.

b) Typical evolution of colony forming units (CFU) numbers during infection of murine BMDM by *B. abortus* strain 2308. After internalisation, the majority of infecting bacteria are cleared by 6 h after infection. Replication starts around 8 h p.i. A mutant deficient for VirB T4SS is unable to reach the rBCV and becomes progressively cleared in macrophage lysosomes. Picture taken from ref 48.

c) Structure of a prototypical T4SS. The schematics is derived from a structure derived from *A. tumefaciens*, another α-proteobacteria. PM = plasma membrane OM= outer membrane, IM= inner membrane. Picture taken from ref 334.

In addition to passively avoid recognition, *Brucella* spp. was shown to actively counteract several immune signalling pathways to promote its replication such as IFN-γ-induced signal transducer and activator of transcription (STAT) 1 signaling, stimulator of IFN genes (STING) (**Figure 3**) or MyD88 (Figure 1)[39–42]. This is often linked with the secretion of "effector proteins" by the type IV secretion system (T4SS) which is also essential for *Brucella* spp. survival, replication and dissemination into host cells in a series of events commonly referred to as *Brucella*'s "intracellular infection cycle" [2].

1.3.2. Intracellular infection cycle

Brucella intracellular infection cycle is a highly regulated process during which the bacteria-containing vacuoles (BCVs) endure sequential maturation phases that are associated with the completion of different steps in the infection cycle (bacterial entry, replication and egress) (**Figure 4.a**) [15]. During the first hours of infection, *Brucella* can be found in an endosomal compartment called the endosomal *Brucella*-containing vacuole (eBCV). Bacterial entry into the host cell, is already fundamental for the outcome of the infection. *Brucella* was shown to produce different adhesins[43] such as BigA that can induce rearrangements of the actin cytoskeleton in the host cell and is required for the invasion of epithelial cells[44]. The entry mechanism differs between virulent (smooth) and non-virulent (rough) strains, the former relying on the presence of cholesterol and GM1 ganglioside-rich lipid rafts for entry by macropinocytosis. This entry pathway is related to an increase in survival and replication in mouse bone marrow-derived macrophages (BMDM)[45] that seems to be linked to a delay in endosome maturation and a decrease in the fusion with the lysosomes in comparison to rough strains[45,46]. However, Starr et al. more recently demonstrated that, in contrast to general belief, the eBCV fuses with functional, proteolytic, lysosomes around 3 h p.i. and that this event is necessary for the completion of the cycle in HeLa and macrophage-like cells[47]. Furthermore, the presence of the endolysosomal marker LAMP-1 and the acidification of the eBCV to a pH around 4 to 4.5 further indicate that the bacteria endure the normal endocytic process. The majority of virulent bacteria (more than 90%) thus get killed after fusion with lysosomes (**Figure 4.b**)[48] giving rise to the concept that lysosomal fusion is a "necessary evil"[15]. Next, these vacuoles fuse with the endoplasmic reticulum (ER)[49] giving rise to the rBCV where the bacteria can massively replicate[15]. The exact mechanism of rBCV formation is not well characterised but it involves membranes derived from the ER exit site (ERES) and the Golgi apparatus[50]. Starting at 48 h post-infection, the rBCV becomes engulfed in multiple membrane with late endocytic features such as low pH and the presence of lysosome-associated membrane glycoprotein 1 (LAMP1). This structure is reminiscent of autophagosome and are dependent on the activity of the autophagic nucleation complex (UNC-51-like kinase 1 (ULK-1), Beclin-1 and Atg14L) but does not involve other autophagy related proteins such as LC3, Atg5 or Atg7. Those structures have nevertheless been called autophagic BCV (aBCV) and are essential to the last step of *Brucella*'s life cycle: the exit of the cell, possibly after the fusion of the aBCV with the plasma membrane in an exocytosis-like manner[15].

Table 1: Recapitulation of identified *Brucella* spp. effectors, their dependence on VirB, when known their function inside host cells and their impact on the infection process.

Effector Name	VirB dependent	Molecular target in the host	Effect on host physiology	Fitness of deletion mutants
BigA	Not investigated	Unknown	Modulation of actin cytoskeleton	Adhesin required for proper invasion of epithelial cells[44].
BPE123	Yes[53]	Alpha-enolase from glycolysis (HeLa cells)	Unknown	Reduced intracellular replication (HeLa cells) which depends on reduced alpha-enolase activity[58]
BPE005	Yes[53]		Leading to collagen deposition and fibrosis in the liver[55]	Normal replication in mice but reduced liver fibrosis[55].
BspA, BspC, BspE	Yes[54]	Unknown	Not investigated	Not investigated
BspB	Yes[54]	Interaction with Golgi-localised COG[50]	Inhibition of host protein secretion and rewiring of intra-Golgi trafficking to provide Golgi-derived vesicles to rBCVs[50]	Reduced rBCV biogenesis and intracellular replication (BMDM)[50]
BspF	Yes[54]	Binding and activation of ACAP1, a GAP towards Arf6[56]	Disruption of vesicular trafficking between recycling endosomes and the Golgi (HeLa)[56]	Reduced replication within the rBCV[56]
BspJ	Seemingly not[54]	Binding and downregulation of CKB and NME2[308]	Inhibition of apoptosis	Decreased intracellular viability in RAW264.7 over time linked to greater apoptosis induction[308].
BspL	Yes	Herp[57]	Induction of ER-associated degradation (ERAD) pathway[57]	Anticipated aBCV formation (HeLa and BMDM)[57]
VceA	Yes[52]	Unknown	Deficiency increases autophagy and decrease apoptosis (in trophoblasts cells)[59]	Not investigated
VceC	Yes[52]	ER chaperone Grp78/BiP[64]	Induction of IRE1 branch of UPR signaling[64] in macrophage and induction of CHOP pathway in trophoblasts[307]	Reduced induction of inflammatory gene expression upon infection in macrophage[64] and reduced induction of cell death upon trophoblast infection[307]
NyxA and NyxB	Yes for NyxA, independent for NyxB	Direct interaction with the SENP3 protease [328]	Formation foci in the cytoplasm positive for SENP3, ribosomal proteins and the ribophagy receptor [328]	SENP3 seems to favour the replication of *Brucella* WT (HeLa cells)[328].

Table 1: Recapitulation of identified *Brucella* spp. effectors, their dependence on VirB, when known their function inside host cells and their impact on the infection process.

Effector Name	VirB-dependent?	Molecular target in the host	Effect on host physiology	Fitness of deletion mutants
SepA	Yes	Unknown	Not investigated	Defect in LAMP-1 exclusion leading to reduced proliferation before 24h p.i. (HeLa, THP-1 and BMDMs)[338].
TcpB (*B. melitensis*) or Btp1 (*B. abortus*)	No[65]	Binding to TIR-domain containing proteins such as TIRAP and association to microtubules	Induction of the UPR[65], reorganization of the microtubule cytoskeleton, inhibition of TLR signalling[341]. Reduction of NAD^+ concentrations in infected HeLa cells[60].	Decreased replication inside HeLa cells due to MAL/TIRAP function[340].

Importantly, *Brucella*'s infection cycle is far from being a passive process as its completion also relies on the secretion of effectors that manipulate different host pathways through the expression of the T4SS VirB (**Figure 4.c**)[15]. Several screens done about 10 years ago identified several *Brucella* effectors[2,51–54] but the molecular characterisation of their role during infection started more recently by an increasing number of studies (see **Table 1**)[50,55–60]. It has been shown that VirB expression is important for the entry of virulent *B. abortus* by macropinocytosis inside macrophages by inducing a large reorganization or the actin skeleton[45] but this VirB-dependency is not confirmed in *B. suis*[46]. VirB has also been shown to be essential for the conversion of the eBCV to the rBCV starting at 8 h p.i.[48]. The requirement for eBCV acidification for the completion of the cycle[61] could be linked to the pH-dependent induction of *virB* expression in *B. suis*[62] and later shown to be linked to the activation of the BvrS/BvrR by exposure to low pH and low nutrient availability in *B. abortus*[63]. The VirB-dependent effectors have been shown to promote *Brucella*'s intracellular fitness by modulating different cellular processes such as protein secretion[54], Golgi-associated vesicular trafficking[50] and also induction of the ER-unfolded protein response (ER-UPR)[64,65]. Lastly, the T4SS has also been shown to be required for the final step of the cycle: the maturation of the rBCV to the aBCV and bacterial egress from the host cell[66].

In conclusion, *Brucella* intracellular fitness and replication relies on the modulation of different cellular pathways and organelles such as vesicular trafficking or the ER-UPR[15]. Several studies done on *B. abortus*-infected macrophages also indicate a possible modulation of mitochondrial activity with reduced expression of nuclear-encoded mitochondrial genes[67] and reduced respiratory capacity of macrophages upon infection by *Brucella abortus*[68]. Mitochondria are indeed increasingly recognized as being important in host-pathogen interactions and reported to be targeted by a number bacterial pathogens such as *Legionella pneumophila, Chlamydiae spp, Simkania negevensis, Salmonella enterica serovar Typhimurium, Mycobacterium tuberculosis* or *Coxiella burnetii*[69,70]. Furthermore, it is becoming more and more documented that the ER and the mitochondria heavily crosstalk through direct physical contact called mitochondrial-associated ER membranes (MAMs) potentially transmitting UPR-activated signalling pathways[71]. The next section will be dedicated to discuss the relevant mitochondrial functions in an infectious context.

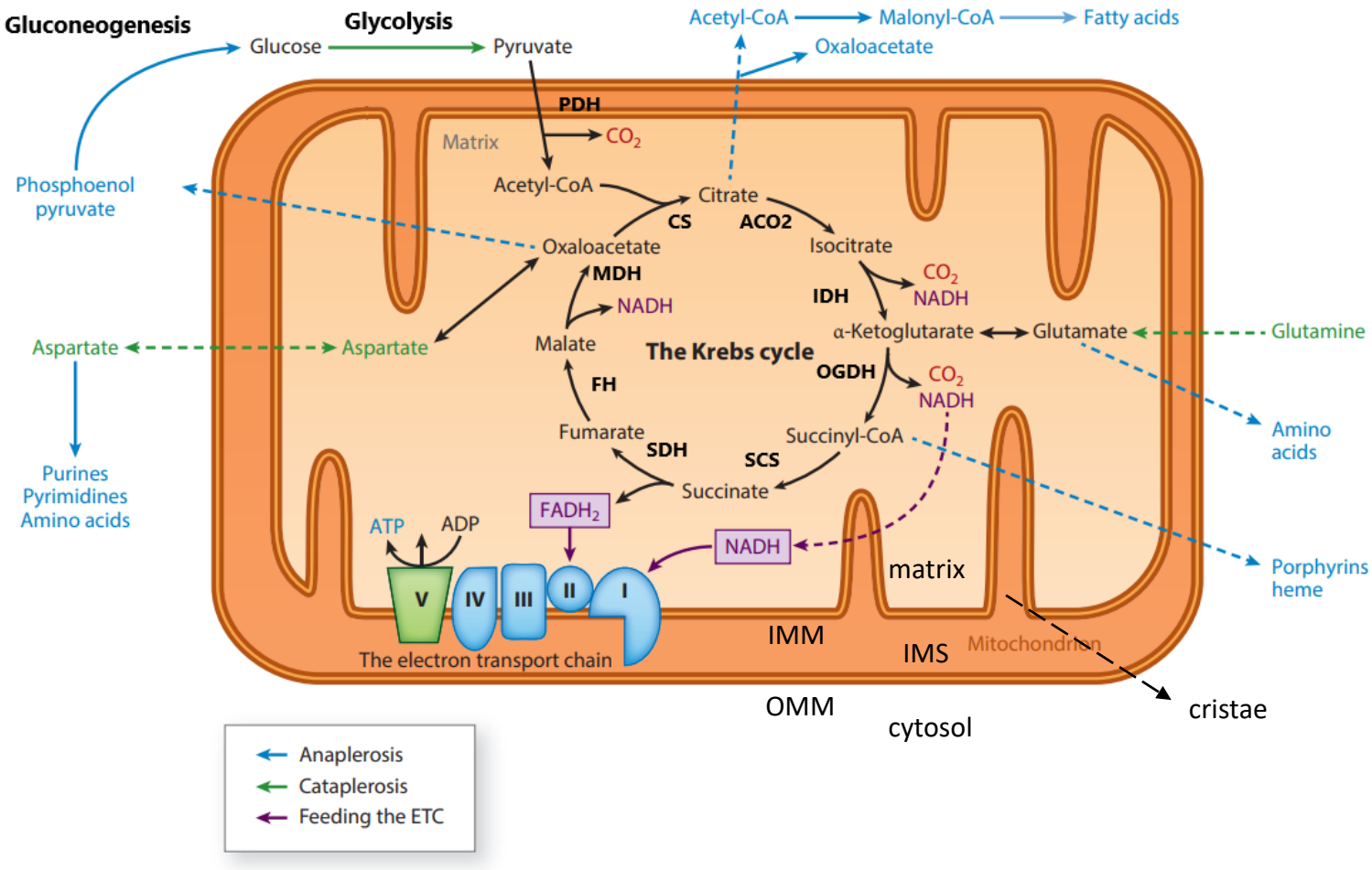

Figure 5: Schematics of mitochondrial ultrastructure and bioenergetics.

The substrate of the Krebs cycles (also called tricarboxylic acid cycle, TCA) is acetyl-CoA, which can be obtained either by oxidation of glucose-derived pyruvate by the pyruvate dehydrogenase (PDH) or by β-oxidation of fatty-acids (not shown). The TCA is constituted of 8 successive enzymatic reactions starting with incorporation of 2C atoms (Acetyl-CoA) on oxaloacetate (4C) to generate citrate (6C). Citrate is then oxidised to generate electron carriers, NADH and $FADH_2$, and decarboxylated twice to regenerate the 4C acceptor for acetyl-CoA (oxaloacetate). Electron carriers can then feed the electron transport chain (ETC) in order to generate ATP by oxidative phosphorylation (ATP). Intermediates of the TCA are used as biosynthetic precursors for a wide range of biomolecules such as amino acids or heme in a phenomenon called "anaplerosis". This is balanced with "cataplerosis" which refers to the ability of some nutrients to replenish the pools of Krebs cycle intermediates such as glutamine or aspartate. Abbreviations: OMM = outer mitochondrial membrane, IMS = intermembrane space, IMM = inner mitochondrial membrane, PDH = pyruvate dehydrogenase, CS= citrate synthase, ACO2= aconitase 2, IDH= isocitrate dehydrogenase, OGDH = α-KG dehydrogenase, SCS = succinyl-CoA synthetase, SDH = succinate dehydrogenase, FH = fumarate hydratase, MDH = malate dehydrogenase. Picture modified from ref 78.

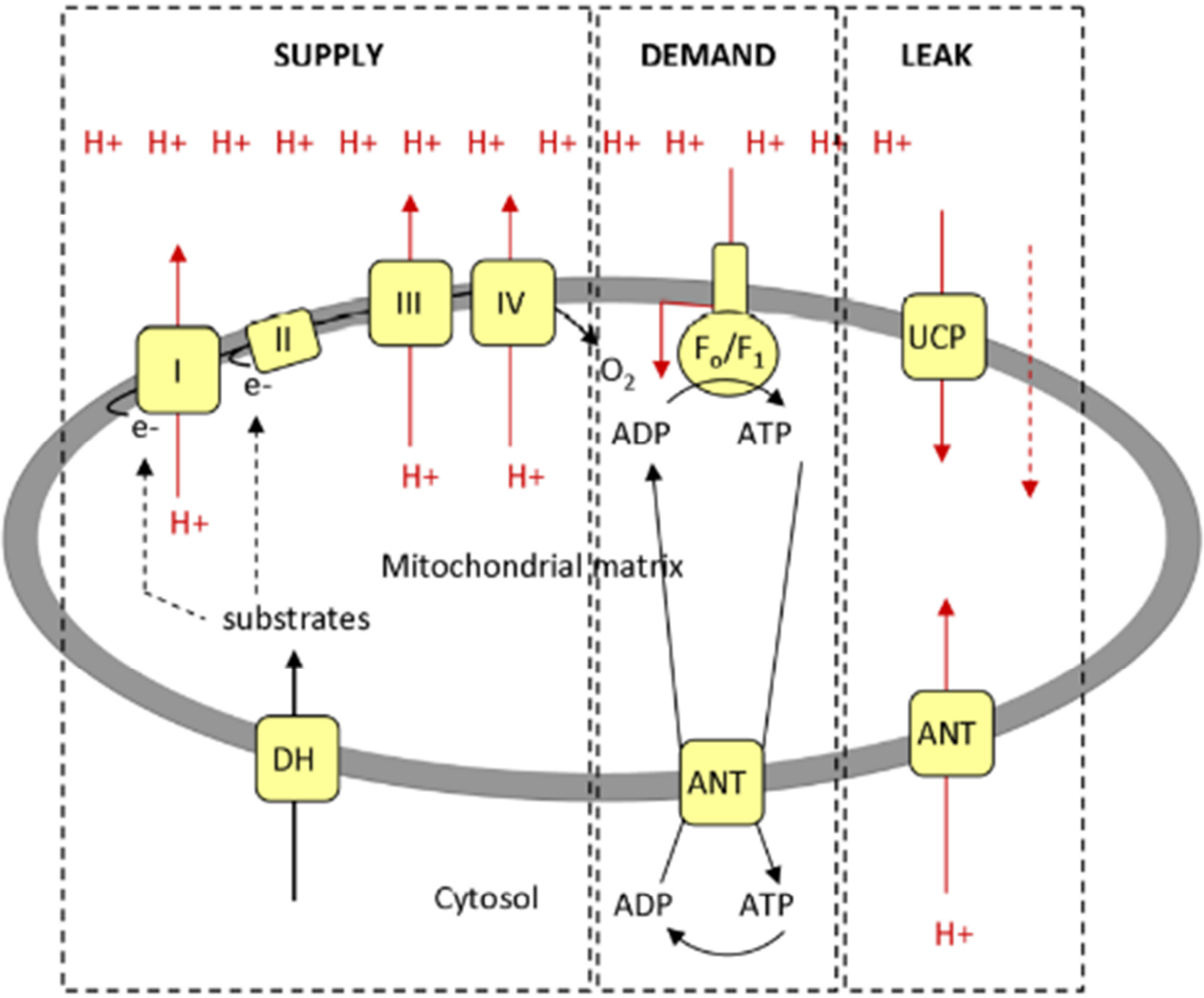

I-IV, respiratory complexes 1-4; ANT: adenine nucleotide translocase; DH: dehydrogenases; F_o/F_1, ATP synthase.

Figure 6: Establishment of mitochondrial membrane potential (MMP).

The mitochondrial electron transport chain is constituted of 4 complexes: CI (NADH dehydrogenase), CII (TCA enzyme succinate dehydrogenase (SDH)), CIII (ubiquinol:cytochrome c oxidoreductase), CIV (cytochrome c oxidase (COX)). Oxidation of respiratory substrates, such as NADH and succinate from the Krebs cycle, are oxidised at complex I and complex II, respectively, generating electron flux in the respiratory chain which is referred to as the supply. The flow of electron in the ETC entrain the pumping of protons (H+) by complex I, III and IV out of the matrix into the IMS giving rise to an electrochemical gradient (also called proton motive force, ΔμH+) composed of a difference in pH (ΔpH) and a difference in charge (ΔΨ) the latter being commonly referred to as mitochondrial membrane potential (MMP, ΔΨm). The MMP is the main component of the ΔμH+ and is also easy to measure with fluorescent probes. Proton re-entry in the matrix can occur through the Fo/F1 ATP synthase which permits the phosphorylation of ADP into ATP but this path relies on the energy demand, meaning the ADP/ATP ratio. Alternatively, proton leak refers to the re-entry of protons independently of the Fo/F1 ATP synthase which leads to energy dissipation as heat. There is a basal proton leak due to the permeability of the IMM but can also be induced in a process termed uncoupling through the expression of uncoupling proteins (UCP). Picture from ref 81.

1.4. The mitochondria and *Brucella*

The mitochondria generally host the central metabolism (tricarboxylic acid (TCA) cycle and OXPHOS) accounting for the majority of ATP production in most healthy eukaryotic cells[72,73]. They are also essential for the biosynthesis of a number of biomolecules (amino acids, lipids, heme, …)[72]. Mitochondria are the descendent of an ancestral bacterium that has been "domesticated" by the last common eukaryotic ancestor (this is the endosymbiotic theory)[74]. This theory explains some of the structural particularity of the mitochondria such as the presence of its own genome (mtDNA), present in multicopies, and expression machinery, particular ribosomes or a double membrane like it is seen in Gram-negative bacteria[75]. The mitochondria are associated with a plethora of functions that can confer advantages to a pathogen and recent research confirmed that the mitochondria constitute a target of choice for different bacterial pathogens[70,76,77]. In the next sections, the relevance of studying the mitochondria in an infectious context will be discussed, after a brief presentation of the mitochondria, its structure, biochemistry, dynamic aspects and homeostasis.

1.4.1. The powerhouse of mammalian cells

Mitochondria are double membrane enclosed organelles which contains several compartments: the matrix, the inner mitochondrial membrane (IMM), the intermembrane space (IMS) and the outer mitochondrial membrane (OMM). Mitochondrial matrix host the TCA cycle, the central metabolic hub where reducing equivalents such as NADH and $FADH_2$ are obtained from acetyl-CoA oxidation (**Figure 5**)[78]. NADH and $FADH_2$ will feed the mitochondrial electron transport chains (ETC) with electrons in several and sequential oxido-reduction reactions before reaching molecular oxygen, the final electron acceptor[79]. Electron flux across the respiratory complex induce the pumping of protons from the matrix to the IMS, thereby generating the mitochondrial membrane potential (MMP) (**Figure 6**) which is an important measure of mitochondrial function[80]. Protons re-entry occurs in most cases mainly through the Fo/F1 ATP synthase that is coupled with the phosphorylation of ADP into ATP, in opposition to an uncoupled state where proton ionophores (which can be chemicals such as carbonyl cyanide-p-trifluoromethoxyphenylhydrazone (FCCP) or, in more physiological settings, uncoupling proteins, UCP) mediate proton re-entry without concurrent ATP synthesis[81,82].

Mitochondria, together with NOXs, are a major source of endogenous ROS that is due to electron leakage from complex I or complex III to molecular oxygen giving rise to superoxide radical anions ($O_2^{\cdot -}$)[72,83]. A too high MMP, referred to as hyperpolarisation, does not necessarily lead to increase in ATP synthesis, which mainly depends on energy demand and ADP/ATP ratio, but it causes exponential rises in proton leakage across the IMM and also in mitochondrial ROS (mtROS) production[84,85]. On the other hand, depolarisation, meaning a substantial drop in MMP, leads to reduced ATP production but its impact on mtROS production is debated[85,86].

Mechanistically, $O_2^{\cdot}$ produced in the matrix side of complex I is converted to H_2O_2 by the mitochondria-localised superoxide dismutase (SOD2) which can exit the mitochondria through porins to exert signalling roles by causing the reversible oxidation of redox sensors[72]. At complex III, $O_2^{\cdot}$ can be formed directly in the IMS which can cross the OMM through porins to exert signalling roles in the cytoplasm either directly or after conversion into H_2O_2 by the cytosolic and IMS-localised SOD (SOD1)[72]. Reversibility of protein oxidation relies on anti-oxidant defences such as thioredoxins (Trx) and glutaredoxins (Grx) that reduce proteins to their original state but a deregulation between ROS generation and anti-oxidant defences can

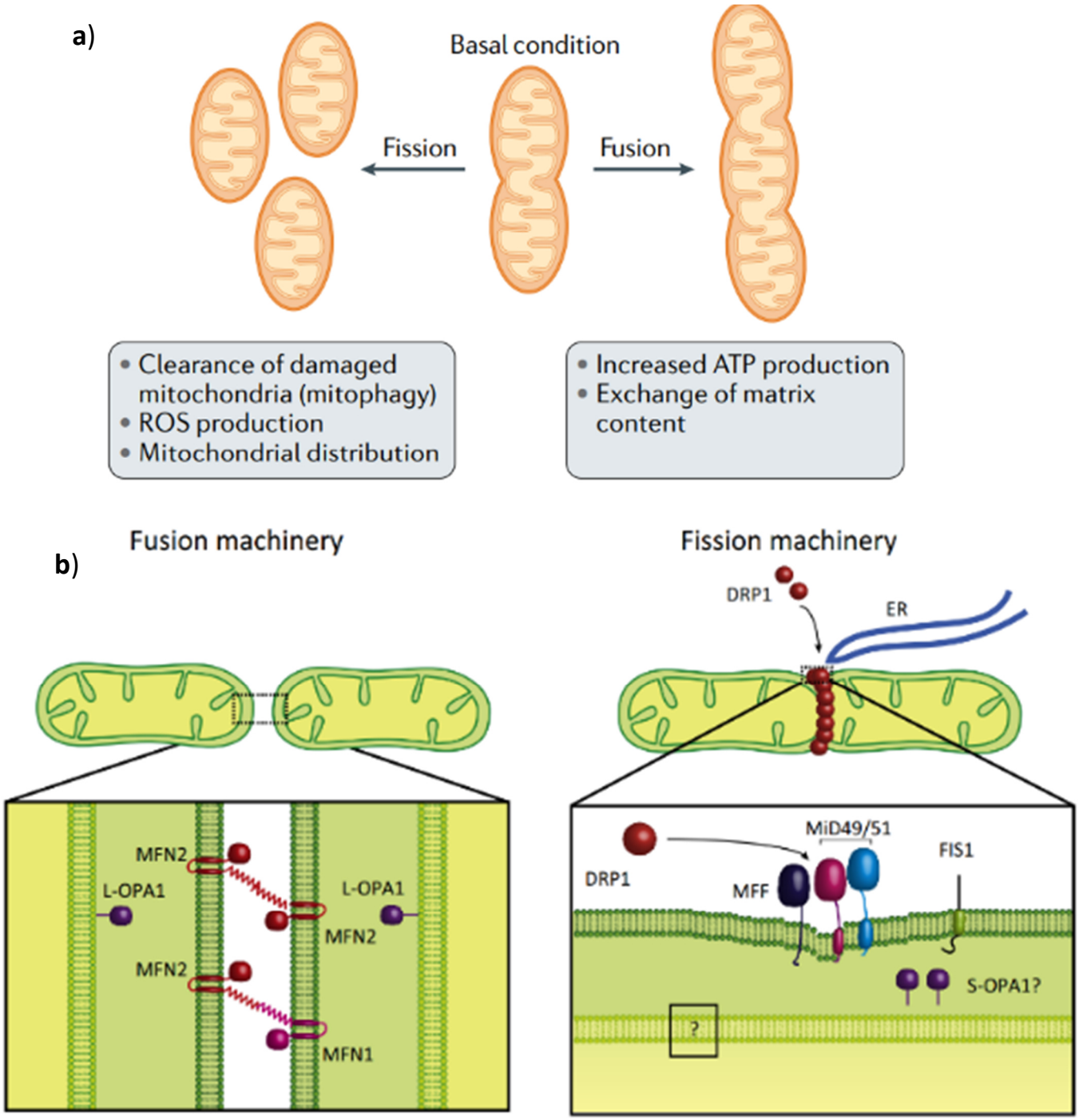

Figure 7: Mitochondrial fusion and fission mechanisms

a) Summary of the biological roles associated with fusion/fission balance. Picture taken from ref 100.

b) Left: mitochondrial fusion the result of the subsequent fusion of OMM by homo or heterotypic association between mitofusins (MFN) 1 and MFN2 followed by IMM fusion which depend on the long isoform of optic atrophy protein 1 (lOPA1). lOPA1 can be cleaved by mitochondrial protease (Ymel1 and Oma1) to yield a short isoform of OPA1 (sOPA1) which is also involved in the fusion process but in an unclear manner.

Right: the main mitochondrial fission pathway depend on the recruitment of the GTPase dynamin-related protein 1 (DRP1) on the mitochondria where it oligomerises into a contractile ring. Fission site are marked by ER tubules where are located DRP1 receptors, mitochondrial fission factor (Mff) and mitochondrial dynamic proteins of 49 kDa (MiD49) or 51 kDa (MiD51). The sOPA1 has been shown to localise to DRP1 fission site and to promote fission (Anand et al., 2014). Pictures taken from ref 327.

lead to irreversible protein (but also lipid or DNA) oxidation which is referred to as oxidative stress[86]. Importantly, mitochondrial bioenergetics and ROS production have been recently linked to dynamics changes in mitochondrial morphology.

1.4.2. Mitochondrial fusion/fission balance

Mitochondria undergo successive fusion and fission events to form reversible interconnected or fragmented networks (**Figure 7a**). During the cell cycle for example, mitochondria are highly connected at S phase but become fragmented during mitosis possibly to allow segregation and partitioning of mitochondria between daughter cells[87]. Fusion has been shown to be necessary to dilute damaged components inside the mitochondria to maintain a homogenous healthy population. However, when a part of the mitochondria become heavily damaged, the activation of fission mechanism and/or the inhibition of fusion mechanism lead to the dissociation of the defective part from the network to allow its selective removal by mitochondrial autophagy (mitophagy)[87]. Furthermore, mitochondria can also be transported throughout the cell on microtubules in order to fulfil subcellular need for ATP at the best[88] and this process requires the presence of small fragments of mitochondria. Mitochondrial morphology is also usually linked to functionality, with elongated networks generally consuming more oxygen and producing more ATP while fragmented states are often associated with ROS production and apoptosis induction[79].

Mitochondrial morphology is dependent on the activity of dynamin related guanosine triphosphatases (GTPase) (**Figure 7b**). The main mitochondrial fission effector is the cytosolic dynamin-related protein 1 (DRP1 also called DNML1) that can polymerize into a contractile ring around the mitochondria which is constricted following GTP-hydrolysis[89]. Multiple DRP-1 OMM-located receptors have been identified: Fis1 in yeast and mitochondrial fission factor (Mff), mitochondrial dynamics protein of 49 or 51 kDa (MiD49 and MiD51) in mammalian cells[89]. In a seminal work, it was shown that DRP1 oligomerisation and thus division sites was determined by ER-mitochondria contacts[90]. Contacts between mitochondria and late endosomes/lysosomes and Rab7 function were also implicated in mitochondrial fission[91].

The outer mitochondrial membrane (OMM) located mitofusin 1 and 2 (MFN1 and MFN2, respectively) and the inner mitochondrial membrane (IMM) protein optic atrophy 1 (OPA1) are responsible for fusion events[88]. MFN1 and MFN2 first tether adjacent mitochondria through homo- or heterotypic interactions and then mediate fusion thanks to GTP hydrolysis[88]. The sequence homology between MFN1 and 2 is high but their depletion induce different fragmentation phenotypes: a high number of small mitochondria fragments and aggregation into clusters, respectively[92]. Reports also indicate that MFN1 is the main fusion effector while MFN2 is associated with other functions[93,94]. Interestingly, a fraction of MFN2 is present at the ER and is be required for physical interactions between the ER and the mitochondria at MAMs[95–97]**.** OPA1 is essential for fusion to occur[98] and its fusion activity is linked to OXPHOS activity[99]. OPA1 is also essential for the formation of cristae, and thus proper OXPHOS functioning[100]. Fragmentation can also occur because of a diminished activity of fusiogenic proteins. Indeed, it was shown that, in mammalian cells, Fis1 recruit another fission effector: TBC1D15 that is independent of DRP1[101]. Fis1 was shown to mediate fission by reducing mitochondrial fusion through direct interaction with MFNs and OPA1 and reduction of their GTPase activity[102]. The fragmentation of the mitochondria is often (but not always), a first step in the degradation of dysfunctional mitochondria by mitophagy.

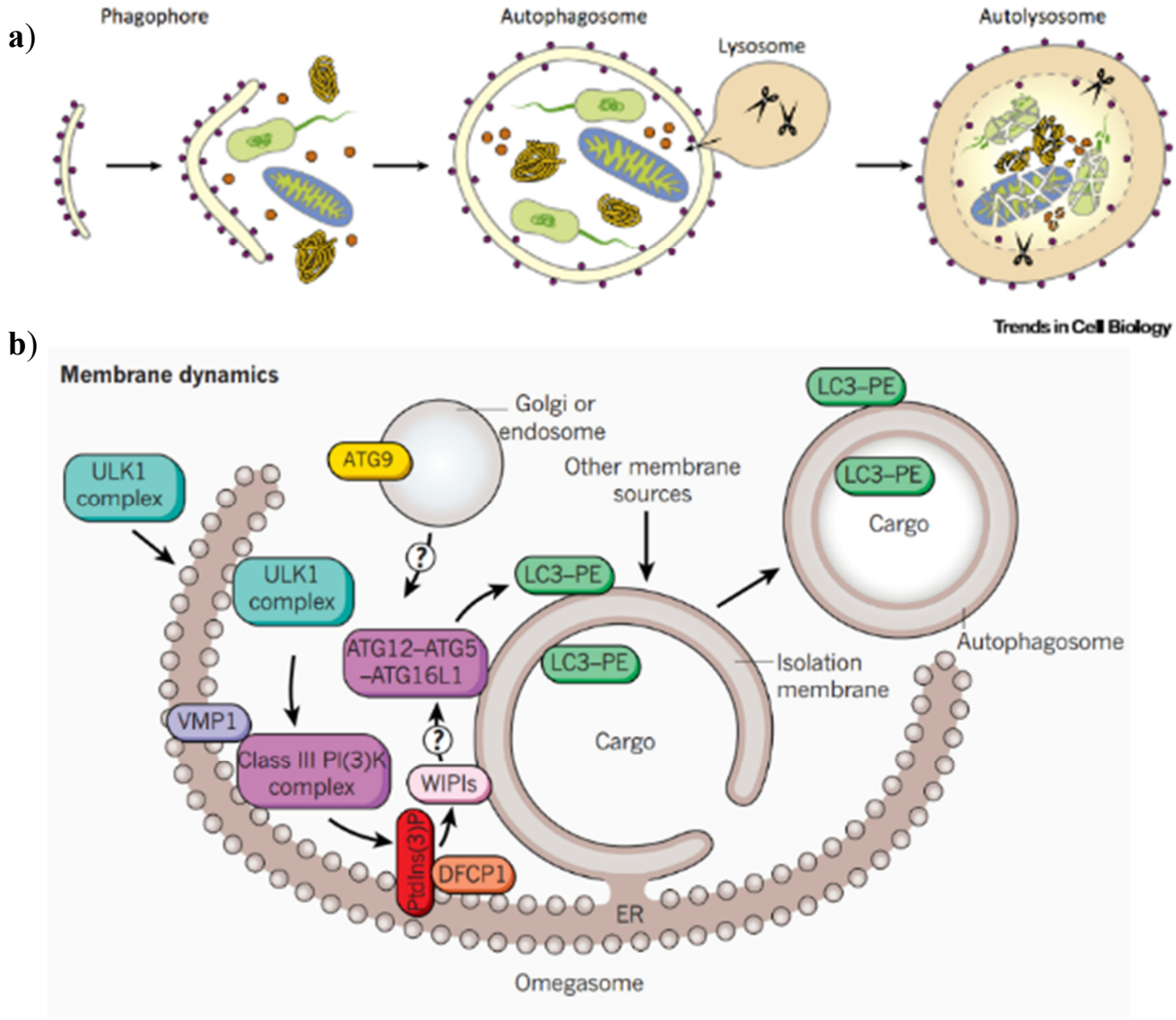

Figure 8: The biogenesis of autophagosome during bulk autophagy

a) The biogenesis of autophagosome has first been studied in the case of starvation induced bulk autophagy. In this case, ER-derived membranes called phagophore or isolation membrane will encapsulate portion of the cytoplasm in a non-specific manner giving rise to a double membrane enclosed compartment called autophagosome. The autophagosome content will then be degraded after fusion with lysosomes leading to autophagolysosome formation. Picture from ref 330.

b) Low nutrient availability leads to a reduced mammalian target of rapamycin (mTOR) activity relieving the inhibition of the ULK initiation complex composed of ULK1/2, ATG13, FIP200 (also known as RB1CC1) and ATG101 that translocate to Atg9 positives regions of the ER (Karanasios et al., 2016; Zachari and Ktistakis, 2020). This recruits the Vps34 phosphatidylinositol-3-phosphate kinase (PI3K) complex (composed of Vps34, Vps15, Beclin1 and Atg14) that phosphorylate surrounding PI phospholipids generating a PI-3-phosphate (PI3P) rich membrane. PIP3 recruits WD-repeat domain phosphoinositide-interacting (WIPI) proteins and double FYVE-containing protein 1 (DFCP1) yielding a particular compartment termed omegasome that will surround the growing phagophore. The growth of the phagophore is associated with the conjugation of phosphatidyl-ethanolamine (PE) to LC3/GABARAP family of ubiquitin-like proteins by the ATG5/ATG12/ATG16L1 complex and their insertion into the autophagosomal membranes. The PE-conjugation to LC3/GABARAPs relies on a ubiquitin-like conjugation system where LC3/GABARAP are activated by ATG7 (E1 enzyme), transferred to ATG3 (E2 enzyme) and ATG12- ATG5 acting as the E3 complex. The PI3P effector WIPI2 was found to dictate LC3-lipidation sites by binding ATG16L1 leading to the recruitement of ATG5-ATG12 on the phagophore leading to the incorporation of LC3-II to both sides of the phagophores and is kept in mature autophagosomes and degraded after fusion with lysosomes. The exact role of LC3/GABARAP family of proteins is unclear but they are involved in phagophore growth and closure during starvation-induced autophagy but their role could differ following the context as formation and closure of mitophagosome is independent of LC3s during Parkin mediated mitophagy. Picture from ref 104.

1.4.3. Mitophagy

Mitophagy is a selective form of macro autophagy (hereafter referred to as autophagy) that selectively targets excess or dysfunctional mitochondria to lysosomal degradation[103]. Mitophagy can be divided in different functional groups: mitophagy can serve as a quality control mechanism to allow the removal of damaged mitochondria either under homeostatic conditions (basal mitophagy) or in response to a stressor (stress-induced mitophagy)[103]. In addition, programmed mitophagy refers to the induction of mitophagy at specific stages of development such as during red blood cell maturation to allow the dynamic remodelling of the mitochondrial network in response to fluctuating metabolic demands[103].

In order to be degraded, target mitochondria must first be separated from the rest of the cell after being engulfed in a double membrane bilayer called isolation membrane or phagophore giving rise, after closure, to a new compartment called autophagosome (**Figure 8a**)[104]. The biogenesis of the phagophore occurs at a transient ER compartment called the omegasome that is formed upon activation of the ULK1 kinase complex following mammalian target of rapamycin (mTOR) complex 1 (mTORC1) inhibition under nutrients (especially branched amino acids) or growth factors deficiency (**Figure 8b**)[105]. In addition, energy deficiency, such as following glucose starvation, activates the AMP-activated protein kinase (AMPK), a master regulator of metabolism that activates autophagy when AMP concentrations rise by inactivating the mTORC1 complex[105]. AMPK activation also promotes autophagy by directly phosphorylating ULK1[106,107]. Interestingly, AMPK activation in HeLa cells[108] and ULK1, along with the downstream autophagy proteins, activation in different macrophage cell lines[109] have both been shown to promote the intracellular multiplication of *Brucella*.

The biogenesis of the phagophore has been reported to occur at MAMs upon amino acids starvation[110]. Different membrane sources in addition to ER origin have been implicated in phagophore growth such as the mitochondria[111], the plasma membrane or endosomes[112]. The maturation of the phagosome is coupled with the conjugation of LC3/GABARAP family of ubiquitin-like proteins to the phospholipid phosphatidylethanolamine (PE) for incorporation into the phagophore by an ubiquitin-like conjugation system: ATG7, ATG3 and the ATG5-ATG12-ATG16L1 complex which function as E1-like, E2-like and E3-like enzymes, respectively[113].

Mechanistically, selectivity of mitophagy relies on mitophagy receptors characterised by a LC3-interacting region (LIR) necessary for binding the phagophore markers LC3/GABARAP family of proteins. Several different mitophagy receptors have been identified that can be broadly separated into two categories: ubiquitin-dependent receptors and ubiquitin-independent receptors (**Figure 9**). On the one hand, following the classical pathway mitochondrial damage, such as an IMM depolarisation triggers the ubiquitination of surface mitochondrial proteins by the E3-ubiquitin ligase Parkin. However, more recently other ubiquitin ligases were involved in mitophagy (**Figure 9a**). Ubiquitin act as an "eat-me" signal that is recognised by specific mitophagy receptors such as optineurin or nuclear dot protein 52 kDa (NDP52)[103]. On the other hand, a number of ubiquitin-independent mitophagy receptors have been identified in the recent years such as BCL2/adenovirus E1B 19 kDa protein-interacting protein 3 (BNIP3) and the closely related BNIP-3L (also called Nix), FUN14 domain-containing protein 1 (FUNDC1) or FK506 binding protein 8 (FKBP8) among others which are linked to mitophagy induced by other stressors than depolarisation, such as hypoxia or iron deficiency (**Table 2**)[114]. Importantly, LC3/GABARAP binding to the LIR is highly regulated by phosphorylation on serine residues (for BNIP3, BNIP3L and FUNDC1)[115,116] or tyrosine residues (FUNDC1)[117] adjacent to the LIR motif (**Figure 9b**).

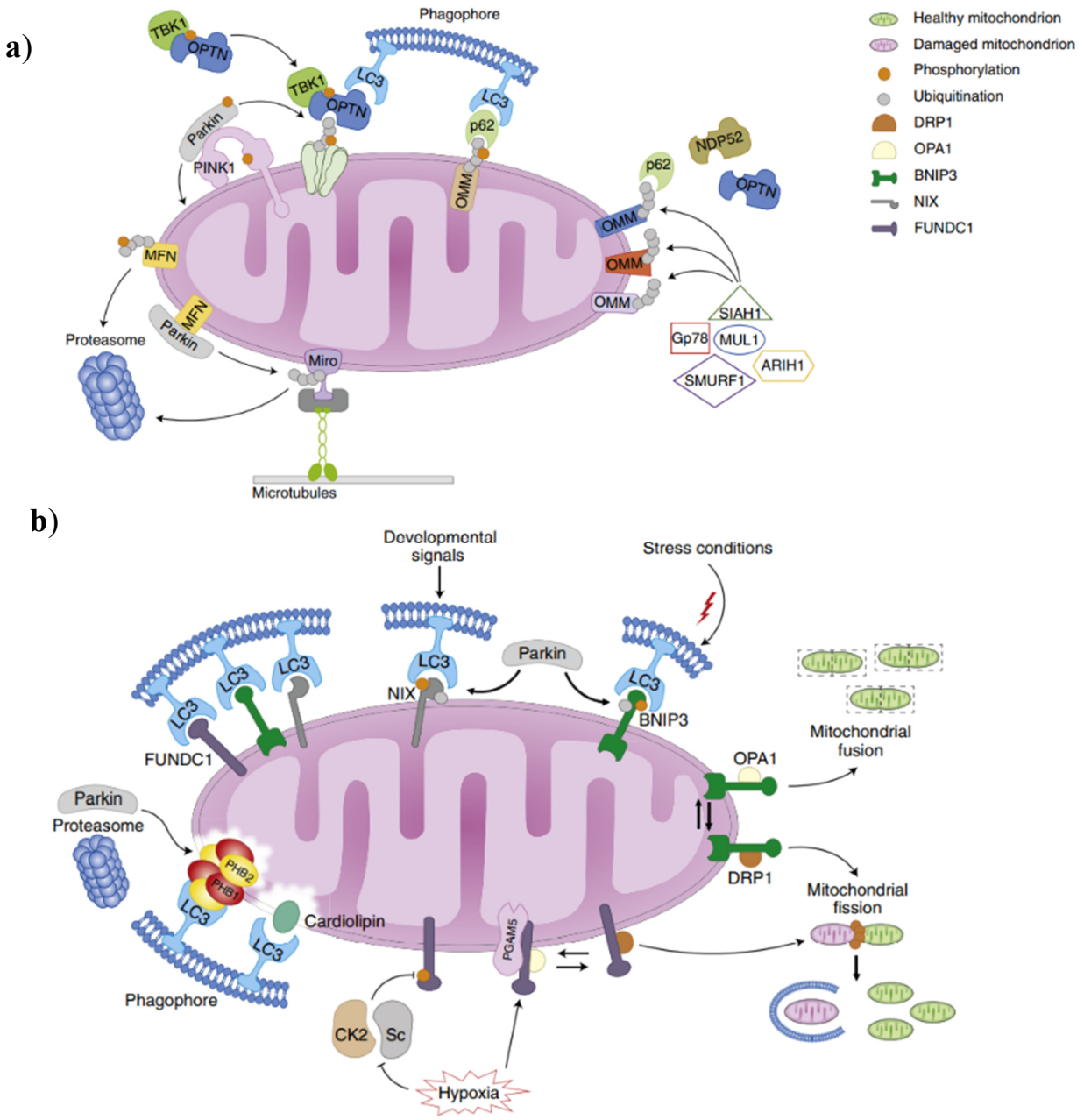

Figure 9: The different pathways of mitochondrial removal by mitophagy

a) Ubiquitin-dependent mitophagy has been extensively studied in the context of Parkin-mediated-mitophagy where widespread depolarisation of mitochondria inhibits the degradation of the kinase PINK1 which is stabilised on the OMM. PINK1 then induces the recruitment of the E3-ubiquitin ligase Parkin leading to widespread ubiquitination of OMM proteins and recruitment of mitophagy receptors (such as optineurin or NDP52) (Sekine and Youle, 2018; Zachari and Ktistakis, 2020). Parkin also triggers the selective removal of OMM proteins by proteasomal degradation such as MFNs and Miros, a Rho-GTPase, leading to reduced mitochondrial fusion and motility, respectively. MFN2, once phosphorylated by PINK1, can also act as receptor for mitochondrial Parkin recruitment. Tank-binding kinase 1 (TBK1) phosphorylates optineurin to enhance its recruitment on mitochondria in a feed-forward loop. The ubiquitination of mitochondria can occur independently of Parkin by different other E3-ubiquitin ligases.

b) Ubiquitin-independent mitophagy receptors are OMM localised proteins which directly interacts- with LC3 and, notably, include FUNDC1, BNIP3, BNIP3L/NIX to allow mitophagy in the absence of Parkin. When OMM integrity is lost, IMM located prohibitin (PHB1)/PHB2 and cardiolipin now at the mitochondrial surface can directly bind LC3 and induce mitophagy. Interactions with regulators mitochondrial morphology such as OPA1 and DRP1 allow mitophagy receptors to induce the removal of dysfunctional part from healthy part of the network to allow specific mitophagic degradation. FUNDC1 is inhibited by a phosphorylation-dependent mechanism mediated by casein kinase 2 (CK2) and Src kinase at S13 and Y18, respectively, which inhibits LC3 binding. Upon mitochondrial stress, phosphoglycerate mutase family member 5 (PGAM5), a phosphatase, dephosphorylates S13 to allow mitophagy. Both BNIP3 and BNIP3L were shown to be involved in Parkin-mediated mitophagy by enhancing its recruitment. Pictures taken from ref 103.

Following the classical/canonical model of mitophagy, these LC3 positive membranes will bind and recruit primed mitochondria harbouring mitophagy receptors before autophagosome closur[114]. However, it has been reported that mitochondria can also be recruited inside fully formed autophagosomes independently of LC3/GABARAP proteins during Parkin-mediated mitophagy[118]. The core initiation machinery including the ULK1 complex can be directly recruited on the damaged mitochondria by the mitophagy receptor NDP52 following mitochondrial depolarisation and initiate *de novo* mitophagosome formation[118,119]. ULK1 recruitment on the mitochondria is needed for FUNDC1- and Bcl-2-like protein 13 (Bcl2-L-13)-mediated mitophagy possibly indicating the formation of the mitophagosome directly onto the mitochondria[120,121]. However, LC3 binding is essential for mitophagosome formation during receptor-mediated mitophagy, in contrast to Parkin mediated mitophagy, but how this is regulated spatio-temporally in regard to mitophagosome formation remains an area of current and intensive investigation[114].

Several crosstalk between mitophagy and mitochondrial dynamics do exist. Several reports indicated that during starvation-induced autophagy, reduced DRP1 activity lead to mitochondrial elongation that was shown to spare the mitochondria from degradation[94,122]. Furthermore, PINK-Parkin-mediated mitophagy leads to degradation of MFN1 and MFN2 in a proteasome-dependent manner and removal of mitochondria upon mitochondrial depolarisation is impaired in DRP1 knock-out (KO) mouse embryonic fibroblasts (MEFs) and cardiomyocytes[123,124]. A number of mitophagy receptors were also shown to induce mitochondrial fragmentation when ectopically over-expressed (Table 2), sometimes dependent on DRP1 such as for BNIP3L[125,126], BNIP3[127,128] or FUNDC1[129,130]. However, FKBP8[131] or Bcl2-L-13[132] induce mitochondrial fragmentation independently of DRP-1. These different observations have led, intuitively, to the assumption that mitochondrial fission is a necessary prerequisite for mitophagy because only small fragmented mitochondria could be engulfed inside autophagosomes[133]. Recent reports nevertheless indicate that mitophagy can still occur in cells having highly elongated networks (DRP1 KO cells)[134]. It has been reported that the machinery responsible for the initiation and elongation of the isolation membrane (including FIP200, ATG14 and WIPIs) was recruited onto tubular mitochondria upon hypoxia or the addition of an iron chelator and is responsible for mitochondrial fission in a DRP1-independent manner[135].

In the recent years, accumulating evidence indicates that bacterial pathogens actively modulate the processes of fusion/fission and mitophagy to their advantage thanks to dedicated effectors[76,77]. Some of the advantages that a pathogen can obtain from the regulation of mitochondrial dynamics will be discussed in the next section.

Table 2: Non-exhaustive overview of currently characterised mitophagy receptors, their ability to recruit LC3 family members following different stimuli and their requirement for DRP1 in the induction of mitochondrial fragmentation

Mitophagy receptor	LC3/GABARAP member	Stimuli	Ability to cause fragmentation
BNIP3	LC3B[333]	Hypoxia[185]	Yes, involvement of DRP1[127]
BNIP-3L/Nix	GABARAP-L1 > LC3A > LC3B[336]	Reticulocyte maturation[332] Depolarisation (CCCP)[337] Ischemia-reperfusion[329] Hypoxia[180]	Yes, involvement of DRP11[125, 126]
FKBP8	LC3A > LC3B[289]	DFP[131]	Yes, DRP1 independent[131]
Bcl2-L-13	LC3B[132]	Depolarisation (CCCP)[132]	Yes, DRP1 independent[132]
FUNDC1	LC3B > GABARAP > LC3A[117]	Hypoxia[117] Depolarisation (FCCP)[293]	Yes, involvement of DRP1[129, 293]
NLRX1	LC3B[158]	*L. monocytogenes* infection[158]	Not known
E2F3d	LC3A, LC3B, GABARAPs[336]	Hypoxia[339]	Yes, mostly DRP1 independent[336]

1.4.4. Roles of mitochondria during bacterial infections

1.4.4.1. Mitochondria and macrophage immunometabolism

In the recent years, it was observed that pro-inflammatory macrophages operate a glycolytic switch, meaning a shutdown of OXPHOS activity with a compensatory increase in glycolysis, a phenomenon commonly called "Warburg effect" (or aerobic glycolysis) as a tribute to Otto Warburg that first observed that in cancer cells[136]. This discovery led to the development of the immunometabolism field in which the mitochondria was found to play a central role[78]. Usually, the glycolytic switch is thought to produce more anabolic precursors to meet the high biosynthetic demand of activated macrophages because of the incomplete oxidation of glucose during glycolysis, that only generates a net gain of 2 ATP/ glucose molecule in contrast to an average of 36 ATP/glucose during OXPHOS[136,137]. This metabolic switch has mainly been studied in LPS-stimulated macrophages and will be further discussed in the section addressed to hypoxia-inducible factor (HIF) 1α **(**see section 1.5.2.**)**. Importantly, the polarisation state of macrophages and the associated metabolism greatly influence *Brucella* fitness and ability to cause a chronic infection[138] and *B. abortus* was shown to preferentially replicate inside M2 macrophages[139]. M2 macrophages have low glycolysis activity and upregulate arginine metabolism (through arginase-1 expression), which leads to increased glucose and arginine-derived polyamines, respectively, which are both used as nutrient source by *Brucella*[139,140].

M1 polarisation by TLR4 or TLR3 agonists is also accompanied with mitochondrial fragmentation as soon as 2 h after stimulation that is due to reduced expression of the fusion factor FAM73B (also called MIGA2) independently of MFN1/2[141]. MIGA2, together with its isoform MIGA1, were shown to constitute one of the downstream effector mechanism of MFN1/2-induced mitochondrial fusion in a still unclear mechanism[142]. In addition, LPS-activated macrophages exhibit mitochondrial fission which is abrogated by DRP1 deficiency and was shown to be important for IL-12 expression[143,144]. In the case of *S. pneumoniae* infection of macrophages, mitochondrial fragmentation was dependent on mtROS-mediated lysosomal permeabilisation and the release of the lysosomal protease cathepsin B[145] which has recently been implicated in *B. abortus* infection of murine macrophages[146]. Direct manipulation of mitochondrial dynamics have been linked with metabolic advantages to bacterial pathogens such as *Chlamydia trachomatis* who inactivates DRP1 mediated fission resulting in mitochondrial elongation and increased ATP synthesis which promote its growth[147,148]. In contrast, *L. pneumophila* actively induce mitochondrial fragmentation through the secretion of a DRP1 stimulating effector, MitF, which downregulates OXPHOS and is required for optimal bacterial replication[149]. Induction of glycolysis in *B. abortus*-infected RAW264.7 macophage-like cells was reported to favour bacterial replication through the consumption of host-derived lactate[68]. Even if mitochondrial fission has been associated with aerobic glycolysis induction in different cell types[150–152], its implication in M1 macrophage polarisation has not been thoroughly determined so far[141,144].

1.4.4.2. Mitochondrial ROS production and anti-bacterial defences

In the recent years, the mitochondria emerged as an essential actor in the antimicrobial defense of macrophages and is exemplified in the upregulation of mitochondrial biogenesis upon TLR stimulation[77]. The mitochondria was further shown to colocalise with bacteria containing vacuoles after engagement of a subset of TLR (TLR2, TLR4 and TLR1) in murine macrophages[153]. Anti-bacterial mtROS-mediated immunity against *S. aureus* was later shown to be dependent on the activation of IRE-1α (a molecular effector of the UPR)[154]. Importantly, an exaggerated stimulation of IRE-1α was shown to be responsible for the induction of macrophage cell death by a rough attenuated *Brucella* strain[155], possibly implicating mtROS.

Accordingly, the inhibition of ETC activity reduce the anti-microbial activity against *E. Coli* and *S. aureus*[156] and the maximal anti-bacterial activity of macrophages against *S. typhimurium* is associated with elongated networks and high MMP[157]. *L. monocytogenes* counteract this defense mechanism by secreting a pore forming toxin, listeriolysin O (LLO), which damages the mitochondria and stimulates its removal by mitophagy to limit mtROS production, which is advantageous for the bacteria[158]. These authors also found that LLO-induced mitophagy was dependent on a new mitophagy receptor: NLRX1 which belong to the NLR family of PRR with the particularity of possessing a mitochondrial targeting sequence and a LIR motif[158]. Interestingly, *B. abortus* was shown to counteract ROS production inside macrophages in several ways[108,159] but a putative involvement of mitophagy has not been investigated so far.

1.4.4.3. Mitochondria as regulators and platforms for innate immune signalling

Multiple immune signaling pathway are affected by the mitochondria. The STING, that is of importance for the containment of *Brucella* infection [40,160] or was reported to rely on mitochondrial dynamics with a reduced activation of the STING pathway upon MFN1 deficiency or after the induction of mitochondrial fission by mitochondrial uncouplers [161]. The mitochondria anti-viral signaling protein (MAVS), was also shown to act as a platform signalling for the antiviral response initiated by RLRs-mediated viral RNA recognition which cause MAVS aggregation on the surface of the mitochondria to allow signal transduction and activation of the IFN response and NF-κB [77]. This pathway was nevertheless involved in type-1 IFN production and the containment of infection caused by bacterial pathogens such as *C. pneumoniae*, *L. pneumophila, M. tuberculosis* or *L. monocytogenes* [162–165]. A good amount of evidence also showed an intricate relationship between the mitochondria and NLRP3 inflammasome activation. NLRP3, along with the DNA-recognizing AIM2 inflammasome, mediate IL-1β production in *B. abortus*-infected macrophages, a pro-inflammatory cytokine found to be involved in the containment of *Brucella* infection in mice[37]. NLRP3 inflammasome is activated in response to a wide variety of DAMPs such as extracellular ATP, alum hydroxide, silica crystals, urea crystals, nigericin [166]. Importantly, NRLP3, an ER-located protein, was shown to relocate to the mitochondria upon activation and especially at MAMs upon complex assembly [167]. NLRP3 was proposed to act as a sensor of mitochondrial dysfunction as it is able to bind mtDAMPs such as oxidised mtDNA and cardiolipin [168,169]. NLRP3 activation is associated with an increase in mtROS production and a decrease in MMP [167]. Accordingly, IL-1β production is totally blunted in LPS/ATP treated macrophages devoid of mtDNA (ρ^0)[170].

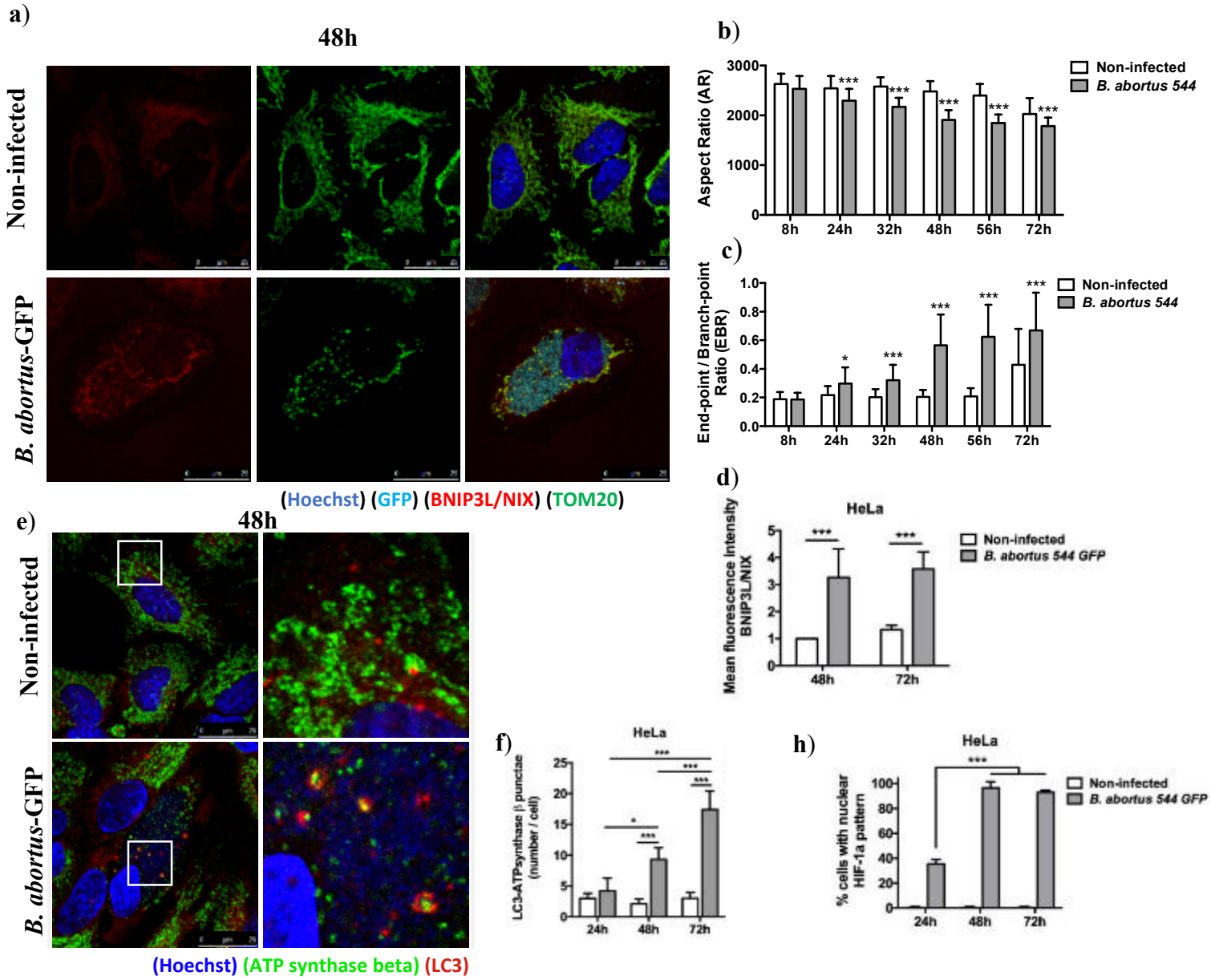

Figure 10: Preliminary results

a) Co-immunostaining of TOM20 and BNIP-3L in *B. abortus*-GFP infected or not HeLa cells (scale bars = 25 µm). Quantification of mitochondrial morphology is in **b** and **c** (n = 3 independent experiments, 75 cells analysed/condition). Quantification of BNIP-3L abundance by flow cytometry is shown in **d** (n = 4 independent experiments).

e) Co-immunostaining of LC3 and ATP-synthase β (IMM marker) in *B. abortus*-GFP infected or not HeLa cells (scale bars = 25 µm). Quantification of colocalisation events is shown in **f** (n = 3 independent experiments, 75 cells analysed/condition)

g) Immunostaining of HIF-1α in *B. abortus*-GFP infected or not HeLa cells (scale bars = 25 µm). Quantification is shown in **h** (n = 3 independent experiments, 75 cells analysed/condition) (Jeremy Verbeke, ongoing PhD thesis, unpublished results).

Moreover, infection of macrophages with the rough *Brucella* strain RB51 lead to the activation of inositol-requiring enzyme 1 (IRE1, a molecular effector of the UPR) which was associated with the release of mitochondrial DAMP into the cytoplasm, and subsequent activation of caspase 1 by the NLRP3 inflammasome [171]. Another study reported that the ER-UPR induced by the smooth strain of *B. abortus* 2308 was contributing to IL-1β secretion in infected-BMDMs [172].Importantly, mitochondrial dynamics (fusion and fission events) regulate inflammasome assembly. Elongated mitochondrial networks due to DRP1 deficiency were associated with an increase in NLRP3 assembly in response to LPS/ATP stimulation of BMDMs [173]. In accordance with NLRP3 being a sensor of mitochondrial damage and dysfunction, mitophagy was repeatedly shown to decrease inflammasome activation and IL-1β release by reducing mtROS production and mtDNA release[170,174–177].

1.4.4.4. Mitochondrial phenotypes associated with *B. abortus* infection

Previous work in the team on infected HeLa cells and RAW264.7 murine macrophage-like cells showed that *B. abortus* strain 544 and *B. melitensis* strain 16M BCVs do physically interact with the mitochondria. An induction of mitochondrial fragmentation that is independent of DRP1 can be observed at 48 and 72 h p.i.[178] (**Figure 10.a,** Verbeke J, ongoing PhD Thesis, unpublished data). Importantly, an involvement of mitochondrial respiration or mtROS production in *Brucella* replication was excluded [178]. In addition, mitochondrial fragmentation is associated with an increase in colocalisation between mitochondria and LC3B, indicative of mitophagy induction (**Figure 10.e**, Verbeke J, ongoing PhD Thesis, unpublished data). In an attempt to identify the mitophagy pathway involved, no widespread mitochondrial depolarisation could be seen in infected *B. abortus*-infected HeLa cells and Parkin-dependent mitophagy was dismissed (Verbeke J., unpublished data). Nevertheless, the mitophagy receptor BNIP3L (Nix) was shown to accumulate on the mitochondria of infected cells at both 48 and 72 h p.i. (**Figure 10.a,** Verbeke J, ongoing PhD Thesis, unpublished data). As BNIP3L is a well known HIF-1α target gene[179,180], the stabilisation and nuclear localisation of the this transcription factor was confirmed which starts at 24h p.i. in both cell types infected with *B. abortus* strain 544 (**Figure 10.g,** Verbeke J, ongoing PhD Thesis, unpublished data).

As the main objective of this master thesis is to pursue the study of the mechanism involved in the fragmentation of mitochondria and mitophagy in *Brucella*-infected cells, we will finish the introduction by reviewing regarding HIF-1α and its known roles during infection.

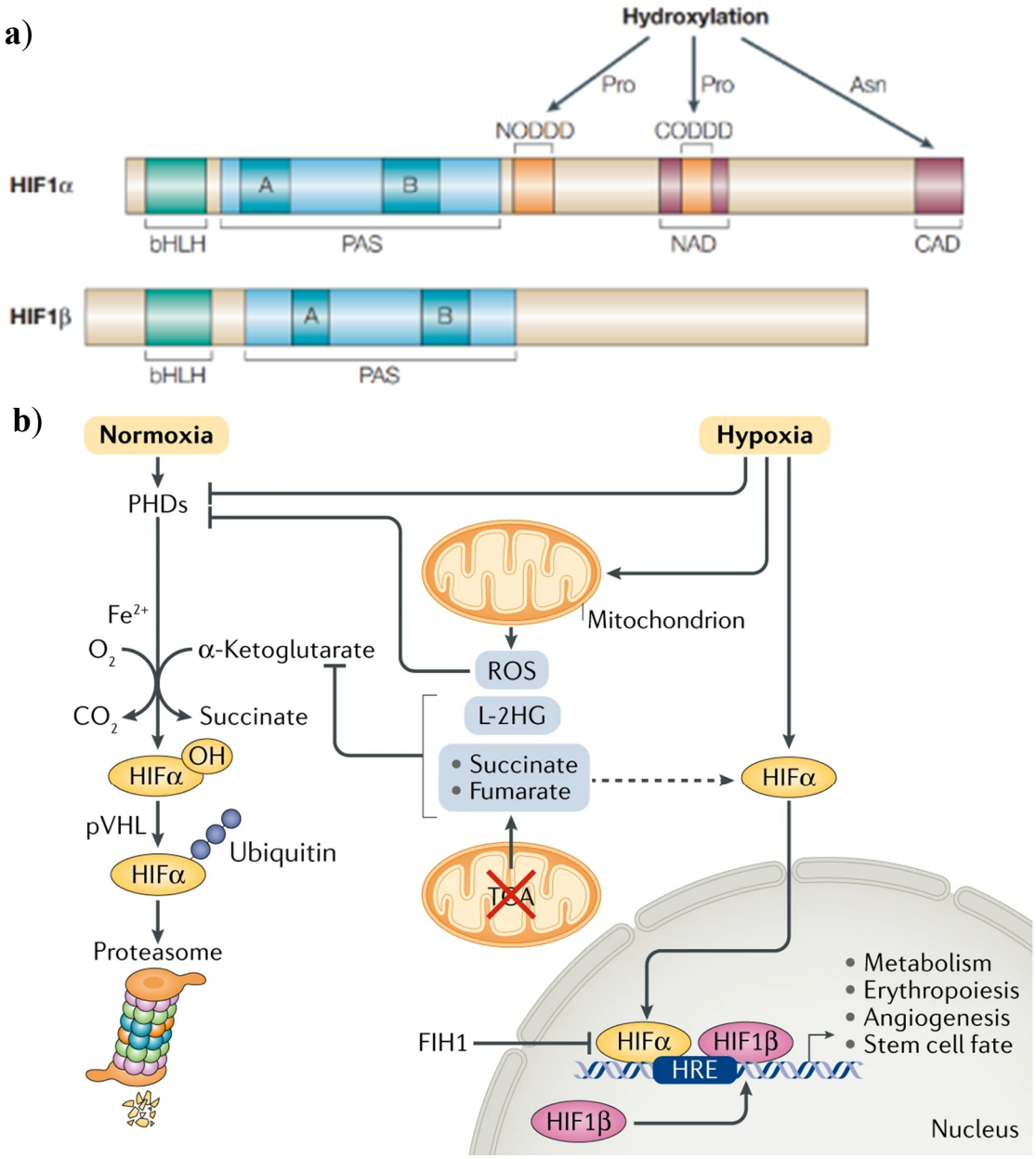

Figure 11: Regulation of HIF-1α stabilisation through prolyl hydroxylation

a) Domain sequence of HIF-1α: at the N-terminal, the per-ARNT-Sim (PAS) domain allow dimerization with HIF-1β and DNA binding through the basic Helix-Loop-Helix domain (pHLH). Oxygen dependent regulation depend on three domains. Prolyl hydroxylation at the N-terminal Oxygen-Dependent Degradation Domain (NODDD) and the C-terminal ODDD (CODDD) regulate protein stability. HIF-1α possess two trans-activating domains, one at the N-terminus (NAD) which contain the CODDD and one at the C-terminus (CAD). Hydroxylation of an asparagine residue in the CAD, which is maintained at lower oxygen concentrations than prolyl hydroxylation, impede its transactivation function leading to a differential regulation between NAD-activated and CAD-activated genes. Picture from ref 187.

b) Oxygen dependent degradation of HIF-1α relies on the activity of a group of enzymes called prolyl hydroxylases which will hydroxylate two proline residues in the oxygen-dependent-degradation domain of HIF-1α. Hydroxylated proline residues will be recognised by the E3-ubiquitin ligase von Hippel Lindau tumour suppressor protein (pVHL) leading to poly-ubiquitination of HIF-1α and its subsequent proteasomal degradation. Under hypoxia, PHD are inhibited, leading to HIF-1α stabilisation which can interact with HIF-1β and translocate to the nucleus. In the nucleus, the HIF-1 heterodimer can bind DNA sequences called “hypoxic response element” (HRE) to initiate the transcription of a wide range of genes involved in biological processes such as metabolism, erythropoiesis, angiogenesis or stem cell fate. Another layer of regulation is brought by factor inhibiting HIF-1 (FIH) which hydroxylate asparagine residues on HIF-1α leading to reduced recruitment of HIF transcriptional co-activators CBP and p300 leading to reduced transcriptional activity. Picture from ref 181.

1.5 . HIF-1α in the host-pathogen relationship

1.5.1. HIF-1α, canonical functions and hypoxia-mediated regulation

HIF-1α is a subunit of the HIF1 transcription factor that is the master regulator of the cell response to hypoxia [181]. The protein, constitutively expressed, is characterised by the presence of an oxygen-dependent degradation domain (ODDD) which induces its rapid degradation under normoxia (**Figure 11.a**)[181]. In addition, 2 isoforms, HIF-2α and HIF-3α have been identified which do also contain an ODDD but their pattern of expression is different than the ubiquitous HIF-1α [182]. HIF-3α functions are not really understood, while HIF-2α has been reported to be activated by less intense hypoxia and remains more stable than HIF-1α overtime giving rise to the idea that HIF-1α is important for response to acute hypoxia while HIF-2α is more linked to chronic hypoxic situations [182]. Even if some target genes are shared between HIF1 and HIF2 such as glucose transporter 1 (*GLUT1*) or vascular endothelial growth factor (*VEGF*), HIF2 seems preferentially involved in the regulation or erythropoiesis and iron metabolism, inducing a greater activation of erythropoietin (*EPO*) or iron uptake (transferrin) for example while HIF1 is more efficient at inducing glycolytic genes such as lactate dehydrogenase a (*LDHA*) [183]. HIF-1α main effects are metabolic through expression of pyruvate dehydrogenase kinase (PDK1) and LDHA which lead to the redirection of pyruvate fluxes from the TCA cycle to the production of lactate, thereby operating a glycolytic switch [184]. Furthermore, HIF1 activity repress mitochondrial respiration to limit the production of damaging ROS under hypoxia and preserve cell viability by inducing mitophagy trough, in the latter case, the upregulation of BNIP3 and BNIP3L mitophagy receptors [184,185]. Induction of BNIP3 mediated mitochondrial clearance by HIF-1α has been shown to mitigate hypoxia-induced ROS production by mitochondria and cell death[185].

HIF-1α protein abundance is directly linked to oxygen availability as regulated by the activity of a prolyl hydroxylase family of enzymes (PHD) which comprises 3 isoforms (PHD1, PHD2, PHD3) [182] with PHD2 being the major actor in normoxic HIF-1α degradation in various cell lines [186]. PHD are non-heme Fe^{2+} containing α-keto-glutarate (αKG, also called 2-oxoglutarate, 2-OG) dependent dioxygenase type of enzymes that use molecular oxygen and αKG to catalyse the hydroxylation HIF-1α on two target proline residues (402 and 564) (**Figure 12**) [187]. Proline hydroxylation of HIF-1α will lead proteasome-mediated degradation (**Figure 11.b**) [187]. When PHD activity is sufficiently reduced, HIF-1α is stabilised and interact with HIF-1β to form a functional HIF-1 complex that induce, after nuclear translocation, the transcription of genes containing an "hypoxia response element" (HRE) DNA sequence [182]. Due to their relatively low affinity for oxygen in comparison to other prolyl hydroxylases, PHD are very sensitive to drops in oxygen concentrations at physiologically relevant ranges [187]. However, PHD inhibition due to lack of oxygen as a substrate is only seen under anoxic conditions (0 to 0.4% O_2) while under hypoxic conditions (1 to 3% O_2) the presence of a functional mitochondrial ETC is needed for HIF-1α stabilisation [188–190]. The exact role of mitochondria is controversial in the literature with data supporting the importance of ROS generation [188] while contrasting reports show that mitochondrial oxygen consumption is crucial for hypoxic HIF-1α stabilisation[191].

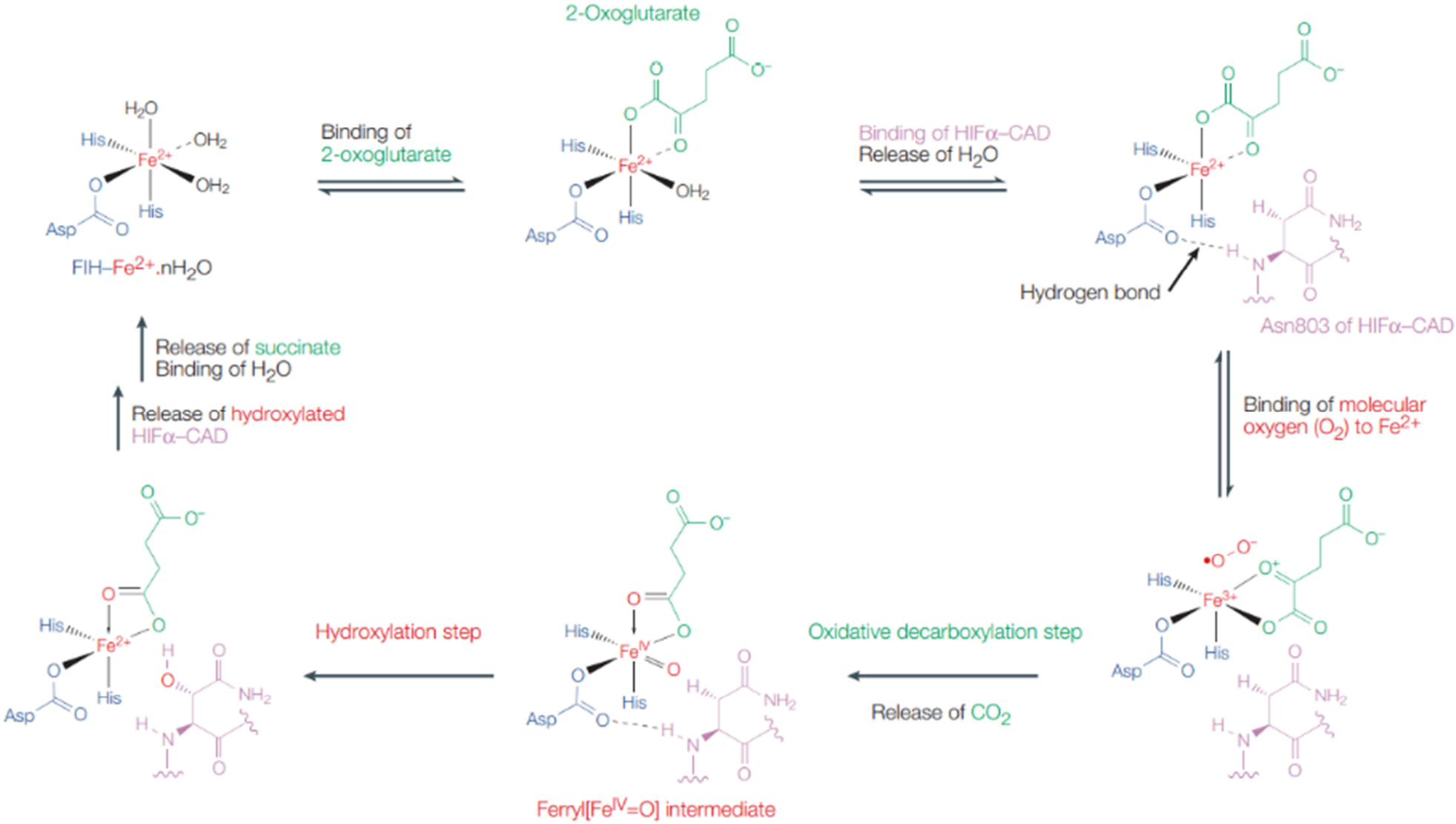

Figure 12: Mechanism of Factor Inhibiting HIF(FIH)-mediated HIF asparagine hydroxylation as a surrogate for general 2-oxoglutarate(OG)-dependent dioxygenases catalysis

The catalytic Fe^{2+} ion is complexed by two histidines and a carboxylate group from aspartate and water molecules. The binding of various substrates is sequential, with first the binding of 2-OG. This is followed by the binding of the prime substrate, here HIF-1α, which is required for the displacement of the water molecule bound to Fe^{2+} allowing the access of O_2 to the catalytic iron. This initiates the oxidative decarboxylation of 2-OG into succinate, generating a highly reactive ferryl intermediate able to hydroxylate a C-H bond on the prime substrate. Picture taken from ref 187.

1.5.2. HIF-1α and immunometabolism in macrophages

In addition to a decrease in partial pressure of oxygen (PO_2), ROS and NO production, iron chelators or TCA intermediates (such as succinate and fumarate) can also inhibit PHD and thus induce HIF-1α stabilisation even under atmospheric oxygen tension (conditions known as pseudohypoxia) [192]. As previously mentioned, HIF-1α can be activated in pro-inflammatory contexts [193] and has been shown to be required for normal myeloid functions such as motility, invasiveness but also anti-bacterial capacity [194]. One of the main function of HIF-1α in LPS-activated macrophages is to upregulate glycolysis genes that are important to sustain macrophage ATP levels [194]. Interestingly, LPS-driven metabolic shift in LPS-activated murine macrophages was shown to be dependent on BNIP3L/NIX-mediated mitophagy [195]. HIF-1α is required for LPS-driven transcriptional upregulation of pro-IL-1β an NOS2 as the promoters of the genes encoding these proteins contain an HRE[196]. Accordingly, the glycolysis switch thus contributes to clear mycobacterial infection in macrophages [197]. However, strikingly, HIF-1α stabilisation has also been shown to favour the replication of some pathogens, such as *C. pneumoniae* [198] but also *B. abortus*[68].

Importantly, HIF-1α stabilisation in a pro-inflammatory context, which is dependent on Myd88 and NF-κB activation, is functionally different from HIF-1α stabilisation under hypoxia, with pro-inflammatory genes such as NOS2 or COX2 being marginally induced by hypoxia in comparison to HIF-1α stabilisation following TLR stimulation[199]. Interestingly, HIF-1α stabilisation can be extended to TLR9 but not TLR3 signalling[199]. Glycolysis upregulation is a general metabolic adaptation to pro-inflammatory stimuli but a decrease in OXPHOS seems to be specific to LPS-treatment and is not seen with TLR2 and TLR3 agonists[200]. This indicates that metabolic modifications are stimuli-specific and allow a specific response in function of the threat.

Mechanistically, LPS-induced HIF-1α stabilisation was shown to be dependent on a rise in succinate concentrations, a TCA intermediate that strongly accumulates in activated macrophages [196]. Succinate drives mitochondrial hyperpolarisation through its oxidation by SDH leading to mtROS generation that are responsible for PHD inhibition [84]. Oxidation of particular cysteine residues in PHD2 leads to enzyme inhibition in response to H_2O_2 treatment, thereby conferring redox sensibility to PHD2[201]. Succinate accumulation relies on the production of itaconate, an immunometabolite, generated by the decarboxylation of *cis*-aconitate into itaconate by *cis*-aconitate decarboxylase (CAD, also called immune-related gene 1 protein, Irg1) which is one of the most upregulated gene in macrophage during inflammation[202]. Regarding *Brucella*, itaconate was recently implicated in the containment of *Brucella* infection by alveolar macrophages (AM) *in vivo*[10]. Furthermore, a very recent study linked glycolysis induction in primary BMDMs infected by *B. abortus* with HIF-1α stabilisation which was dependent on succinate accumulation and an associated mtROS production[203].

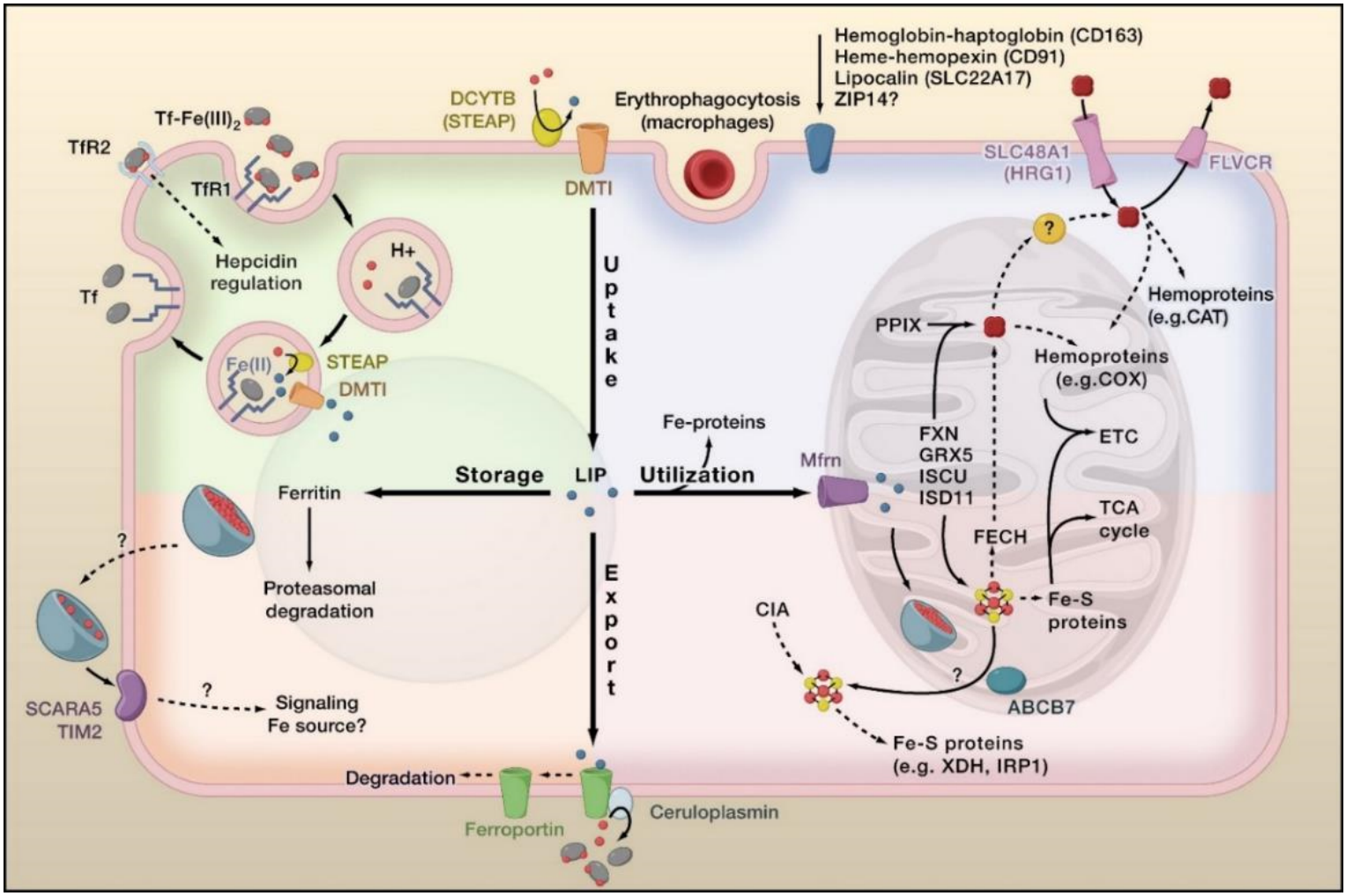

Figure 13: Cellular iron trafficking, regulation and its partitioning into the mitochondria

Iron can enter the cells by in several forms that are classically divided between non-transferrin-bound iron (NTBI) and TBI which depends on specific transporters (such as ZIP8 or ZIP14) and the endocytosis of the transferrin receptor 1 (TfR1), respectively. In the latter case, the acidification of the endosome lead to the release of Fe^{3+} from transferrin and its receptor, which is then reduced to Fe^{2+} by the Steap3 metalloreductase before being imported in the cytoplasm by the transporter DMT1 to enter the LIP. The empty receptor is then recycled back to the plasma membrane to restart another cycle. In other contexts, iron-containing molecules such as ferritin, haemoglobin or hemin can be imported inside cells.

A substantial proportion of cell iron is transported to the mitochondria where it is processed into iron containing prosthetic groups (Fe-S clusters and heme) that are essential for the proper function of proteins involved in the mitochondrial electron transport chain (ETC) and tricarboxylic acid (TCA) cycle. Heme synthesis starts in the matrix from TCA intermediate succinyl-CoA catalysed by the aminolevulinic synthase (ALAS) which is present in two isoforms in mammals: the ubiquitously expressed ALAS1 that ensures routine heme synthesis and ALAS2 which supports heme synthesis mainly during reticulocyte differentiation. After a cytosolic part, heme synthesis ends in the mitochondria with the incorporation of iron into protoporphyrin IX (PPIX) ring by ferrochelatase (FECH) to give functional heme. Mitochondria also host the early iron-sulfur cluster synthesis (ISC) machinery, composed of the following proteins: frataxin (FXN), iron-sulfur assembly enzyme (ISCU), cysteine desulfurase (NFS1) and ISD11. The ISC are essential to generate Fe_2S_2 clusters which can be either incorporated directly into mitochondrial proteins. Some proteins, such as ACO2 and IRP1, require Fe_4-S_4 clusters that are synthetized in the mitochondria or in the cytosol, respectively. Fe_2S_2 clusters can indeed a shuttled to the cytosol where the cytosolic Fe-S assembly (CIA) machinery metallate cytosolic proteins. FXN has also been implicated in heme synthesis by acting as an iron donor for the ferrochelatase.

In conditions of iron excess, iron can be stored inside ferritin polymers in a biologically inactive Fe^{3+} form and be later released by proteasomal or autophagic degradation of ferritin. Iron can also be exported through the SLC40A1, commonly referred to as ferroportin (FPN). Export is coupled with oxidation from Fe^{2+} to Fe^{3+} by the membrane-bound ferroxidase hephastin or by the serum ferroxidase ceruloplasmin. Degradation of ferroportin and iron export in response to the ligation of the liver hormone hepcidin is crucial to maintain stable plasma iron levels and for whole body iron homeostasis. Picture taken from ref 216.

1.5.3. Iron-dependent regulation of HIF-1α

Iron availability has also been linked to HIF-1α stabilisation in various contexts [204,205]. The treatment of dendritic cells with LPS triggers an increase in iron storage by ferritin leading to the depletion of the intracellular iron pools [206]. In those conditions, PHD activity is greatly reduced and HIF-1α is stabilised in a totally oxygen-independent manner [206]. ROS-mediated oxidation of Fe^{2+} to Fe^{3+} was also shown to be responsible for oxidative stress-induced HIF-1α stabilisation in different contexts such as oncogene signalling, NO production, aerobic glycolysis or arsenite-treated cells which can be recovered by treatment with excess Fe^{2+} or vitamin C [207–209]. Indeed vitamin C inhibits or reduces HIF-1α stabilisation following different stimuli such as $CoCl_2$, chelation of iron by DFO, growth factors (IGF-1 and insulin) and moderate (1 to 3% O_2) but not severe (0.1 to 0.4 % O_2) hypoxia[189]. Vitamin C effect is thought to act by increasing PHD catalytic activity by, most likely, reducing Fe^{3+} to Fe^{2+}. More recently, it was shown that reduced glutathione (GSH) can functionally replace vitamin C[189,210]. Importantly, HIF-1α stabilisation during infection of macrophages by different *enterobacteriacae* (which includes *S.* Typhimurium) was shown to be totally dependent on the production of bacteria-derived iron-chelating metabolites called siderophores [211]. Furthermore, iron supplementation was shown to mitigate the glycolytic switch induced by *S. enterica* infection of macrophages [212], highlighting the preponderant role of this transition metal in the host-pathogen relationship.

1.6. On the central role of iron during bacterial infections

1.6.1. Iron: an ubiquitously sought for nutrient

Iron is central to (nearly) all living organisms from bacteria to mammals because it can balance easily between 2 oxidation states (Fe^{2+} or Fe^{3+}) making it an essential cofactor for many enzymes involved in essential biological process such as DNA synthesis and mitochondrial respiration [213]. Iron (with other trace metals) plays a central role in the host-pathogen relationship as iron is absolutely required for the growth of nearly all pathogens (viral, fungal, bacterial or eukaryotic parasites). The pathogen iron dependency is leveraged by the immune system as a defence mechanism to prevent the growth of pathogens. This mechanism is referred to as nutritional immunity and involves systemic, as well as cellular, rewiring of iron trafficking to limit iron availability to pathogens [214].

1.6.2. Cellular iron handling in physiological and infectious context

At the cellular level, the majority of intracellular iron is found inside heme or iron-sulfur (Fe-S) clusters that act as essential cofactors for the function/activity of a great number of proteins/enzymes [215]. The amount of cytoplasmic "free iron", meaning available for incorporation into iron-containing proteins, is called the "labile iron pool" (LIP) [216], that is rather thought to be constituted of low molecular weight iron complexes (iron-citrate, iron-ATP_2 or GSH-iron complexes) [217,218]. The LIP must be sufficiently large to allow the synthesis of iron containing proteins without inducing iron toxicity. Indeed, the high redox capability of iron is also at the basis of its toxic effects as excess free Fe^{2+} can lead to the formation of the highly toxic ROS $HO^{\cdot}$ (hydroxyl radical) following the Fenton reaction: $Fe^{2+} + H_2O_2 \rightarrow Fe^{3+} + HO^{\cdot} + OH^{-}$ [219]. Dysregulation of iron metabolism leading to important increase in the LIP are associated with different programmed cell deaths (PCD) such as apoptosis or the newly discovered ferroptosis pathway for which the stress-induced release of iron from intracellular stores have been proposed to act as second messengers [219].

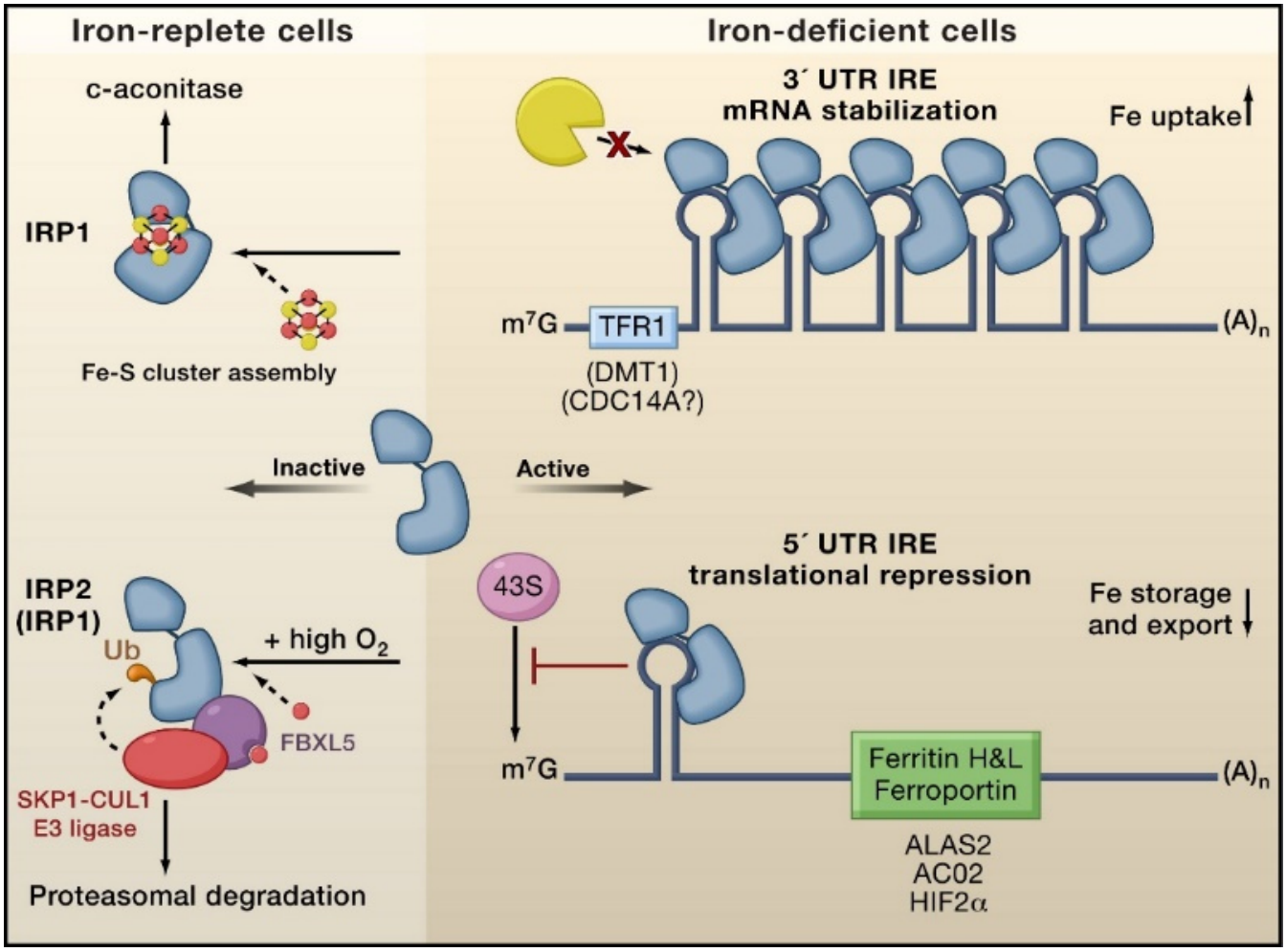

Figure 14: Post-transcriptional regulation of iron homeostasis-related proteins by the IRP system

The IRP system is activated in response to iron deficiency in order to re-establish iron homeostasis. Under sufficient iron concentrations in the cell, IRP1 binds to a 4Fe-4S cluster (holo-IRP1) and possess a cytosolic aconitase activity (ACO1) while IRP2 is degraded by the proteasome after its binding to the iron sensor F-box and leucine-rich repeat protein 5 (FBXL5) which is part of an E3-ubiquitin ligase complex (Muckenthaler et al., 2017). When iron concentrations decrease, IRP1 loses its 4Fe-4S cluster (apo-IRP1) while IRP2 becomes stabilised due to FBXL5 inactivation. Apo-IRP1 has also been reported to be targeted for degradation by FBXL5. Apo-IRP1 or IRP2 then bind conserved hairpin structures called iron responsive elements (IRE) in the 5' or 3' untranslated regions (UTR) of regulated mRNAs. 5' UTR IRE-containing transcripts are LIP-reducing agents such as *ferritin* (storage), *ferroportin* (export), the erythroid-specific isoform of the δ-aminolevulinic acid synthase (*ALAS2*, heme synthesis), mitochondrial aconitase (ACO2, a Fe-S cluster containing enzyme) or *HIF-2α* (erythropoiesis that is very iron consuming). IRP binding on 5'-UTR inhibit cap-dependent translation leading to reduced protein levels. IRP1/2 binding on 5'UTR IRE reduce translation initiation and thus protein levels of iron-depleting transcripts. In contrast, IRP1/2 binding on the 3'UTR IRE in transcripts of iron import proteins such as DMT1 and TfR increase mRNA stability, translating in increased protein levels and thus iron import to recover iron homeostasis. In addition to iron, FBXL5 activity relies on oxygen concentrations and hypoxia induces IRP2 protein levels (Wang et al., 2020). IRP1 can also be activated due to oxidation of its Fe-S cluster by H O or NO. Picture taken from ref 216.

In consequence, the LIP is highly regulated and is the result of a delicate balance between iron import, cellular consumption of iron, iron storage and iron export (**Figure 13**) [216]. The main iron import pathway (albeit not the sole) is the clathrin-mediated endocytosis of plasma holo-transferrin (Fe_2-Tf) after its binding to the transferrin receptor 1 (TfR1) present on the cell's surface. Elemental iron export depends on the expression of the Fe^{2+} transporter SLC40A1 (ferroportin, FPN) [216]. Cytosolic excess of Fe^{2+} from the LIP can also be oxidised to Fe^{3+} and stored inside ferritin in all cell types [220]. Ferritin turnover is mainly mediated by receptor-mediated autophagy dependent on NCOA4 or ,alternatively, by proteasomal degradation [221,222].

Cellular iron trafficking is mainly regulated post-transcriptionally by iron-sensing proteins called iron regulatory protein 1 and 2 (IRP1/2) (**Figure 14**) [216]. When iron concentrations decreases, IRP1/2 bind on specific sequences called iron-responsive elements (IRE) in the transcript of iron related genes leading to the downregulation of LIP-reducing agents such as ferritin (storage) or FPN (export) and the upregulation of LIP-uplifting genes such as *TfR1* and *Dmt1* (encoding for the Fe^{2+} importer divalent metal (Ion) transporter 1 (DMT1))[216]. KO of IRP1 and IRP2 in mice revealed that IRP2 is the major iron regulatory system *in vivo* [223]. In addition, a number of iron related genes are positively regulated at the transcriptional level by HIF-1α such as TfR1 or heme oxygenase 1 (HO-1), an enzyme involved in heme catabolism [224] and more recently the ferritinophagy receptor NCOA4 [225,226] with hypoxia and HIF-1α stabilisation increasing cellular iron levels.

1.6.3. Rewiring of iron trafficking upon bacterial infections

At a basal level, iron concentrations are maintained low in the plasma as iron is always bound to iron scavenging proteins like transferrin and haemoglobin, the latter, being the largest store of iron in the body [227]. Iron withholding is further exacerbated during an infection as inflammation triggers a hypoferrimia that will lower down plasma iron concentrations. Mechanistically, this relies on the downregulation of FPN at the transcriptional, mediated by TLR signaling, and post-transcriptional levels through the liver hormone hepcidin and/or cytokines such as tumor necrosis factor (TNF)-α [214,227].

However, while increasing iron retention inside macrophages limits the growth of extracellular pathogens, it increases iron availability to intracellular pathogens such as *Salmonella* [214] and possibly *Brucella*[228]. Macrophages thus evolved mechanisms to deprive intracellular pathogens of iron by inducing a hyperferrimic response [214] which is associated with IRP1/2 function in macrophages [229]. In macrophages, iron is stored inside ferritin in the cytosol in a biologically inactive form that is, in theory, inaccessible to intra-phagosomal pathogens [213]. However, pathogens can access ferritin-entrapped iron and ferritin even constitute an iron source for *S. typhimurium* inside macrophage as the bacteria secrete iron-chelating molecules called siderophores (see next section), a process inhibited by the IRP1/2-dependent expression of Lipocalin 2 (Lcn2) [229]. IFN-γ signalling also leads to an increase in FPN expression in pro-inflammatory macrophage [214] that is thought to overpass the hepcidin-induced FPN degradation [228,230]. Mechanistically, the production of NO by iNOS/NOS2 in inflammatory macrophages leads to the stabilisation of the transcription factor Nrf2 which promotes the expression of the gene encoding FPN [214]. This mechanism has been shown to be important for the antimicrobial role of NO against *Salmonella* as iron chelation do rescue the decrease in anti-microbial activity in *Nos2*$^{-/-}$macrophages [230]. Iron depletion mediated by an increase in FPN expression has also been observed in RAW264.7 macrophages infected with *B. abortus* which was dependent on Lcn2 expression [231].

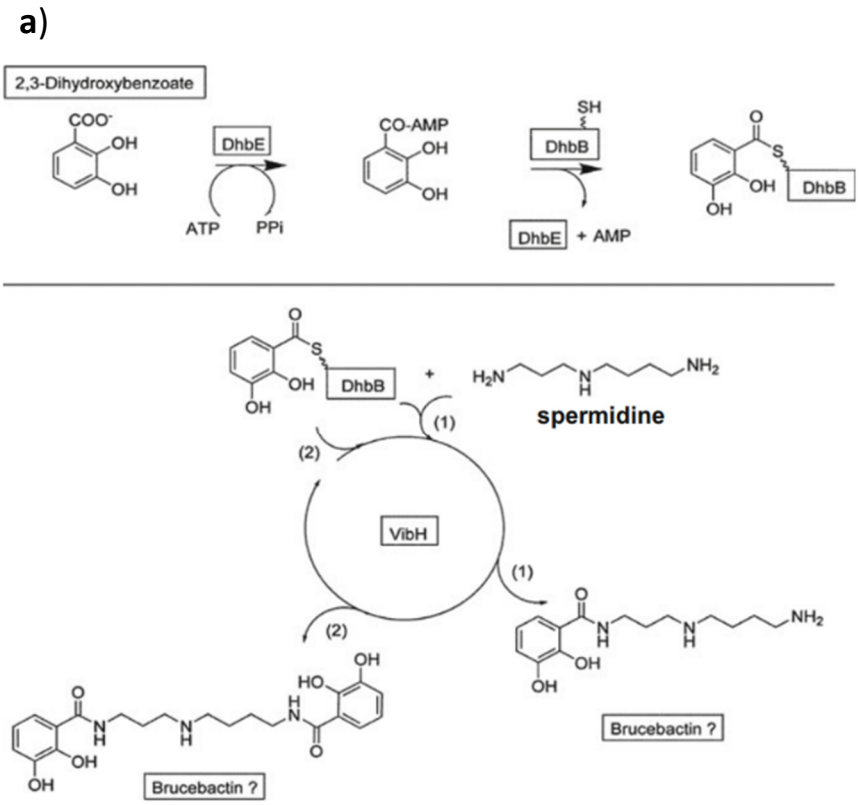

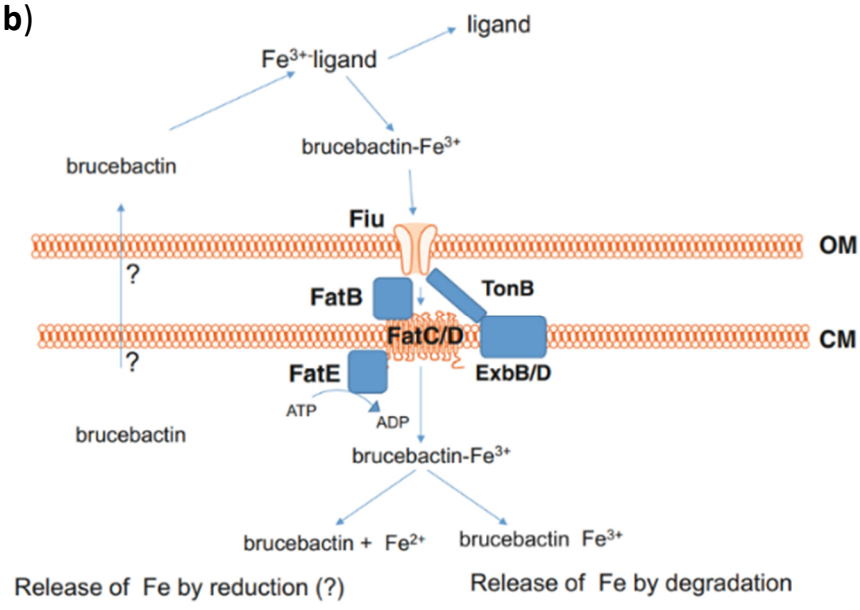

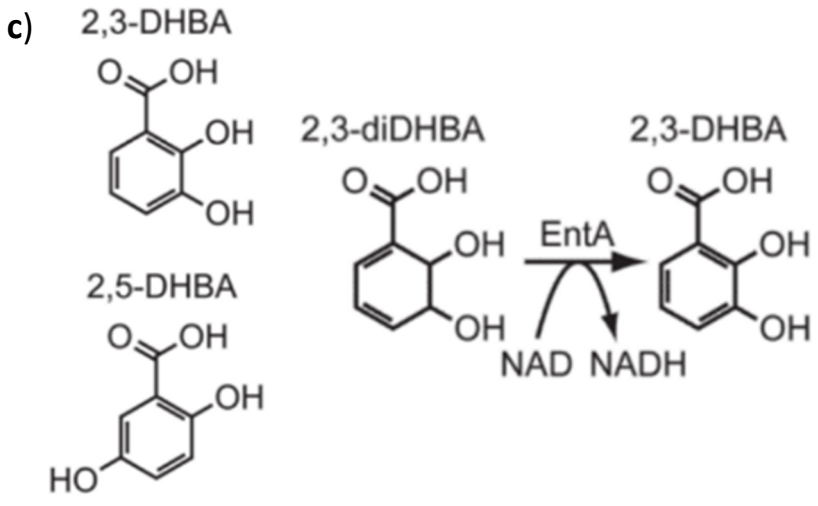

Figure 15: Synthesis and import of the siderophores 2,3-DHBA and brucebactin in *B. abortus*

a) Proposed mechanisms of brucebactin synthesis from 2,3-dihydrobenzoate (2,3-DHBA) which is obtained by condensation of 1 or 2 2,3-DHBA with a non-identified polyamine. This is catalysed by the VibH homolog of *B. abortus*, also called entF. Brucebactin, in contrast to 2,3-DHBA, has a sufficiently high affinity for iron to allow competition with transferrin Picture taken from ref 228.

b) Transport of Fe^{3+}-siderophore complexes across the outer membrane of Gram- bacteria relies on a ExbBD-TonB dependent system. Siderophore transport is energy consuming but, as ATP is not present in the periplasm, the ExbBD-TonB system transfer energy from the inner membrane, most likely proton pumping, to the siderophore transporter/permease located in the outer membrane (Klebba, 2016). The identity of the outer membrane (OM) TonB-dependent permease has not been elucidated to date but current candidates are Fiu and Cir that are responsible for Fe^{3+}-2,3-DHBA and Fe^{3+}-2,3-DHBA-serine complexes import into *E. coli*, respectively. The Fe^{3+}-siderophore complex is then transported through the inner membrane by an ABC-type transporter encoded in the *fatBDCE* operon. Once in the cytoplasm, the Fe^{3+}-siderophore complex releases its bound iron either after reduction of the Fe^{3+} atom and/or through the degradation of the siderophore but the exact mechanism in the case of brucebactin is not known. Picture taken from ref 228.

c) Comparison of bacterial (2,3-DHBA) and mammalian siderophore (2,5-DHBA). In bacteria, 2,3-DHBA synthesis is catalysed by EntA enzyme but it can be functionally replaced by its mammalian homolog BDH2 *in vitro* which is normally involved in 2,5-DHBA synthesis. Picture taken from ref 246.

1.6.4. Bacterial iron acquisition as a virulence determinant

Pathogens evolved in response sophisticated iron import systems that are closely related to the virulence of the pathogen, implying that iron partitioning plays a central role in the outcome of an infection [227]. Some bacteria can circumvent iron withholding by secreting small iron-chelating metabolites called siderophores that, due to their higher binding affinity to iron, can steal iron bound to transferrin [227]. The most-well characterised siderophore is enterobactin, produced by *E. coli* and other enterobacteria, but the use of this siderophore is prevented during the innate immune response by Lcn2 synthetized by activated macrophages and neutrophils [227,232]. Pathogenic enterobacteria produce another siderophore called salmochelin that evades Lcn2 binding due to its hyper-glycosylated state. This succession of innovations shows clearly that iron metabolism constitute a strong selection pressure in the weapon race that oppose host to pathogens (referred to as co-evolution) [227]. Importantly, the expression of the salmochelin biosynthetic locus in a commensal strain of *E. Coli* renders it pathogenic and deadly to infected mice, showing that the subversion of nutritional immunity is central to virulence [233]. Siderophore are nevertheless not the only bacterial iron acquisition systems as direct transport of Fe^{2+}, heme or heme scavenging proteins (e.g. transferrin) are associated with the virulence of numerous bacterial pathogens [227].

In the case of *B. abortus*, a proteomic study performed on infected macrophages 48 h p.i. showed that the bacteria highly remodels its iron-associated proteome with upregulation of the iron-deficiency regulator (Irr) and upregulation of different iron transport systems indicating that *Brucella* face iron starvation inside cells [234]. Three different iron acquisition systems have been identified. First, *B. abortus* 2308 was shown to produce two siderophores when cultured *in vitro* in a low iron environment: the monocatechol 2,3-dihydroxybenzoic acid (2,3-DHBA) and the lastly identified more complex siderophore: brucebactin (**Figure 15**) [228]. A more recent structural study showed that brucebactin is likely to be two 2,3-DHBA linked by a polyamine (such as spermidine) supporting the hypothesis that 2,3-DHBA is a synthetic precursor of brucebactin, which is a more effective siderophore [228]. This is very likely as 2,3-DHBA is also a precursor for many other siderophores in other bacterial species such as enterobactin, vibriobactin or bacillibactin [228]. The role of siderophores in *Brucella* is far from being clear as it is host-dependent. In fact, *B. abortus* strains deficient for brucebactin and 2,3-DHBA biosynthetic genes are "extremely attenuated during infection of pregnant ruminants" but this is not seen upon infection of mice[228]. Supplementation of macrophage cultures with 2,3-DHBA increased the intracellular survival of *B. abortus* [235] but *Brucella* mutant for 2,3-DHBA synthesis or import are still able to replicate similarly to the wild-type (WT) strain inside different epithelial or macrophage cell line [236,237]. One hypothesis to explain this discrepancy has been linked to the catabolism of a four carbon atoms sugar alcohol called erythritol that is present in high concentrations in their natural hosts's trophoblasts. Erythritol catabolism has been shown to be very iron consuming and siderophore-mediated iron acquisition is important to meet this increase in iron demand [237,238].

In addition, *Brucella* do also possess a heme import system and a high-affinity Fe^{2+} transporter that are important for the maintenance of chronic infection in the spleen of mice infected by the intraperitoneal route [239,240].

1.7. On the relationship between iron and the mitochondria in infectious context

1.7.1. Reciprocal dependency between iron metabolism and mitochondrial function

Mitochondria constitute one of the major iron pool inside eukaryotic cells, 20% of total iron in lung carcinoma cells [218]. Mitochondria is, at the same time, centrally involved in Fe-S cluster and heme biosynthesis (see figure 12) and a major consumer of these prosthetic groups[218] that are required for the activity of mitochondrial enzymes from the ETC or the TCA cycle [218]. Accordingly, iron was shown to be essential for proper mitochondrial function[205,241].

1.7.2. Getting iron into the mitochondria: unexpected link with siderophores

The exact source of iron imported into the mitochondria is not really known. First observed in erythroid before epithelial cells, transferrin-bound iron (TBI) can be directly shuttled to the mitochondria without transit by the LIP through direct contact with Tf-containing endosomes [242]. Non-transferrin-bound iron (NTBI) can also access the mitochondria in cardiac cells in a manner insensitive to iron chelators. This indicates that NTBI does not transit by the LIP, supporting a model in which a system of chaperones specifically deliver iron to the mitochondria [243]. Iron transport across the OMM has been proposed to rely on porins [218] but the divalent ion transporter DMT1 has also been localised to OMM and reported to contribute to iron transport [244]. Transport across the IMM relies on mitoferrins (MFR) 1 and 2 which seem to have non-redundant functions as MFR1 but not MFR2 is essential for heme synthesis during reticulocyte development [245].

Interestingly, in mammals, mitochondrial iron loading was shown to be dependent on the synthesis of a mammalian siderophore 2,5-DHBA [246]. 2,5-DHBA is very similar to 2,3-DHBA, a precursor for siderophore synthesis in numerous bacteria such as *E. coli* [246] and, as previously mentioned, also *Brucella* spp. [228]. 2,5-DHBA synthesis relies on the 3-hydroxybutyrate dehydrogenase (Bdh2) enzyme which is homologous to the bacterial EntA [246]. Interestingly, nutritional immunity involves the regulation of 2,5-DHBA availability as Bdh2 is downregulated following stimulation of several TLRs, including TLR4**,** TLR2 and TLR9[247] which are relevant to *Brucella* infection[31,33,248]. The siderophore 2,5-DHBA was shown to promote *E. coli* growth in vitro under iron-deficient conditions and mice deficient for *bdh2* had increased resistance to *E. coli* infection. These observations indicate that the mammalian siderophores 2,5-DHBA could represent a relevant iron source during bacterial infections[247]

1.7.3. Iron deficiency induces mitophagy

Importantly, the treatment of multiple cell lines with an iron chelator, such as DFO or deferiprone (DFP), induces a decrease in respiratory metabolism together with a switch to glycolysis and induction of Parkin-independent mitophagy [249]. Several selective autophagy receptors have already been implicated in iron chelation-induced mitophagy such as NCOA4, FKBP8 and FUNDC1 [131,250,251]. Furthermore, tristetraprolin (TTP), a RNA-binding protein induced under iron deficiency, could also be linked to mitochondrial fragmentation as a result of the downregulation of MFN1 and OPA1 levels [252,253]. Interestingly, siderophores from the pathogenic bacteria *P. aeruginosa* induce the stabilisation of HIF-1α, mitochondrial stress and mitophagy in *C. elegans* [254,255]. Moreover, the BNIP-3L homolog of *C. elegans* was involved in the mitophagy induced by iron deficiency [256] further emphasizing the relevance of these actors.

1.8. Objectives

In this master thesis, the regulation of the stability of the transcriptional regulator HIF-1α and its relation with the mitochondria during *B. abortus* infection of non-myeloid (HeLa) and myeloid (BMDM) was explored.

The main objectives were to:

1) Identify and characterize the different molecular actors that could impair PHD activity in *Brucella*-infected cells based on an *a priori* approach aiming at testing the putative role of PO_2, succinate, mtROS and iron.
2) Determine whether HIF-1α stabilisation is responsible for the expression of the mitophagy receptor BNIP-3L and thus possibly involved in the alterations in mitochondrial morphology observed in *B. abortus*-infected cells.
3) Define the contribution of the bacteria and/or the host in the onset of the perturbation at the origin of the stabilisation of HIF-1α in *B. abortus*-infected cells.

2. Materials and Methods

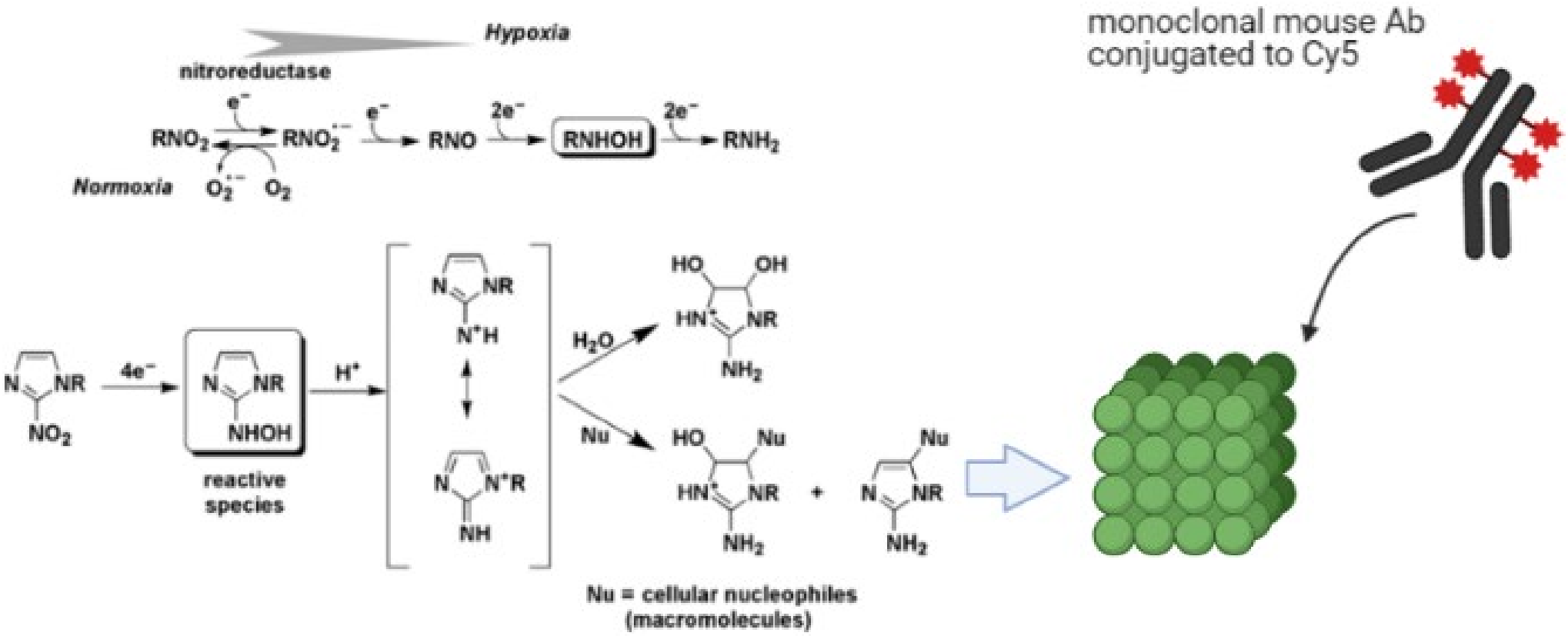

Figure 16: Molecular mechanism of the oxygen-sensitivity of EF-5-like compounds.

EF-5 is first reduced by a group of enzymes called nitroreductases to a reactive nitro radical anion intermediate. Different enzymes have been associated with this step such as NADPH-dependent cytochrome P450 or xanthine oxidase. Under normal oxygen tension conditions, this radical is reoxidised by oxygen in a "futile cycle" yielding a super oxide anion. However, under hypoxia, this radical is stabilised and able to react and oxidise adjacent biomolecules to form covalent bonds. This yield macromolecular adducts that can be recognised by monoclonal antibodies conjugated to the fluorophore Cyanine 5. Picture from ref 266.

2.1. Eukaryotic cell culture

HeLa cells (ATCC: Amercian Tissue Cell Collection), a cancer cell line derived from Henrietta Lacks, a Black woman, affected by cervical cancer who died in 1951[257], were maintained in T75 (75 cm^2) cell culture plates (Corning-Costar) with 15 ml of Minimum Essential Medium (MEM) (MEM-Glutamax, Gibco) supplemented with non-essential amino acids (1 %), 1 mM pyruvate and 10 % Fetal Bovine Serum (FBS) and maintained at 37 °C in a humidified incubator with 5 % CO2. For cell sub-cultures and passages, cells were detached with trypsin + ethylenediaminetetraacetic acid (EDTA) (Gibco) during 5 min and plated at a 1:4 dilution for 2 days or 1:8 for 4 days.

Immortalized bone marrow-derived macrophages (BMDMs, a generous gift from Salcedo S., Laboratory of Molecular Microbiology and Structural Biochemistry, CNRS UMR5086, Université de Lyon, France) were maintained in T25 cell cultures plates (Corning-Costar) in 6 ml Dubbelco's Modified Eagle's Medium (DMEM) with pyruvate and 4.5 g/L glucose (Gibco, 41966-029) supplemented with 10 % FBS (Foetal Bovine Serum) and 10 % conditioned media from L929 fibroblasts to provide macrophage colony-stimulating factor (M-CSF). Cells were maintained at 37 °C in a humidified incubator with 5 % CO2. For cell passages and maintenance of the culture, cells were rinsed once with 5 ml PBS and detached with trypsin + EDTA during 3 min before being plated at a density of 1:20 for 2 days or 1:40 for 3 days.

2.2. Bacterial cell culture

Brucella abortus 544-GFP from frozen stocks were cultured on Tryptic Soy Broth (TSB) (211825, BD Biosciences) agar (214530, BD Biosciences) plates (639102, Greiner bio-one) for 4 days at 37 °C. Then, 2 colonies were transplanted in 10 ml liquid TSB (211825, BD Biosciences) the day before the infection and incubated for 16 h at 37 °C.

2.3. Validation of EF-5 as a probe for hypoxia detection.

HeLa cells were seeded on glass coverslips in 24-well cell culture plates at a density of 15 000 cells/well in 1 ml of the appropriate culture medium. Three days later, cells were incubated with 150 µM (2-(2-Nitro-1H-imidazol-1- yl)-N-(2,2,3,3,3-pentafluoropropyl) acetamide (EF-5, Sigma-Aldrich, EF5014) solubilised in CO2-independent culture medium (Gibco, 18045-054) and subsequently submitted to hypoxia. Hypoxia was triggered by pumping gaseous nitrogen under pressure (0.4 bars) inside a sterilised incubator (99 % ethanol treatment). Oxygen leaks out by an air outlet creating a progressive hypoxia. The "strong" hypoxia condition was obtained by letting oxygen flowing out for a duration of 3 min while the "intermediate" hypoxia condition was obtained after 90 s of air flushes. Then, nitrogen pumping was stopped and cells were incubated in low oxygen for 3 h allowing the formation of EF-5 adducts. Indeed, EF5 selectively binds to hypoxic cells and forms adducts (**Figure 16**)[258]. Cells were then prepared for immunofluorescence and confocal microscopy analysis to visualise EF-5 adducts as detailed in section 2.5. A mouse monoclonal antibody, clone ELK3-51 which is directly conjugated to Cyanine 5 was used to selectively bind the EF5 adducts [258].

Table 3: list of the antibodies (Ab) used in immunofluorescence (IF) and/or flow cytometry.

	Antibody	specie	type	dilution	provider	Catalogue number	Used in Figure n°
Primary Ab	***Anti-HIF-1α***	Rabbit	monoclonal	1:100	Abcam	Ab179483	18b, 20, 21, 22, 23, 24, 26, 31 Suppl. 1, Suppl. 2, Suppl. 3
	Anti-ATPs-β	Mouse	Monoclonal IgG1	1:100	Invitrogen	A-21351	27
	Anti-LC3B	Rabbit	Polyclonal	1:100	Sigma-Aldrich	L7643	27
	Anti-TOM20	Rabbit	Monoclonal	1:200	Abcam	Ab186735	32
	Anti-TOM20	Mouse	Monoclonal	1:100	Abcam	Ab56783	20, 26, 29, 31 Suppl. 2 Suppl. 3
	Anti-BNIP-3L	Rabbit	Monoclonal	1:100	Cell signaling	12396S	28, 29
	Anti-EF5-Cyanine5	Mouse	monoclonal	1:100	Sigma-Aldrich	EF5012	18, Suppl. 1
Secondary Ab	***Anti-rabbit-Alexa 568 nm***	Goat	Polyclonal IgG	1:1000	Invitrogen	A-11011	18b, 20, 21, 22, 24, 26, 27, 28a, 29, 31 Suppl. 1, Suppl. 2, Suppl. 3
	Anti-mouse-Alexa 633 nm	Goat	Polyclonal IgG	1:1000	Invitrogen	A-21050	20, 26, 27, 29, 31 Suppl. 2, Suppl. 3
	Anti-rabbit-Alexa 633 nm	Goat	Polyclonal IgG	1:100	Invitrogen	A102215	23, 28c

2.4. Infection of eukaryotic cells with *B. abortus*

B. abortus 544-GFP liquid culture in logarithmic expansion phase (optical density between 0.4 and 1) were first centrifuged (6000 g, 3 min) and the pellet were rinsed with 10 ml phosphate-buffered saline (PBS: 10 mM phosphate buffer; pH 7.4, 150 mM NaCl) 2 times to removes culture wastes. For the last wash, bacteria are resuspended in 10 ml of the appropriate culture media for HeLa and/or BMDM (see 'Eukaryotic cell culture') before measuring the culture optical density (DO) of a 10 times-diluted sample at 600 nm. From the DO, the bacterial cell number of the liquid culture can be calculated (as a DO of 1 is equivalent to 3 x 109 bacteria/ml). Bacteria were then diluted in culture medium to accommodate the desired multiplicity of infection (MOI) (MOI: 2000 for HeLa cells and 200 for BMDMs) to obtain a suspension called "inoculum". A volume of 500 µl of the inoculum was next added on cells before centrifugating the cells (500 g, 10 min) to synchronize bacterial entry (t=0). Cells were then incubated for 1 h at 37°C to start the infection in an incubator containing a humidified atmosphere with 5% CO2. At the end of the incubation, culture media were refreshed with 500 µl of the appropriate culture media containing a high gentamycin concentration (50 µg/ml) for 1 h in order to kill extracellular, non-infecting, bacteria. The cells were next incubated with 500 µl of culture medium containing a lower concentration of gentamycin (10 µg/ml) for the rest of the experiment to avoid new infection events.

At this step and when indicated in the legends of the figures, cells were also treated with different concentrations of either desferrioxamine mesylate (DFO: 150 µM or 1 mM) (D9533, Sigma-Aldrich), 500 µM iron (II) chloride tetrahydrate (44939, Sigma-Aldrich), iron-poor (apo-) or iron-saturated 2,5-dihydroxybenzoic acid (holo-2,5-DHBA, Sigma-Aldrich, 149357), 10 µM Mito-Tempol (MT-Tpl) or *N*-acetylcysteine (NAC, Sigma-Aldrich, A7250) at 500 or 5000 µM. Alternatively, these molecules were sometimes added to the culture media at 24 h p.i. to limit their potential negative effect on rBCV maturation and/or bacterial replication.

2.5. Immunofluorescence analysis and confocal microscopy observation

2.5.1. Immunostaining of HIF-1α, TOM20 and BNIP-3L in *B. abortus*-infected cells.

HeLa cells or BMDM were seeded on glass coverslips in 24-wells plates at a density of 15 000 cells/well and 10 000 cells/well respectively. About 16 h later, cells were infected with *B. abortus* strain 544-GFP following the protocol described above (see section 2.4). At several times post-infection, cells were rinsed once with 1 ml PBS at room temperature (RT) before fixation with 1 ml of 4% paraformaldehyde (PFA) for 30 min. Cells were then rinsed 3 times with 1 ml of PBS before permeabilisation with 500 µl PBS-1% Triton X-100 for 10 min. Unspecific antibody binding sites were blocked by rinsing the cells 3 times for 10 min with 500 µl of PBS-2% Bovine Albumin Serum (BSA).

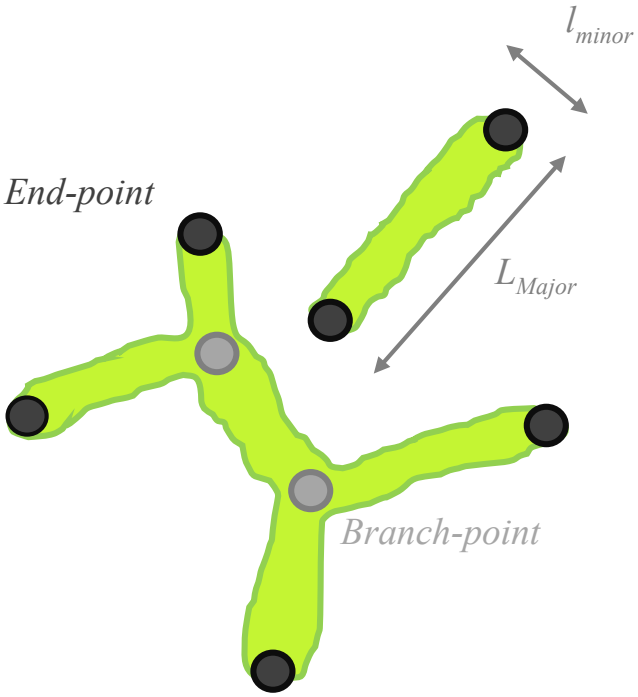

$$Aspect\ Ratio = \frac{L_{Major}}{l_{minor}}$$

$$EP/BP\ Ratio = \frac{\Sigma end\ points}{\Sigma branch\ points}$$

Figure 17: Schematic representations of the quantitative measures of the mitochondrial network morphology i.e. the aspect ratio (AR) and the end-point/branch-point ratio (EP/BP).

To detect HIF-1α, TOM20 or BNIP-3L, cells were incubated with the appropriated primary antibodies (see **Table 3**) in a wet chamber for 2 h at room temperature (RT) (except for the rabbit anti-TOM20 antibody, (see **Figure 32**) for which the incubation was performed overnight at 4 °C). Residual antibodies were rinsed with 500 µl PBS-2% BSA 3 times before incubating the cells with the specie-appropriated secondary antibodies (see **Table 3**) and the Hoechst probe (Abcam, 33258) to stain the nuclei (dilution 1:500) for 1 h at RT (in a wet chamber and protected from light). Excess of secondary antibodies were removed by rinsing the cells 3 times with PBS- 2% BSA and, at the end, excess of salts was removed by rinsing the cells twice with distilled water. Finally, the cells on the coverslips were mounted using Mowiol (Sigma-Aldrich) before observation by confocal microscopy (TCS SP5 II, Leica microsystems).

2.5.2. Co-immunostaining of LC3B and ATP synthase subunit β in *B. abortus*-infected cells.

HeLa cells were seeded on glass coverslips in 24-wells plates (Corning Costar) at a density of 15 000 cells/well. About 16 h later, cells were infected with *B. abortus* strain 544-GFP following the protocol described above (see section 2.4). At several times post-infection, cells were rinsed once with 1 ml PBS at room temperature (RT) before fixation with ice-cold methanol (Merck, Germany) for 15 min at 4 °C. Cells were then rinsed 3 times with 1 ml of PBS. Then, without permeabilisation step, unspecific antibody binding sites were blocked by rinsing the cells 3 times for 10 min with 500 µl of PBS-2% Bovine Albumin Serum (BSA).

To detect LC3B and ATP synthase subunit β (ATPs-β), cells were incubated with the appropriate primary antibodies (see Table 3) in a wet chamber for 2 h at room temperature (RT). Residual antibodies were rinsed with 500 µl PBS-2% BSA 3 times before incubating the cells with the specie-appropriated secondary antibodies (see Table 3) and the Hoechst probe (Abcam, 33258) to stain the nuclei (dilution 1:500) for 1 h at RT (in a wet chamber and protected from light). Excess of secondary antibodies were removed by rinsing the cells 3 times with PBS- 2% BSA and, at the end, excess of salts was removed by rinsing the cells twice with distilled water. Finally, the cells on the coverslips were mounted using Mowiol (Sigma-Aldrich) before observation by confocal microscopy (TCS SP5 II, Leica microsystems).

2.5.3. Quantitative analysis of confocal micrographs

Quantitative analysis of the mitochondrial network morphology, assessed by the aspect ratio and the end-point on branch point of the mitochondrial fragments (**Figure 17**) in single cells sections, was performed as described by De Vos and Sheetz[259] using the ImageJ 64 software. The mean AR and EP/BP was calculated for each cell and considered as 1 biological replicate for statistical analysis (except for figure 9 where the mean values for 1 experiment were considered as a biological replicate). The analysis of the number of colocalisation events between LC3B and ATPs-β were also performed on ImageJ 64 software by defining a threshold dissociating LC3 puncta from diffuse signal in single cell sections. The ATPs-β signal corresponding to the mitochondrial network was also separated from background noise using the threshold option. The number of colocalisation events for each cell were monitored by creating an overlay between both processed micrographs (Process > Image Calculator option "AND"). This value was considered as 1 biological replicate for statistical analysis. The number of cell analysed is specified in the figure legends.

2.6. Imaging of mitochondrial ROS production with Mito-SOX in *B. abortus* infected cells

HeLa cells were seeded in 24-well cell culture SensoplateTM with glas-bottomed wells suitable for live microscopy (Greiner bio-one, 662892) at a density of 15000 cells/well and were infected according to the classical protocol described above for *B. abortus* strain 544-GFP (see section 2.4.). When indicated, cells were incubated with 10 µM of Mito-Tempol (Abcam, ab144644) added at 2 or 24 h p.i. At 48 h p.i., cells were incubated at 37 °C for 30 min with 0.5 µM Mito-SOX in an incubator containing a humidified atmosphere with 5 % CO2. Cells were then rinsed to remove the probe and were observed using a reverse microscope (ECLIPSE Ti2, Nikon).

2.7. Flow cytometry analysis of the abundance of HIF-1α and BNIP-3L in *B. abortus* infected cells

HeLa cells were seeded in 6-well cell culture plates (Corning Costar) at a density of 10^5 cells/well in 2 ml of the appropriate medium. For the different controls, some cells were used to assess the autofluorescence, some cells were infected but not immunostained (to assess the effect of GFP expressed by the Brucella strain) and some cells were non-infected but immuno-stained with the fluorophore-conjugated secondary antibody alone (to assess the background fluorescence of the fluorophore). The next day, cells were infected with *B. abortus* strain 544-GFP following the already described protocol (see section 2.4.) with the only difference that the volume of medium added at each step was 1.5 ml instead of 500 µl. At the appropriate time point p.i., cells were rinsed with 1 ml with PBS (RT) before being detached for few min with 160 µl of trypsin-EDTA at 37 °C. Trypsin was inactivated with 3 ml ice-cold PBS and cell suspensions were transferred into 15 ml Centrifuge Tubes (Corning, 430791) for centrifugation (5 min, 500 g, 4 °C). Cells were then rinsed twice by a resuspension in 500 µl ice-cold fluorescence-activated cell sorting (FACS) buffer (0.5 % BSA and 2 mM EDTA diluted in PBS). After the second centrifugation, cells were resuspended in 200 µl eBioscienceTM IC Fixation Buffer (Invitrogen, 00-8222-49) and incubated at RT for 30 min. At this point, all further manipulations were done at RT. Next, the IC Fixation Buffer was removed by centrifugation (5 min, 500 g) and cells were resuspended in 200 µl of 10 times diluted eBioscienceTM Permeabilisation Buffer (10X) (Invitrogen, 00-8333-56). Samples can then be left at 4°C until the next day.

After removal of Permeabilisation Buffer by centrifugation, cells are incubated (1h at RT in the dark) with 100 µl of the appropriated primary antibody (see Table 3) diluted 100 times in Permeabilisation Buffer. Then, the primary antibody is removed by centrifugation and cells are washed once with Permeabilisation Buffer (resuspension + centrifugation). Except for EF-5 immunostaining, cells were incubated (30 min, RT in the dark) with 100 µl the specie-appropriated secondary antibodies coupled to Alexa-633 nm diluted 100 times in Permeabilisation Buffer. Cells are then washed once in Permeabilisation Buffer (centrifugation, remove supernatant, resuspension and centrifugation) before resuspension of cells with 500 µl FACS buffer. Samples can be stored at 4°C in the dark for a couple of days. Samples are then transferred into FACS glass tubes before analysis by flow cytometry (BD FACSVerse^{TM}). The engine is first calibrated with technical control samples (that measure autofluorescence, background fluorescence of secondary antibody and GFP-fluorescence for *B. abortus*-infected samples) whose fluorescence intensity is subtracted to the fluorescence intensity of experimental conditions.

2.8. Determination of viable intracellular bacteria by the colony-forming unit (CFU) assay

Cells were seeded in 24-well cell culture plates at a density of 15000 cells/well and were infected with *B. abortus* strain 544-GFP according the protocol described above (see section 2.4.). After 2 hours of infection, dedicated wells were treated with 500 µM iron. After 2 h of infection, appropriated infected cells were incubated with 500 µM iron. At the appropriate time post-infection (6, 24 or 48 h), cells were rinsed once with 1 ml PBS before being lysed for 10 min in 500 µl ml of PBS-0.1 % Triton X-100. This is followed by mechanical lysis through scratching and flushing the cells with 1000 µl tips. Twenty µl of each sample was then diluted by serial dilutions in 180 µl PBS before plating on TSB-agar bacteria culture plates (639102, Greiner bio-one). Three different dilutions were plated for each time-point. In the case of HeLa cells, at 6 h p.i. time point the non-diluted, 10 and 100 times diluted samples; at 24 h p.i. time point the 10, 100 and 1000 times diluted samples and for the 48 h p.i time point are plated the 100, 1000 and 10000 dilution of the samples. In the case of BMDM, due to the better infection efficiency, the plated samples were 10 times more diluted in comparison to the corresponding dilution for HeLa cells for each time point. Plates are then placed in an incubator at 37 °C for 4 days before counting of the colonies. Knowing the volume of lysate plated (20 µl) and the number of dilutions, the number of CFU/ml can be calculated for each dilution. The mean number of CFU/ml across the dilutions from the same technical replicate is then calculated and transformed into logarithmic (log_{10}) scale. The plotted values were the mean CFU/ml between triplicates.

2.9. Effect of 2,5-DHBA treatment on mitochondrial iron by live imaging with Ferro-Orange

HeLa cells were seeded in 8-wells LabTek™ chambered coverglass (Thermo Scientific Nunc™, 155411) at a density of 2000 cell/well. After 24 h, DFO at 150 µM was added in the culture medium to the cells in order to deplete the basal levels of intracellular iron. The next day, 500 µM of either Fe (500 µM), 2,5-DHBA (apo-DHBA, at 150 µM or 500 µM) or iron-saturated 2,5-DHBA (holo-DHBA, 500 µM) which is obtained after a 1h incubation of apo-DHBA with iron in a 1:1 concentration ratio, were added or not (control cells) to the culture media for 24 h. Cells were next rinsed once with serum free culture medium and then incubated for 30 min in an incubator (37 °C, 5 % CO_2) with 1 µM Ferro-Orange (DOJINDO Laboratories, F374) and 100 nM of Mito-Tracker™ Green FM (Invitrogen, M7514) solubilised in serum-free culture medium. After 1 wash with serum-free culture medium to remove the excess amount of probe, loaded cells were subsequently observed by confocal microscopy (LSM 980 Airyscan 2 microscope (Zeiss)). Transept analysis were done on Image J software and the resulting data were plotted on Prism 9 GraphPad (San Diego, USA).

2.10. Statistical analyses

The quantitative data and results were expressed as means ± 1 standard deviation (SD), unless otherwise stated. Data were tested for normality distribution (Shapiro-Wilk and Kolmogorov-Smirnov tests) and homogeneity of variance (homoscedasticity) using Spearman's test. If both conditions were present, the means between more than two conditions were compared by two-way ANOVA analysis followed by Bonferroni's post-hoc tests. When data followed a normal distribution but did not filled the homoscedasticity condition, conditions were compared with unpaired t-tests with Welch's correction for heteroscedasticity. When both conditions were absent, comparison was performed by rank sum testing (Mann-Whitney's tests). Comparisons between proportions/percentages was performed using 1 by 1 z tests. A p-value < 0.05 was considered as statistically significant. All calculations and graphs were realised on Prism Graphpad 9 software (San Diego, USA) except for z-tests that were performed on SigmaPlot 12.5 (Systat Software, Chicago, IL, USA).

3. Results

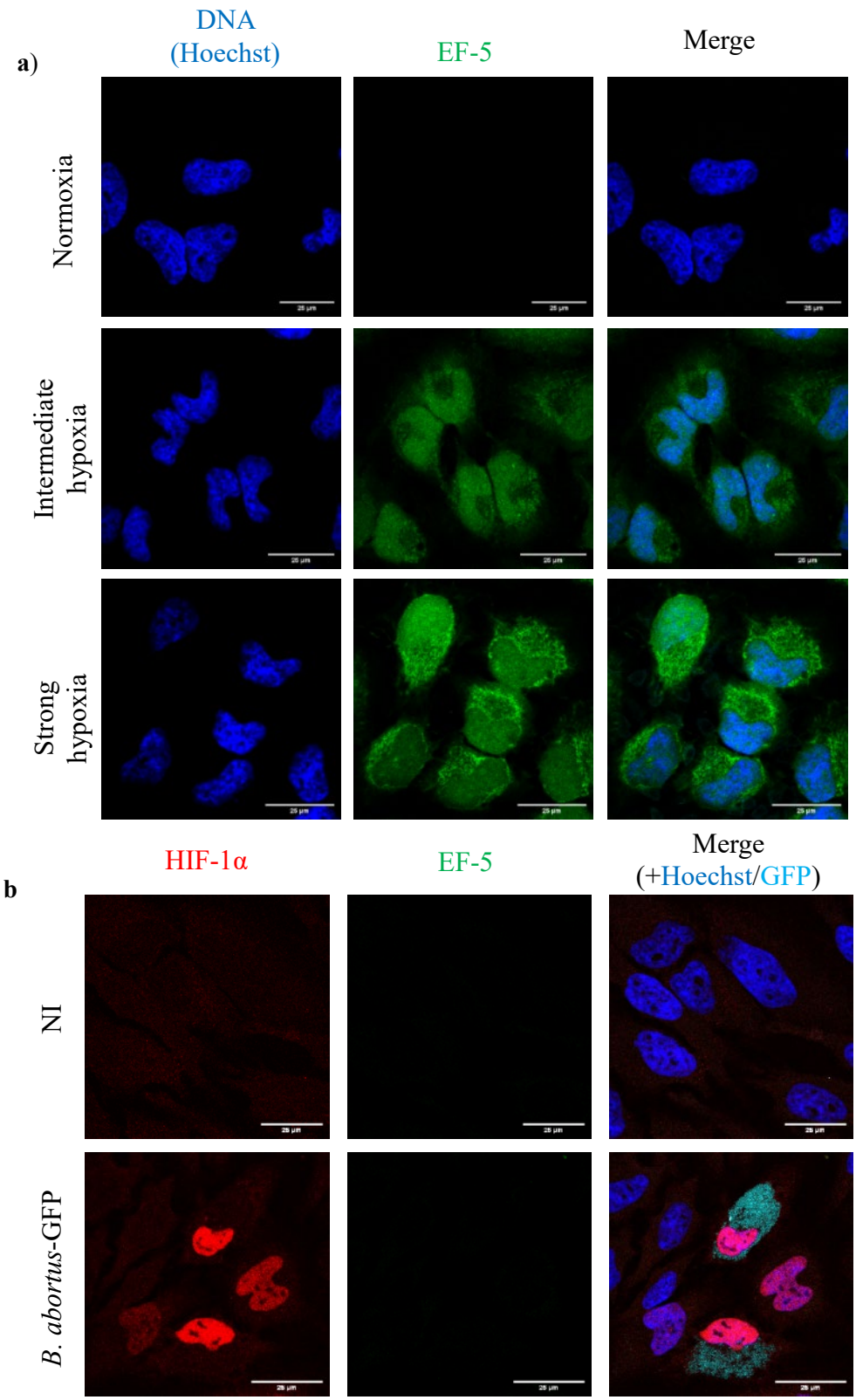

Figure 18: **Detection of hypoxia microenvironments in *B. abortus*-infected HeLa cells with the EF5 probe.**

a) Immunostaining of EF5 in HeLa cells after 3 h of incubation with 100 µM of EF5 while being under hypoxic (strong or intermediate) or normoxic conditions. After cell fixation and permeabilisation, EF5 adducts were immunolabelled with a monoclonal antibody conjugated with the fluorophore cyanin 5 before observation by confocal microscopy (scale bars = 25 µm).

b) Co-immunostaining of EF-5 and HIF-1α in fixed and permeabilised HeLa cells infected or not (non-infected controls, NI) with *B. abortus*-GFP for 48 h and observed by confocal microscopy. During the last 3 h, cells were incubated with 100 µM EF-5 in normoxic conditions to allow adduct formation. Micrographs are representative of n = 4 independent experiments (scale bars = 25 µm).

3.1. Testing the putative involvement of different molecular actors in *B. abortus*-induced HIF-1α stabilisation

3.1.1. Effect of *B. abortus* on oxygen partial pressure in infected-cells

Brucella spp. are aerobic bacteria, meaning that they use oxygen as terminal acceptor of their electrons transport chain[260]. Even if *Brucella* species are classified as obligate aerobes, they can nevertheless survive and grow in oxygen-limited environment such as liver granulomas or macrophage phagosomes[261,262]. This ability relies on the expression of respiratory complexes with high affinity for oxygen[261] which were associated with optimal replication inside cultured macrophages (THP-1)[263]. These considerations, in addition to the remarkably high number of intracellular bacteria found at late stages of *in vitro* infection[15] prompted us to hypothesise that *B. abortus* oxygen consumption might induce a subcellular hypoxia leading to HIF-1α stabilisation.

Intracellular oxygen concentration was monitored with the hypoxia probe EF5[258], a compound analogue to pimonidazole that was already used to detect hypoxic conditions induced by other bacterial pathogens such as *S. aureus* and *Bartonella henselae*[264,265]. The immune-detection of EF-5 macromolecular adducts is in inverse correlation with oxygen tensions allowing the detection of hypoxic micro-environments[266]. We first confirmed the ability of EF-5 to stain HeLa cells exposed to hypoxic conditions (**Figure 18.a**). A strong immunostaining was observed in response to a severe hypoxia and the intensity of the fluorescent signal was lower for intermediate/mid hypoxia, suggesting that the probes is a useful tool to detect intracellular hypoxic conditions. However, hardly any EF-5 immunostaining could be detected in *B. abortus*-infected HeLa cells at 48 h post-infection (p.i.) which did not differ from the signal found in non-infected (NI) control cells (**Figure 18.b**) or any of the other time point studied (Supplementary Figure 1). In these conditions, a strong fluorescent signal was observed for the immunostaining of HIF-1α in the nucleus of *Brucella*-infected cells. While we cannot completely exclude that the level of hypoxia might not be detected in *B. abortus*-infected cells as the fluorescent probe might not be sensitive enough, it is unlikely that hypoxia is the main driver *B. abortus*-induced HIF-1α stabilisation and nuclear accumulation in these experimental conditions. We thus next explore oxygen-independent mechanisms to try to explain the HIF-1α stabilisation observed in bacteria-infected cells.

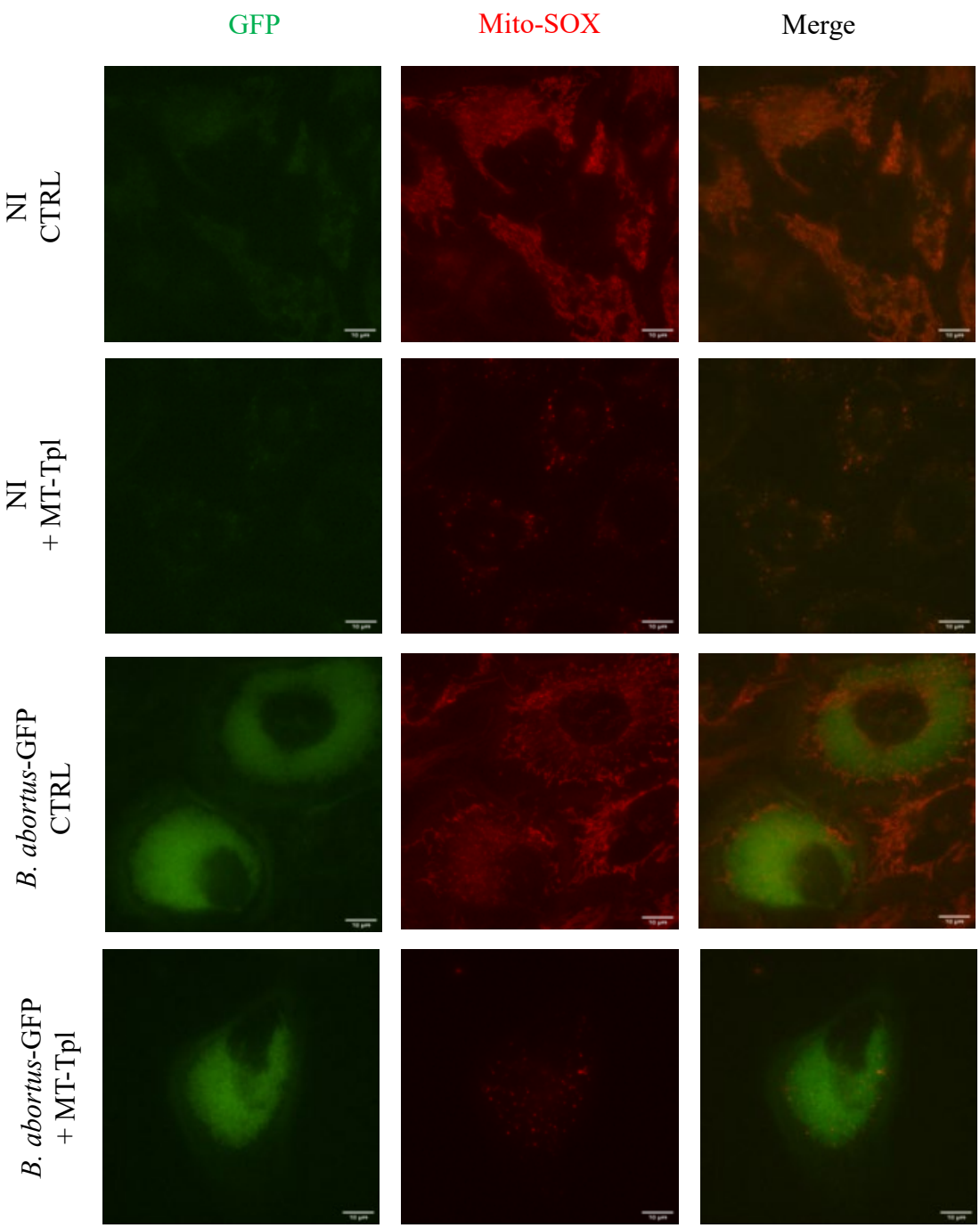

Figure 19: Effect of *B. abortus* infection and Mito-TEMPOL treatment on mitochondrial superoxide anion production.

Mitochondrial ROS detection in *B. abortus*-GFP-infected or not (non-infected, NI) HeLa cells at 48 h post-infection visualised in cells loaded with the Mito-SOX probe (0.5 µM) for 30 min. When applicable, cells were treated with 10 µM Mito-TEMPOL (MT-Tpl) or not (controls, CTRL) at 24 h post infection. Micrographs were taken using a reverse microscope (ECLIPSE Ti2, Nikon) (scale bars = 10 µm).

3.1.2. Involvement of reactive oxygen species in *B. abortus*-induced HIF-1α stabilisation and mitochondrial fragmentation.

Recently, much attention was drawn on HIF-1α stabilisation in the context of immuno-metabolism because it supports the inflammatory and anti-bacterial functions of macrophages[194,267]. Indeed, MyD88 activation following stimulation of some TLR, such as 2, 4 or 9, leads to HIF-1α stabilisation in an oxygen-independent manner[193,199]. Mechanistic studies reported the accumulation of succinate inside activated M1 murine macrophages as responsible for LPS-induced HIF-1α stabilisation[196]. Our attempts to pharmacologically modulate subcellular succinate concentrations were not conclusive (data not shown).

However, HIF-1α stabilisation mediated by LPS-induced succinate accumulation depends on mitochondrial ROS that, most likely, directly inhibits the PHDs[84]. This mechanism has been implicated in *B. abortus*-induced HIF-1α stabilisation in primary mouse macrophages in response to the stimulation of the innate immune receptor STING[203]. To test the putative involvement of mtROS in our model, mitochondrial superoxide anions production was detected using the Mito-SOX probe that becomes fluorescent upon oxidation[203,268]. Importantly, the fluorescence intensity of the Mito-SOX probe was similar between NI and *B. abortus*-infected HeLa cells at 48h p.i. (**Figure 19**). As we could not exclude the involvement of an acute production of mtROS before 48h p.i. in *B. abortus*-induced HIF-1α stabilisation, *B. abortus*-infected HeLa cells were treated with the mitochondria specific anti-oxidant Mito-TEMPOL[269]. Mito-TEMPOL is an analogue of Mito-TEMPO which was reported to totally abrogates STING-induced HIF-1α stabilisation during *B. abortus* infection[203]. We first confirmed the ability of 10 µM of Mito-TEMPOL to abrogate super oxide anion production (as assessed through Mito-SOX staining) for at least 24 h (**Figure 19**).

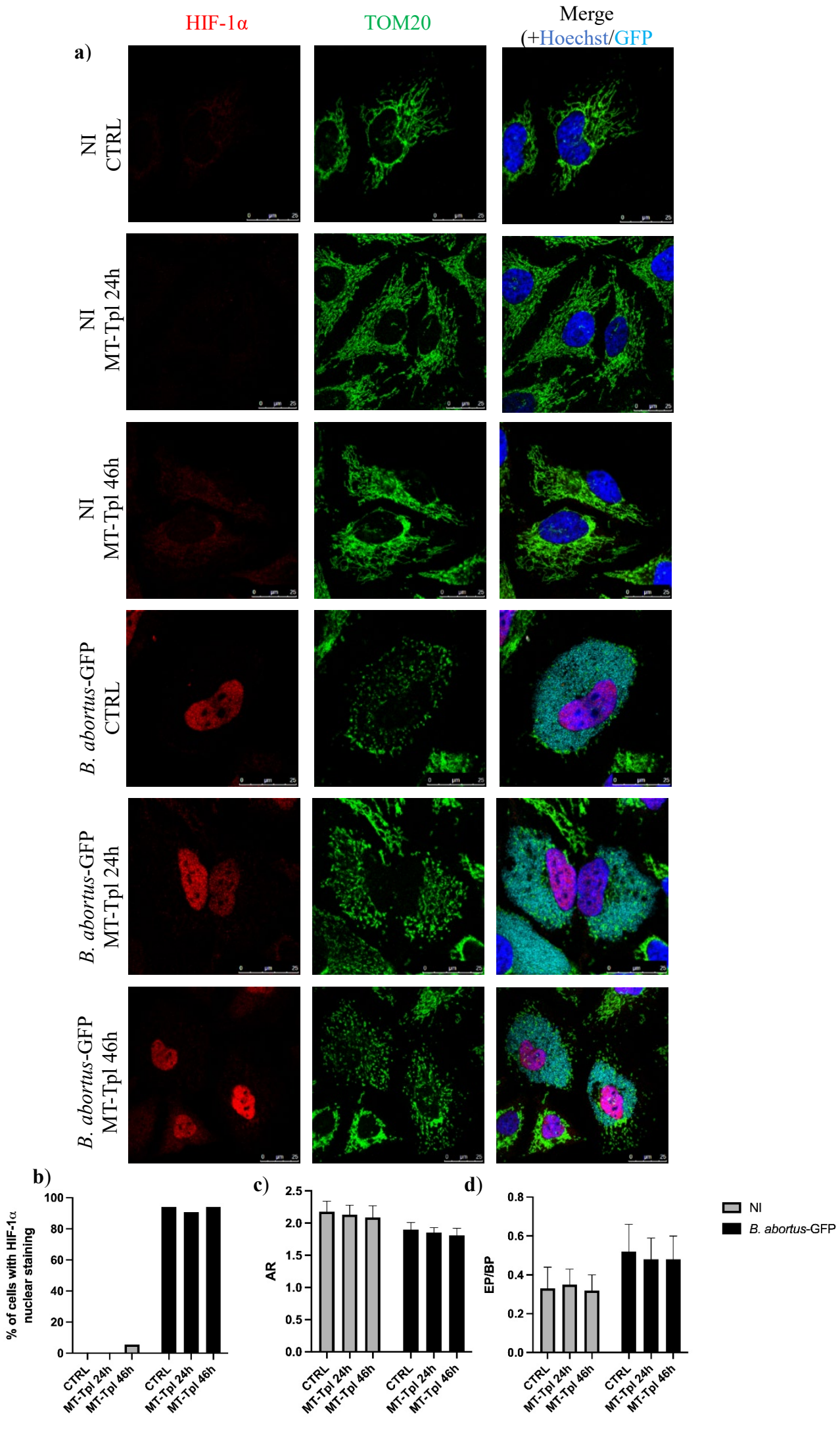
HIF-1α
TOM20
Merge
(+Hoechst/GFP
a)
NI
CTRL
NI
MT-Tpl 24h
NI
MT-Tpl 46h
B. abortus-GFP
CTRL
B. abortus-GFP
MT-Tpl 24h
B. abortus-GFP
MT-Tpl 46h
b)
% of cells with HIF-1α
nuclear staining
100
80
60
40
20
0
CTRL
MT-Tpl 24h
MT-Tpl 46h
CTRL
MT-Tpl 24h
MT-Tpl 46h
c)
AR
2.5
2.0
1.5
1.0
0.5
0.0
CTRL
MT-Tpl 24h
MT-Tpl 46h
CTRL
MT-Tpl 24h
MT-Tpl 46h
d)
EP/BP
0.8
0.6
0.4
0.2
0.0
CTRL
MT-Tpl 24h
MT-Tpl 46h
CTRL
MT-Tpl 24h
MT-Tpl 46h
NI
B. abortus-GFP

Figure 20: Effect of Mito-TEMPOL treatment on *B. abortus*-induced HIF-1α stabilisation and mitochondrial fragmentation.

a) HIF-1α and TOM20 co-immunostaining of HeLa cells infected or not (non-infected controls, NI) with *B. abortus*-GFP and treated or not (controls, CTRL) with 10 µM Mito-TEMPOL (MT-Tpl) at either 2 h or 24 h p.i. (representative of 2 independent experiments, scale bars = 25 µm). HIF-1α stabilisation was quantified in **b**) as the % of non-infected (NI in grey) or infected (in dark) cells that presented a nuclear HIF-1α staining (an average of 15 cell analysed/conditions from the first experiment). The aspect ratio (AR) (**c**) and the end point on branch point ratio (EP/BP) (**d**), metrics of the length and connectivity of mitochondrial fragments, respectively, are represented as the mean ± 1 SD calculated on 15 cells/condition from the data of the first experiment.

Strikingly, the incubation of *B. abortus*-infected HeLa cells with Mito-TEMPOL at either 2h or 24h post-infection does not reduce the percentage of infected cells that display a nuclear localisation of HIF-1α (**Figure 20.a** and **20.b**). In addition, the presence of the mitochondrial antioxidant does not reduce the fragmentation of the mitochondrial network as assessed by the quantification of the aspect ratio (AR) and the end-point on branch-point ratio (EP/BP) (**Figure 20a**, **20.c** and **20.d**).

However, while mtROS do not seem to be implicated in *B. abortus* infection, results in agreement with previous results from our group[178], this does not exclude the involvement of ROS. Indeed, ROS derived from other sources, such as NOX-derived ROS, were already implicated in *B. abortus* infection of HeLa and primary mouse macrophages[108]. NOX-derived ROS were also involved in HIF-1α stabilisation following stimulation of several TLRs that can be prevented by the addition of the broad spectrum anti-oxidant *N*-acetylcysteine (NAC)[201,270,271]. However, the presence of 5 mM of NAC, a concentration showed to be sufficient to prevent NOX-induced HIF-1α stabilisation in other models[201,270] and to promote survival of *B. abortus* in RAW264.7 macrophages-like cells[272], did also not reduce *B. abortus*-induced HIF-1α nuclear localisation nor mitochondrial fragmentation (Supplementary Figure 2). Together, these results does not support an involvement of host-induced ROS production in the stabilisation of HIF-1α during *B. abortus* infection of HeLa cells and drove us to explore the putative role of iron, another central molecular actor in the regulation of PHD[198] and in the host-pathogen relationship[213].

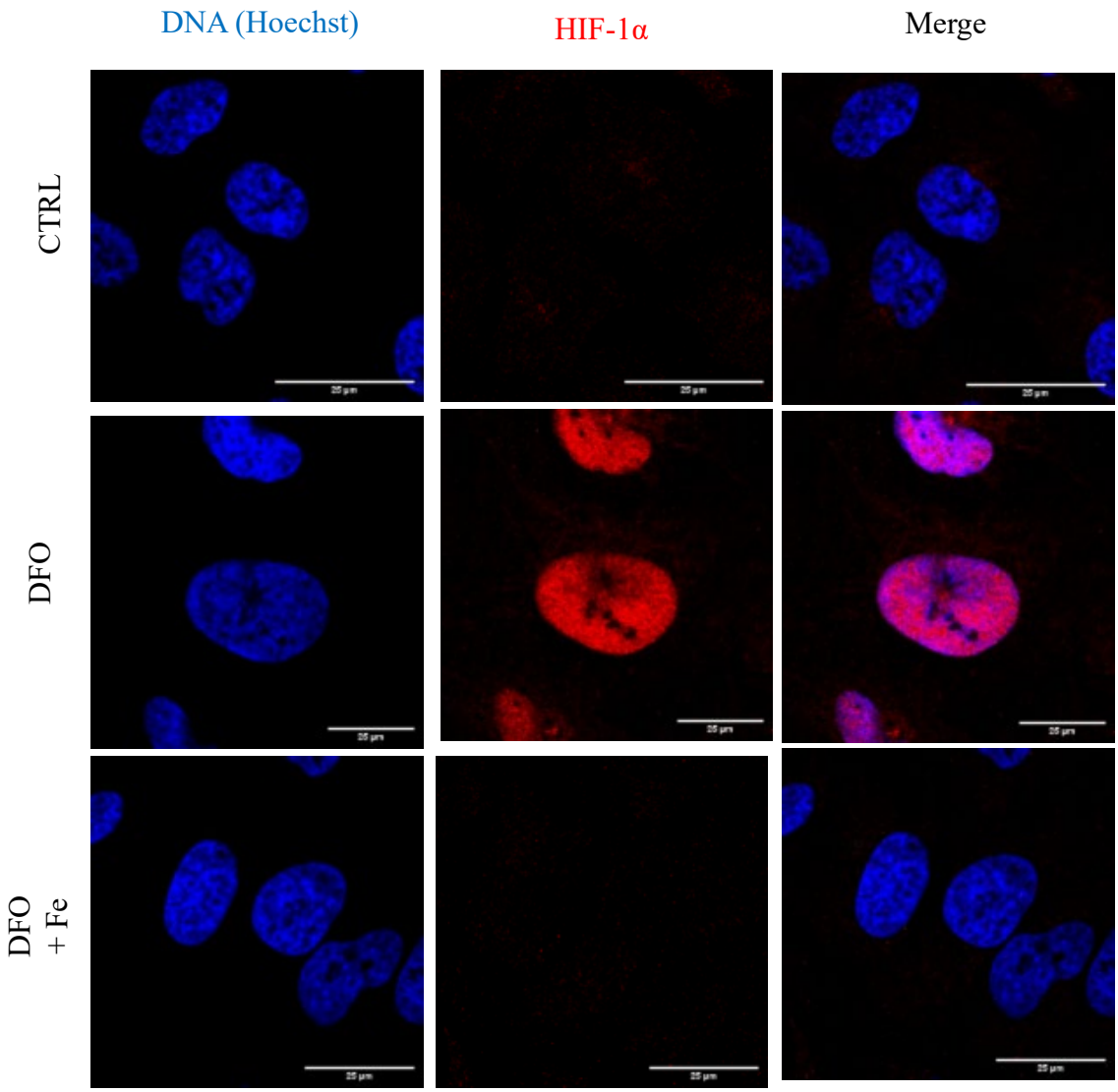

Figure 21: **Effect of the treatment with an iron chelator (DFO) on HIF-1α abundance and localisation in HeLa cells.**

Immunostaining of HIF-1α in non-infected HeLa cells 46 h after an incubation or not (CTRL: control cells) with either 150 µM desferrioxamine (DFO) alone or DFO combined with 500 µM iron chloride tetrahydrate (Fe) (scale bars = 25 µm).

3.1.3. Effect of iron supplementation on *B. abortus*-induced HIF-1α stabilisation.

Iron is an essential micronutrient required for the growth of bacterial pathogens[227], including *Brucella* species[228]. In response to the iron dependency of pathogens, the host evolved mechanisms dedicated to starve pathogens from iron (i.e. nutritional immunity). Against intracellular pathogens, these mechanisms involve an increase in iron storage and in iron export mediated by the upregulation of ferritin and ferroportin, respectively, leading to reduced intracellular iron levels[213]. It is known that host-mediated reduction of intracellular iron concentrations are responsible for HIF-1α stabilisation in LPS-treated DC[206]. Intracellular iron depletion was also observed upon *B. abortus* infection of RAW 264.7 macrophage-like cells due to an increase in the expression of the gene encoding ferroportin[231]. Additionally, high affinity bacterial iron import mechanisms are expressed during infection promoting bacterial proliferation and virulence[227]. This includes the production of iron-chelating metabolites called siderophores which are responsible for HIF-1α stabilisation during intracellular infection by enterobacteria[211,273]. *B. abortus* was also reported to secrete such iron scavenging molecule[228].

Importantly, we confirmed that the treatment of HeLa cells with the iron chelator desferrioxamine (DFO, a siderophore secreted by the bacterium *Streptomyces pilosum*) is able to induce a strong HIF-1α stabilisation and nuclear localisation in an iron-dependent manner (**Figure 21**), emphasizing the essential contribution of iron in HIF-1α regulation. We therefore hypothesized that the massive intracellular replication of *B. abortus*, associated with a putative induction of nutritional immunity mechanisms, could drastically decrease intracellular iron concentrations leading to an impairment of PHD catalytic activity and subsequent HIF-1α stabilisation.

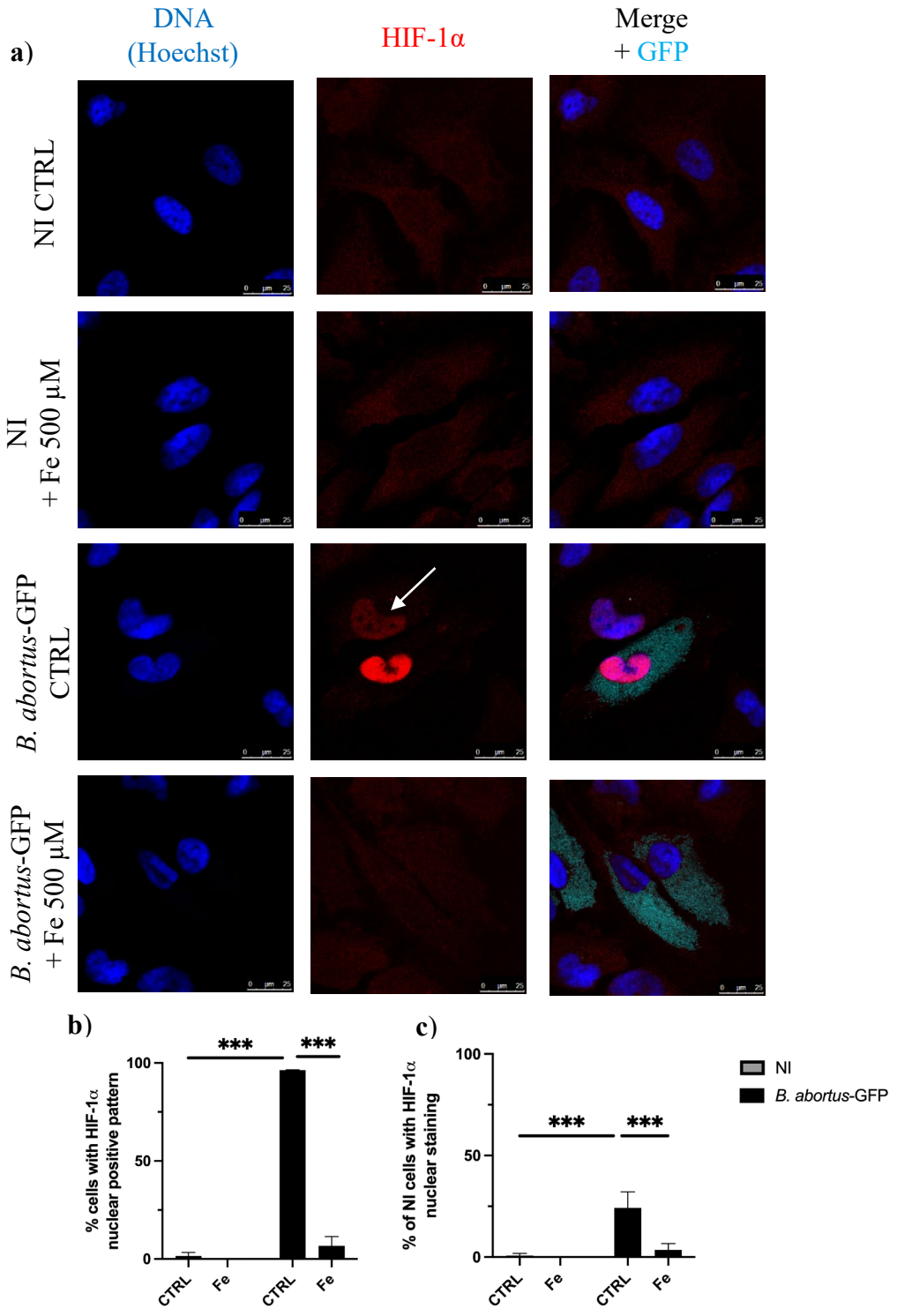

Figure 22: Effect of iron supplementation on *B. abortus*-induced HIF-1α nuclear localisation in HeLa cells.

a) Immunostaining of HIF-1α in HeLa cells 48h after infection or not (non-infected controls, NI) with *B. abortus*-544-GFP (representative of n=5 independent experiments). When indicated, 500 µM Fe was added to the culture medium 2 h post-infection or not (controls, CTRL). The percentages (%) of infected (or NI) cells that display a staining for HIF-1α in the nucleus is shown in **b**. Results are expressed as the means ± 1 SD for n = 4 independent experiments with an average of 30 cells analysed/experiment for each condition. To quantify the extent of HIF-1α stabilisation in non-infected (NI) cells adjacent to *B.* abortus-infected cells (an example is indicated by the white arrow), the percentages of non-infected (NI) presenting a nuclear staining of HIF-1α in each condition were determined and are shown in **c**. Results are expressed as means ± 1 SD for n = 3 independent experiments with an average of 35 cells analysed/experiment for each condition. Statistical analysis: the frequencies of HIF-1α nuclear localisation events from the same conditions were added together for the different experiments (n= 120 cells for each condition in **c** and n = 105 in **d**). The associated proportions of HIF-1α positive cells for each condition were subsequently tested by z-tests (***: $p < 0.001$), (scale bars = 25 µm).

In order to test this hypothesis, *B. abortus*-infected HeLa cells were supplemented with iron choride tetrahydrate (Fe). Strikingly, Fe supplementation drastically prevents *B. abortus*-induced nuclear localisation of HIF-1α (**Figure 22.a** and **22.b**). Interestingly, about 20 % of non-infected (NI) cells present in close proximity to infected cells do also present a nuclear HIF-1α, albeit weaker in intensity than what is seen in *B. abortus*-infected cells (see white arrow on **Figure 22.a**). The percentages of NI cells in the close vicinity of *B. abortus*-infected cells presenting a nuclear localisation of HIF-1α is also strongly decreased upon Fe supplementation (**Figure 22.c**) suggesting that the mechanism at the origin of HIF-1α stabilisation is similar in both cases. Furthermore, flow cytometry analysis of *B. abortus*-infected HeLa cells exposed to Fe supplementation confirmed, in a more quantitative manner, the inhibitory effect of iron on *B. abortus*-mediated HIF-1α stabilisation (**Figure 23**).

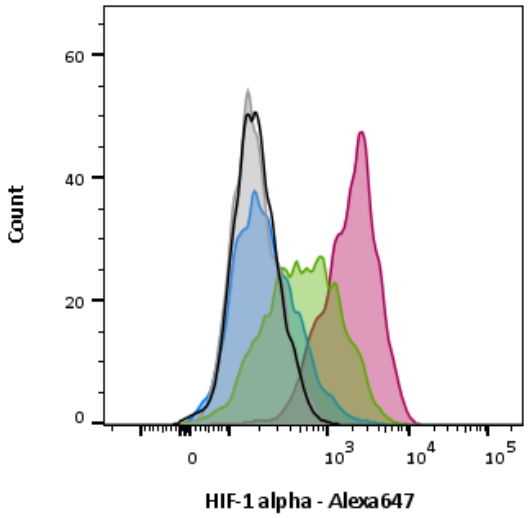

	Sample Name	Subset Name	Count	Median : Alexa 647-A
☐	HIF1a_48h_ctrl.fcs	DownsampleDP	1745	180
☐	HIF1a_48h_Fer.fcs	DownsampleDP	1745	174
☐	HIF1a_48h_544GFP.fcs	DownsampleDP	1745	535
☐	HIF1a_48h_544GFP+Fer.fcs	GFP-positive	1745	213
☐	HIF1a_48h_DFO.fcs	DownsampleDP	1745	1977

Figure 23: **Effect of iron supplementation on *B. abortus*-induced increase in HIF-1α abundance in HeLa cells.**

Quantification of HIF-1α abundance by flow cytometry in HeLa cells (representative of n = 2 independent experiments) infected or not with *B. abortus*-544-GFP for 48 h. When indicated, cells were treated with 500 µM of Fe ("Fer") at 2h post-infection. Some non-infected control cells were subjected to a treatment with 1 mM DFO for 24 h before fixation and used as a positive control. Results represent the frequency distribution of fluorescence intensities.

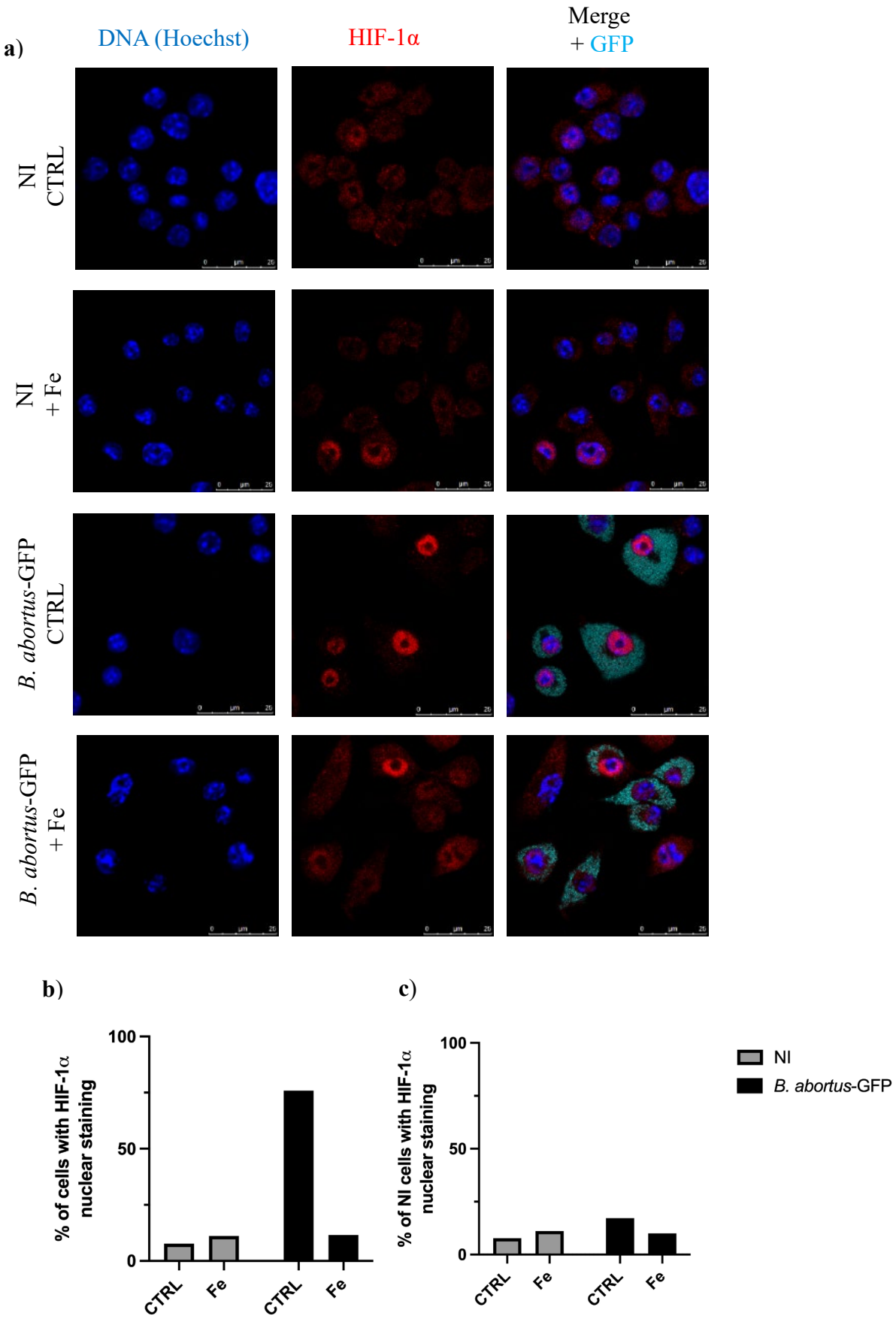

Figure 24: Effect of iron supplementation on *B. abortus*-induced HIF-1α nuclear localisation in BMDM.

a) Immunostaining of HIF-1α in BMDMs infected or not (NI: non-infected cells) with *B. abortus*-544-GFP for 48 h and treated or not (CTRL: control cells) with 500 µM iron chloride tetrahydrate (Fe). The percentages (%) of infected or non-infected as well as non-infected (NI) cells in the vicinity of infected cells that are positive for a HIF-1α nuclear staining for n=1 experiment are shown in **b** and **c**, respectively (scale bars = 25 µm).

Importantly, the inhibitory effect of iron supplementation on *B. abortus*-induced HIF-1α stabilisation can be reproduced upon infection of bone marrow-derived macrophage (BMDM)-derived cell line in a preliminary experiment (**Figure 24.a** and **24.b**). The apparent relevance of our findings to *B. abortus*-infected BMDM is important because BMDMs are a much more relevant cellular model in regard to *Brucella in vivo* infection. However, the difference in the percentages of HIF-1α nuclear localisation between NI cells in close proximity to *B. abortus*-infected cells and cells from control conditions was much less pronounced complicating the interpretation of the effect of iron supplementation in this context (**Figure 24.c**). Nevertheless, these results will need to be confirmed.

In conclusion, *B. abortus*-induced HIF-1α stabilisation in HeLa cells, and apparently also in BMDMs, is due to an iron stress that, we suppose, is negatively affecting PHD catalytic activity. This claim would however require confirmation. We subsequently tried to determine what functional impact this putative iron depletion stress could have during *B. abortus* infection.

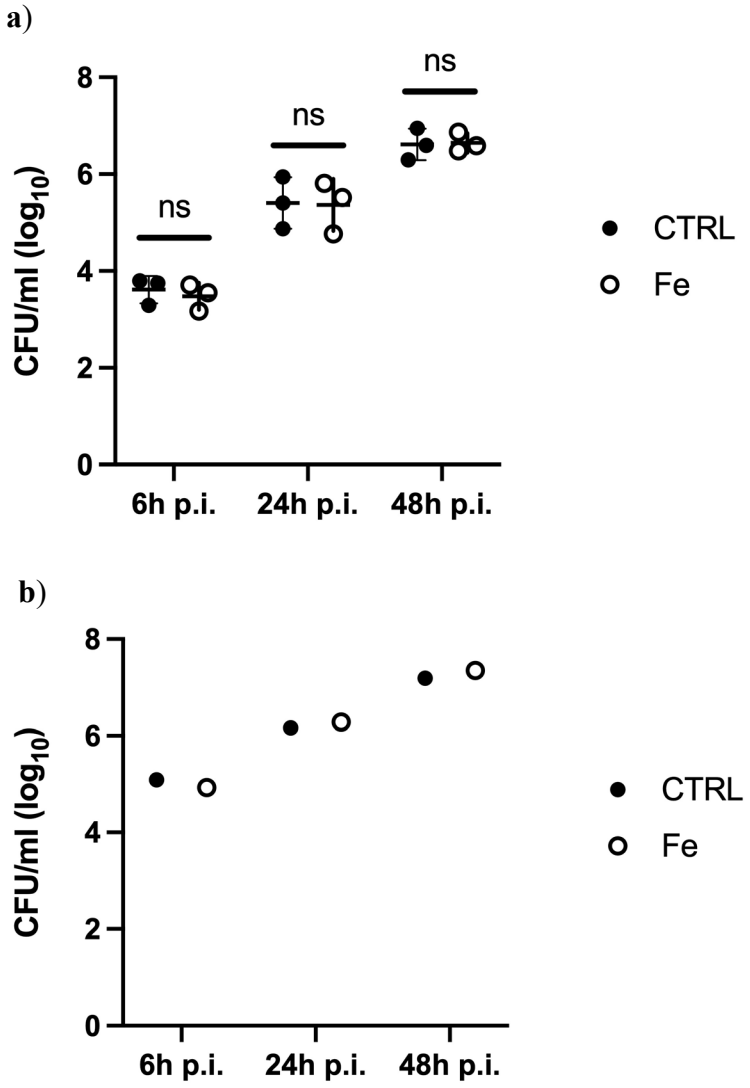

Figure 25: Effect of iron supplementation on *B. abortus* intracellular proliferation.

Colony-forming units (CFU) of *B. abortus*-GFP-infected HeLa (**a**) and BMDM (**b**) cells analysed at 6, 24 or 48 h post-infection times for cells incubated or not (CTRL) with iron chloride tetrahydrate (Fe)-treated (500 µM) from 2 h p.i. In **a**), results represent as the means ± 1 SD (n = 3 independent experiments) of the number of CFU per ml (in $\log_{10}$ units). Statistical analysis: two-way ANOVA followed by Bonferroni's multiple comparisons between CTRL (black dots) and Fe-treated samples (white dots) (ns: no-significant differences). In **b**), results are shown as the mean of CFU per ml (in $\log_{10}$ units) for n = 1 experiment.

3.2. Effect of iron supplementation on *B. abortus* intracellular replication.

Given the very low number of *B. abortus*-infected cells showing HIF-1α nuclear localisation upon iron supplementation (**Figure 22**), this could be used to indirectly assess a putative effect of HIF-1α stabilisation on the intracellular replication of *Brucella*. We thus tested the putative effect of iron supplementation on the bacterial colony-forming unit (CFU) number and found that the supplementation does not have any effect on the proliferation of the bacteria during the course of infection (**Figure 25**). Two conclusions can be drawn from this experiment. First, HIF-1α stabilisation does not contribute to the anti-bacterial defences against *Brucella* in our model in contrast to what was reported during *in vivo* infection. This would however requires confirmation for Fe-treated BMDMs by reiterating the experiment. In addition, iron concentrations are probably not a limiting factor for *Brucella* intracellular replication in our conditions indicating that the different iron import pathways expressed by *Brucella*[228] are apparently sufficient to meet the nutritional needs of the bacteria for iron.

We next focused our attention on our main objective: to determine the potential effects of this putative intracellular iron depletion responsible for HIF-1α stabilisation on the mitochondria of the infected host cells.

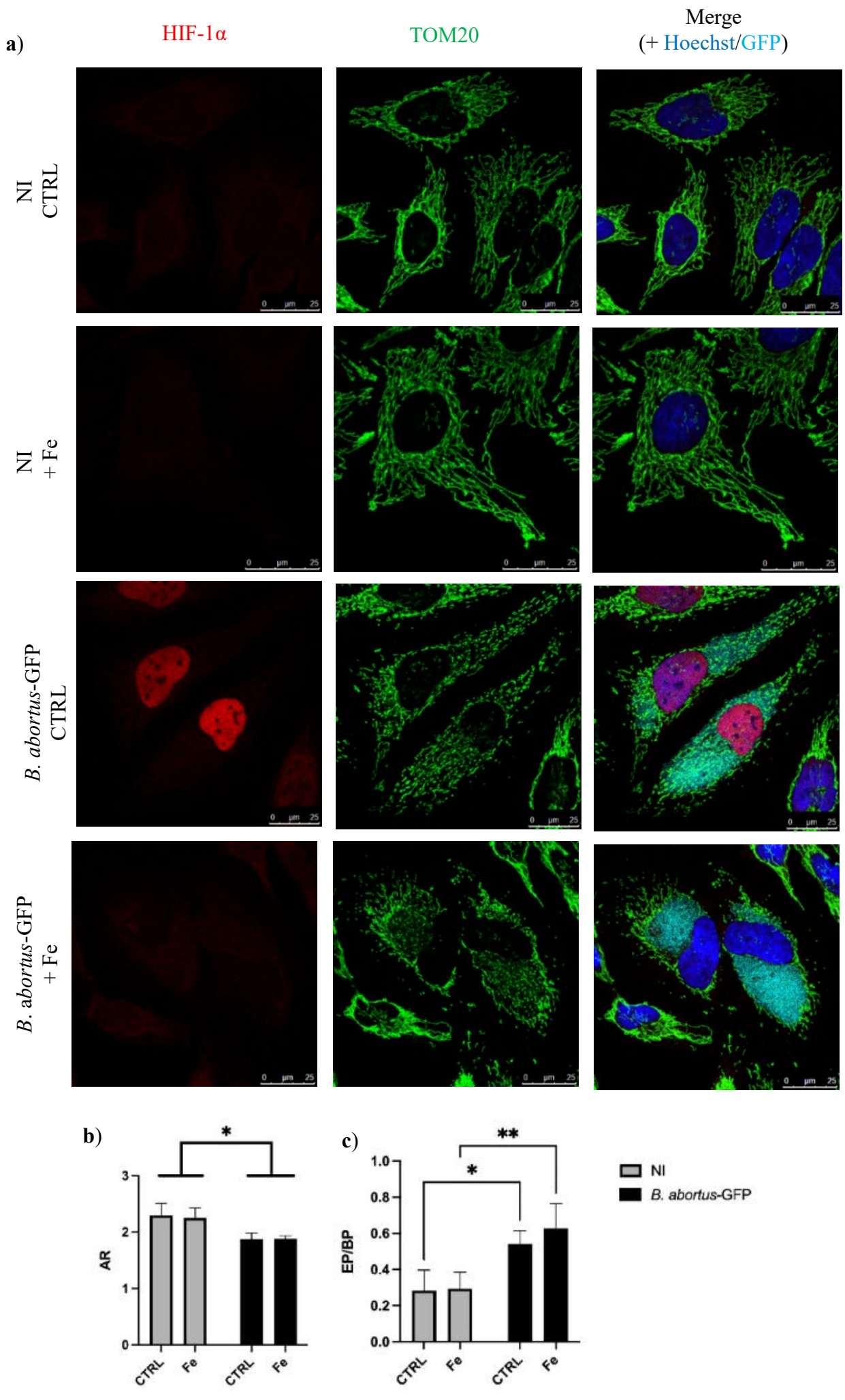
a)
HIF-1α
TOM20
Merge
(+ Hoechst/GFP)
NI CTRL
NI + Fe
B. abortus-GFP CTRL
B. abortus-GFP + Fe
b)
AR
CTRL
Fe
CTRL
Fe
c)
EP/BP
CTRL
Fe
CTRL
Fe
NI
B. abortus-GFP

Figure 26: Effect of the supplementation of iron on *B. abortus*-induced mitochondrial fragmentation.

a) Co-immunostaining of TOM20 and HIF-1α in HeLa cells infected or not (NI) with *B. abortus*-GFP for 48 h treated with 500 µM iron chloride tetrahydrate (Fe) at 2h post-infection time or not (controls: CTRL) (scale bars = 25 µm). Quantitative analysis of the mitochondrial morphology was performed by the determination of the aspect ratio (AR, **b**) and the end-point/branch-point ratio (EP/BP, **c**) of TOM20-stained cells. Results are expressed as the means ± 1 SD for 4 independent experiments (n = 4) for TOM20 (an average of 25 cells were analysed by experiment and for each experimental condition giving a total of 100 cells per condition in total). Statistical analysis: two-way ANOVA followed by Bonferroni's multiple comparison (*: $p < 0.05$ and **: $p < 0.01$)

3.3. Exploration of the interplay between iron, HIF-1α and mitochondrial phenotypes associated with *B. abortus* intracellular infection.

3.3.1. Effect of iron supplementation on *B. abortus*-induced mitochondrial fragmentation.

As it was possible to indirectly modulate HIF-1α stabilisation by modulating iron concentration, we tested whether the suppression of HIF-1α stabilisation in response following iron treatment had any effect on *B. abortus*-induced mitochondrial fragmentation. Surprisingly, the mitochondrial morphology of *B. abortus*-infected HeLa cells stayed fragmented upon iron supplementation and was comparable as the one observed for non-supplemented infected-cells as assessed by AR and EP/BP quantification (**Figure 26**). These results strongly suggest that HIF-1α stabilisation and the mitochondrial fragmentation associated with a putative induction of mitophagy are two unrelated events during *B. abortus* intracellular infection. These observations are also supported by the fact that HIF-1α stabilisation in non-infected cells that are adjacent to *B. abortus*-infected HeLa cells does not seem to trigger mitochondrial fragmentation, at least 48 h after infection (Jeremy Verbeke, unpublished data).

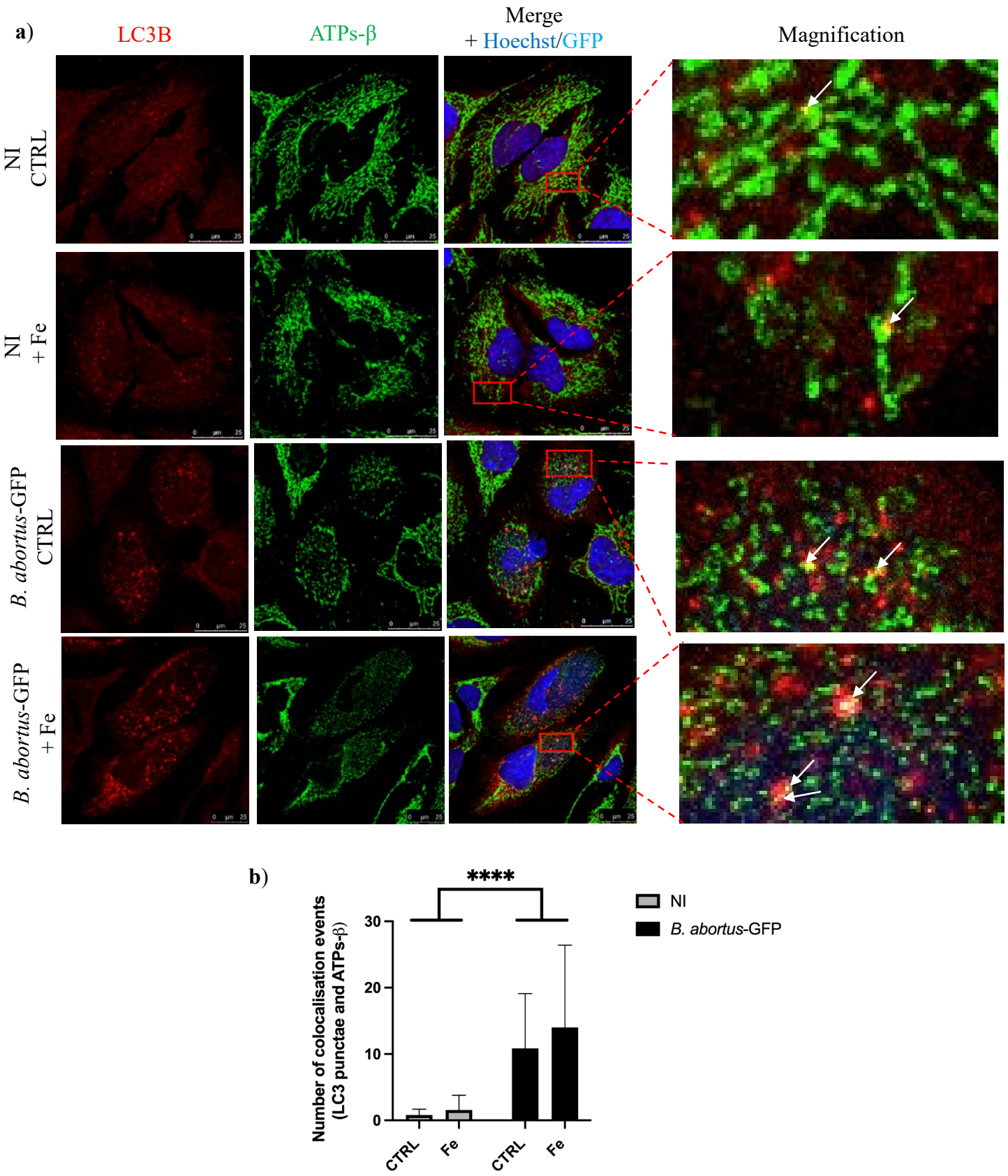

Figure 27: Effect of iron supplementation on *B. abortus*-induced increase in LC3-mitochondria colocalisation events.

a) Co-immunostaining of LC3B and ATP synthase-β subunit (ATPs-β) in HeLa cells infected or not (NI) with *B. abortus*-GFP for 48 h and treated with 500 µM iron chloride tetrahydrate (Fe) at 2h post-infection or not (CTRL: control cells). The zoomed micrographies at the right are derived from the areas delimited by the red boxes (scale bars = 25 µm). **b**) Quantification of LC3B-ATPs-β co-localisation events. Results are expressed as the mean numbers of co-localisation events (indicated by white arrows) between LC3B and the mitochondrial marker ATPs-β and represent means ± 1 SD for 1 experiment (an average of n=15 cells were analysed/condition). Statistical analysis: rank sum test (Mann-Whitney's test, ****: $p < 0.0001$).

3.3.2. Effect of iron supplementation on *B. abortus*-induced putative mitophagy.

To assess the possibility that HIF-1α could be potentially involved in the putative mitophagy observed in *Brucella*-infected HeLa cells, as a downstream event of the mitochondrial fragmentation, the effect of an iron supplementation in *B. abortus*-infected HeLa cells was tested on the number of co-localisation events between LC3B and ATP synthase-β subunit (ATPs-β), markers of autophagosomes and mitochondria, respectively (**Figure 27**). We observed that iron supplementation does not have any any significant effect on the co-localisation between autophagosome and mitochondrial markers.

These results do not support an implication of HIF-1α in the alterations of mitochondrial morphology observed in HeLa cells infected with *B. abortus*.

a)

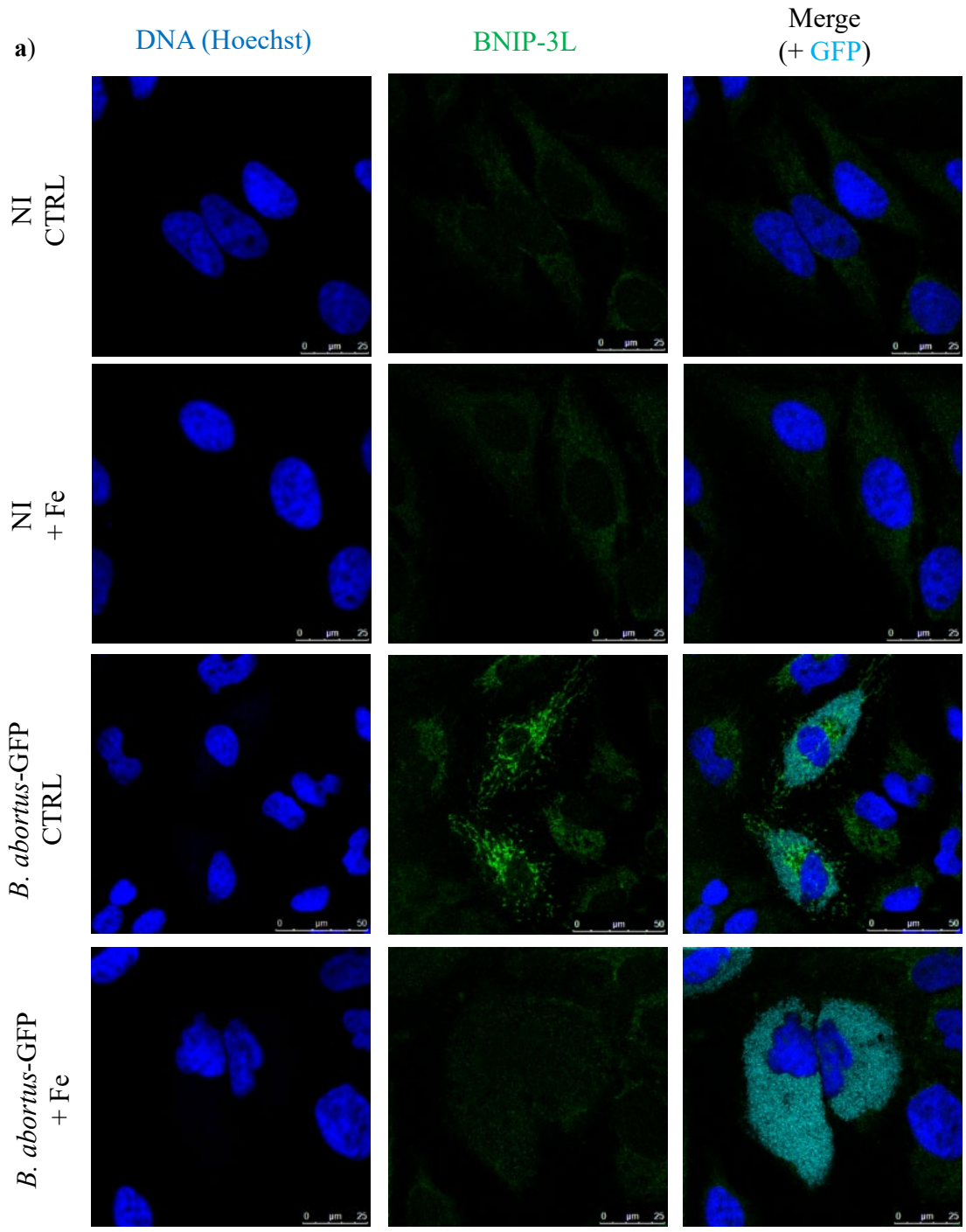

b)

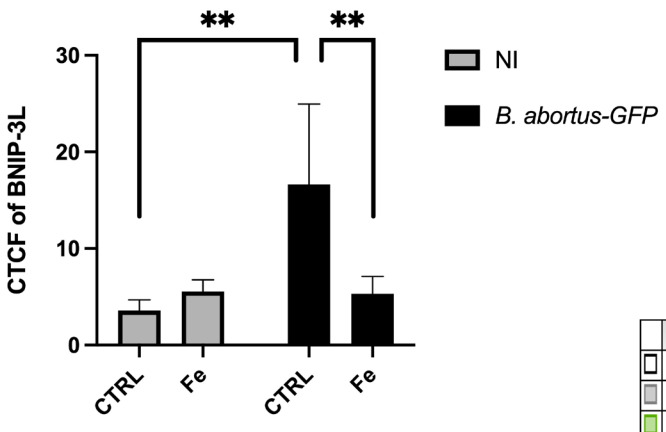

c)

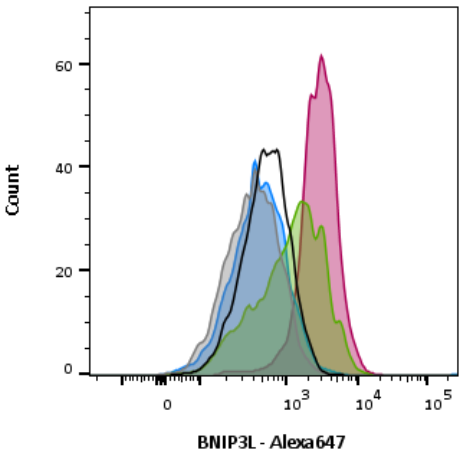

	Sample Name	Subset Name	Count	Median : Alexa 647-A
	BNIP3L_48h_ctrl.fcs	DownsampleDP	1833	568
	BNIP3L_48h_Fer.fcs	DownsampleDP	1833	402
	BNIP3L_48h_544GFP.fcs	DownsampleDP	1833	1272
	BNIP3L_48h_544GFP+Fer.fcs	GFP-positive	1833	468
	BNIP3L_48h_DFO.fcs	DownsampleDP	1833	2816

Figure 28: Effect of iron supplementation on *B. abortus*- induced increase in BNIP-3L abundance.

a) Immunostaining of BNIP-3L in HeLa cells infected or not (non-infected controls, NI) with *B. abortus* at 48 h post-infection observed with confocal microscopy. Where indicated, 500 µM of iron chloride tetrahydrate (+Fe) was added to the culture medium at 2 h post-infection or not (controls, CTRL) (scale bars = 25 µm). The corrected total cell fluorescence (CTCF) shown in **b** was calculated by subtracting the fluorescence of the background from the integrated fluorescence density of each cell using the ImageJ software. Results are represented as the means ± 1 SD calculated on an average of n=10 cells/condition (1 experiment). Statistical analysis: unpaired t-tests with Welch's correction (**: $p < 0.01$).

c) Quantification of BNIP-3L abundance by flow cytometry (1833 cells analysed/condition) in HeLa cells infected or not (ctrl) with *B. abortus*-544-GFP for 48 h. When indicated, cells treated with 500 µM Fe 2 h post-infection or not (ctrl). As a positive control, non-infected HeLa cells were incubated with 1 mM DFO for 24 h before fixation. Results are shown as the frequency distribution of fluorescence intensities for n=1 experiment.

3.3.3. Effect of iron supplementation on *B. abortus*-induced increase in BNIP-3L abundance.

The results showing that HIF-1α stabilisation and the different mitochondrial phenotypes indicative of mitophagy induction during *B. abortus* infection are two unrelated events was really surprising to us. Indeed, as we have seen at the end of the introduction (see section 1.4.4.4. related to preliminary data generated by Jeremy Verbeke, ongoing PhD thesis), one the canonical target genes of the HIF-1α transcription factor, the mitophagy receptor BNIP-3L[180,195,274], localises on the mitochondria in *Brucella*-infected HeLa cells at 48 and 72 h p.i. (see preliminary results **Figure 10**).

Nevertheless, we decided to determine whether BNIP-3L could also be regulated by changes in iron concentrations. Strikingly, the supplementation of *B. abortus*-infected cells with Fe dramatically impaired the increase in BNIP-3L abundance as observed by immunofluorescence and confocal microscopy observation at 48 h p.i. (**Figure 28.a** and **28.b**). Furthermore, these results were confirmed by the quantification of BNIP-3L abundance at 48 h p.i. by flow cytometry performed on a higher number of infected-cells (**Figure 28.c**). Even if these experiments need to be repeated, these results suggest that the accumulation/stabilisation of HIF-1α is responsible for BNIP-3L expression in *B. abortus*-infected cells. This is in total agreement with the known function of HIF-1α as a positive regulator of BNIP-3L[180,274]. However, these result do not support our initial hypothesis assuming that BNIP-3L is the effector responsible for the induction of a putative mitophagy during *B. abortus* infection.

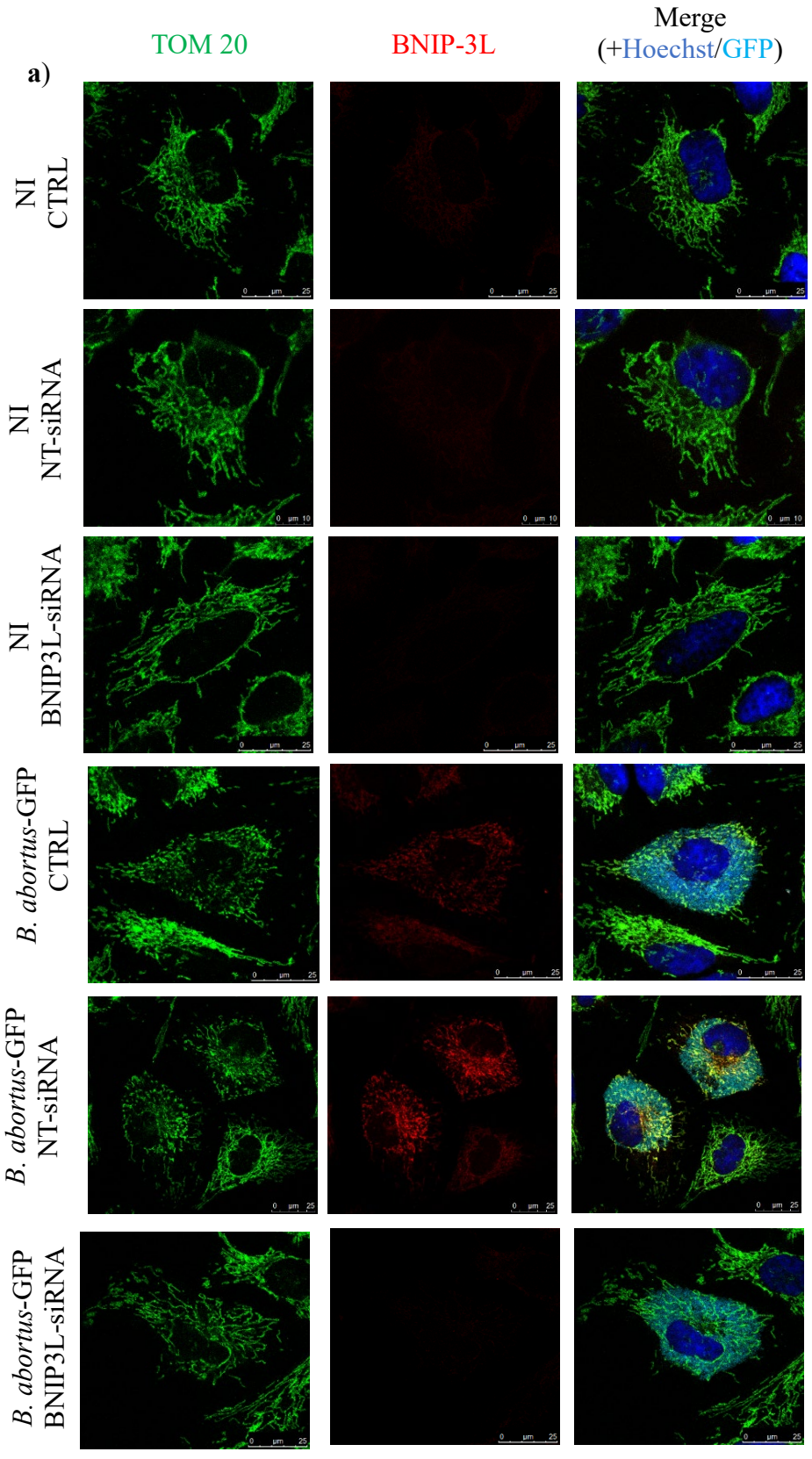

Figure 29: Effect of BNIP-3L silencing on *Brucella*-induced mitochondrial fragmentation in HeLa cells.

a) Co-immunostaining of TOM20 and BNIP-3L in HeLa cells infected with *B. abortus*-GFP or not (NI non-infected control) for 48 h and transfected or not (CTRL controls) with either a non-target siRNA (siNT) or a siRNA directed against BNIP-3L (siBNIP3L). Quantification of mitochondrial morphology was performed by determining the aspect ratio (AR) in **b** and the end-point/ branch-point ratio (EBP) in **c**. Results are expressed as the mean ± 1 SD. 35 cells were analysed/experiment for n = 2 independent experiments. Statistical analysis: two-way ANOVA followed by Tukey's post-hoc analysis (Lisa Martin., master thesis, 2022).

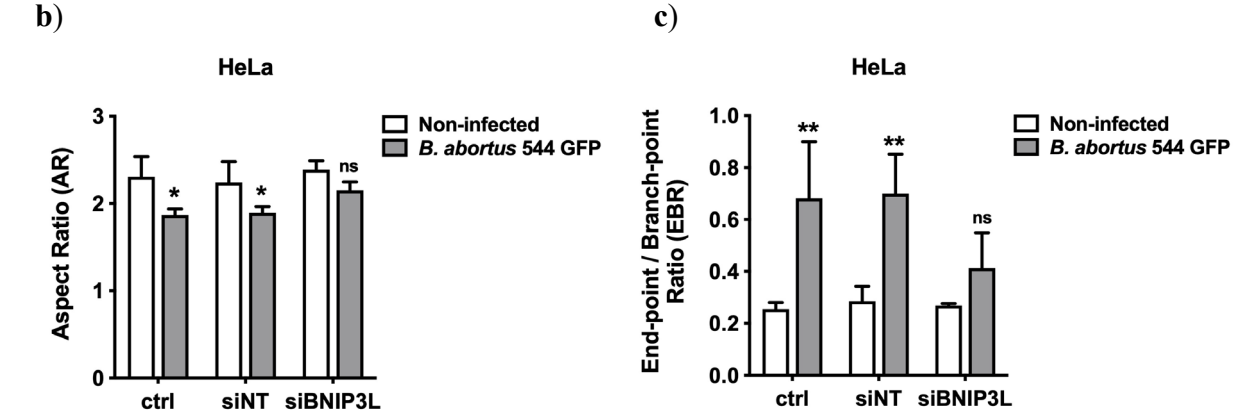

3.3.4. Effect of BNIP-3L silencing on the mitochondrial fragmentation induced by *B. abortus*.

In order to test whether BNIP-3L could play a role in the fragmentation of mitochondria observed in *Brucella*-infected cells, we tested the effects of a small-interfering RNA (siRNA)-directed against BNIP-3L expression on the mitochondria morphology of infected cells (**Figure 29**). The efficiency and controls of these tools were performed by Lisa Martin (master thesis, 2022). We observed that the silencing of BNIP-3L does significantly reduces *B. abortus*-induced mitochondrial fragmentation in HeLa cells (**Figure 29**). Surprisingly, this observation is in contradiction with our previous results showing that accumulations of HIF-1α (**Figure 22** and **23**) and BNIP-3L (**Figure 28**) in *Brucella*-infected cells are unrelated to the induction of mitochondrial fragmentation (**Figure 26**) and/or mitophagy (**Figure 27**) in cells infected with *B. abortus*.

Three hypothesises can be proposed to try to explain this discrepancy: first, iron supplementation could not be as efficient as siRNAs to prevent BNIP-3L accumulation but this is not very likely as the abundance of BNIP-3L in iron-treated *B. abortus*-infected HeLa cells is very similar than in non-infected control cells (**Figure 28**).

In a second time, the iron-mediated suppression of BNIP-3L is less specific and can thus not phenocopy siRNA-mediated knock-down (KD) for a still unknown reason. For example, we might assume that a high concentration of iron might also generate an aspecific stress, such as oxidative stress linked to iron-catalised Fenton reactions[219] leading to a fragmentation that would mask the protection confered by BNIP-3L absence. Indeed, iron overload was linked to the induction of mitochondrial fragmentation (this has been mainly studied in neuronal and cardiac cells), already at a concentration of 100 µM of ferric citric acid[275]. However, no defined induction of mitochondrial fragmentation nor mitophagy could be observed in control HeLa cells treated with 500 µM iron chloride tetrahydrate (see **Figure 26** and **27**). We might thus assume that iron overload might induce aspecific effects only in *B. abortus*-infected cells. Interestingly, the mitochondrial fragmentation induced by iron overload in neuronal cells is dependent on ER stress[276], so we might hypothesise that, because *Brucella* was shown to trigger an ER-UPR response[64,65,172], *B. abortus* infection could sensitize cells to iron overload-induced ER stress and subsequent mitochondrial fragmentation.

In contrast, *B. abortus*-infected cells resistance to iron-mediated ROS production could be similar or even higher than non-infected cells for two reasons. First, following our current hypothesis, *Brucella* is probably depleting intracellular iron stores during its replication. Thereby, it is reasonable to think that a putative oxidative stress induced by iron supplementation would be less intense in *B. abortus*-infected cells than in NI cells because in the formers iron would also be partly consumed by the developing bacteria. In a second time, *Brucella* infection does not lead to an increase in ROS production, atleast by the mitochondria in our model (**Figure 19**), that can thus not explain a putative increase in the iron-catalysed Fenton reaction[219]. Furthermore, *Brucella* spp. were shown to actually upregulate the anti-oxidant defenses in infected cells such as peroxiredoxin (Prdx) 5 and 6 and downregulate pro-oxidants (thioredoxin-interacting protein, TXNIP) in a LPS and VirB-dependent manner to counteract macrophage's oxidative burst[159,272,277]. Importantly, Prdx5 was shown to negatively regulate iron overload induced mitochondrial fragmentation in neurons[276], we thus could hypothetise that *B. abortus*-infected cells would be more resistant than naïve cells to iron-mediated oxidative stress. To test those hypothesises, staining of mitochondrial-derived ROS on *B. abortus*-infected HeLa cells could be performed after iron treatment. In addition, monitoring mitochondrial morphology after NAC treatment of iron-supplemented *B. abortus*-infected HeLa cells could allow to reveal a production of potential damaging ROS linked to the iron treatment as NAC was shown to alleviate iron overload-induced mitochondrial fragmentation[276].

In a third time, we might also consider that the this apparent contradiction between iron-mediated and siRNA-mediated BNIP-3L depletion on mitochondrial morphology is not due to an aspecific effect of iron, but rather due to the fact that both treatment do target the same pathway at different levels. Indeed, the main difference between the two scenarios is that, upon BNIP-3L KD, HIF-1α remains, most probably, stabilised and thus active (Martin L., master thesis) while this is not the case following iron supplementation. HIF-1α regulates a large set of genes in addition to BNIP-3L and the disruption of the normal HIF-1α-dependent signaling events in an more "artificial" way, such as through siRNA mediated KD, could lead to unexpected results. This could also explain the different phenotypes associated with both ways to supress BNIP-3L expression. Importantly, the specific targeting of HIF-1α through a siRNA based KD could give valuable information in favour of either one of these two latter possibilities.

In the end, in an attempt to adress these sets inconsistent data, we assumed that the elemental iron treatment we used was not able to recover/replete mitochondrial Fe levels because of a putative downstream regulator that could be affected during *B. abortus* infection. Importantly, it was reported that mitochondrial iron uptake is impaired in the absence of the mammalian siderophore 2,5-dihydroxybenzoic acid (2,5-DHBA)[246]. Intriguingly, 2,5-DHBA has a similar structure to 2,3-DHBA, an intermediate in bacterial siderophore synthesis[246], to the point that 2,5-DHBA can be imported by the same transporter as 2,3-DHBA to mediate iron import in *E. coli*[247]. Importantly, 2,5-DHBA supplementation was shown to enhance mice suceptibility to *E. coli* infection[247]. 2,3-DHBA is also synthetised by *Brucella* spp. under iron-deficient conditions[228] leading us to hypothetise that 2,5-DHBA could be consumed during the massive intracellular replication of *B. abortus* leading to the depletion of intracellular 2,5-DHBA pools. In those conditions, the additionnal iron that is added in the culture media of the cells could reach the cytosolic compartment (recovering PHD activity and leading to HIF-1α degradation), but not the mitochondria. The depletion of 2,5-DHBA would thus explain why the supplementation of iron does not prevent *B. abortus*-induced mitochondrial fragmentation and mitophagy because iron is unable to accumulate into the mitochondria.

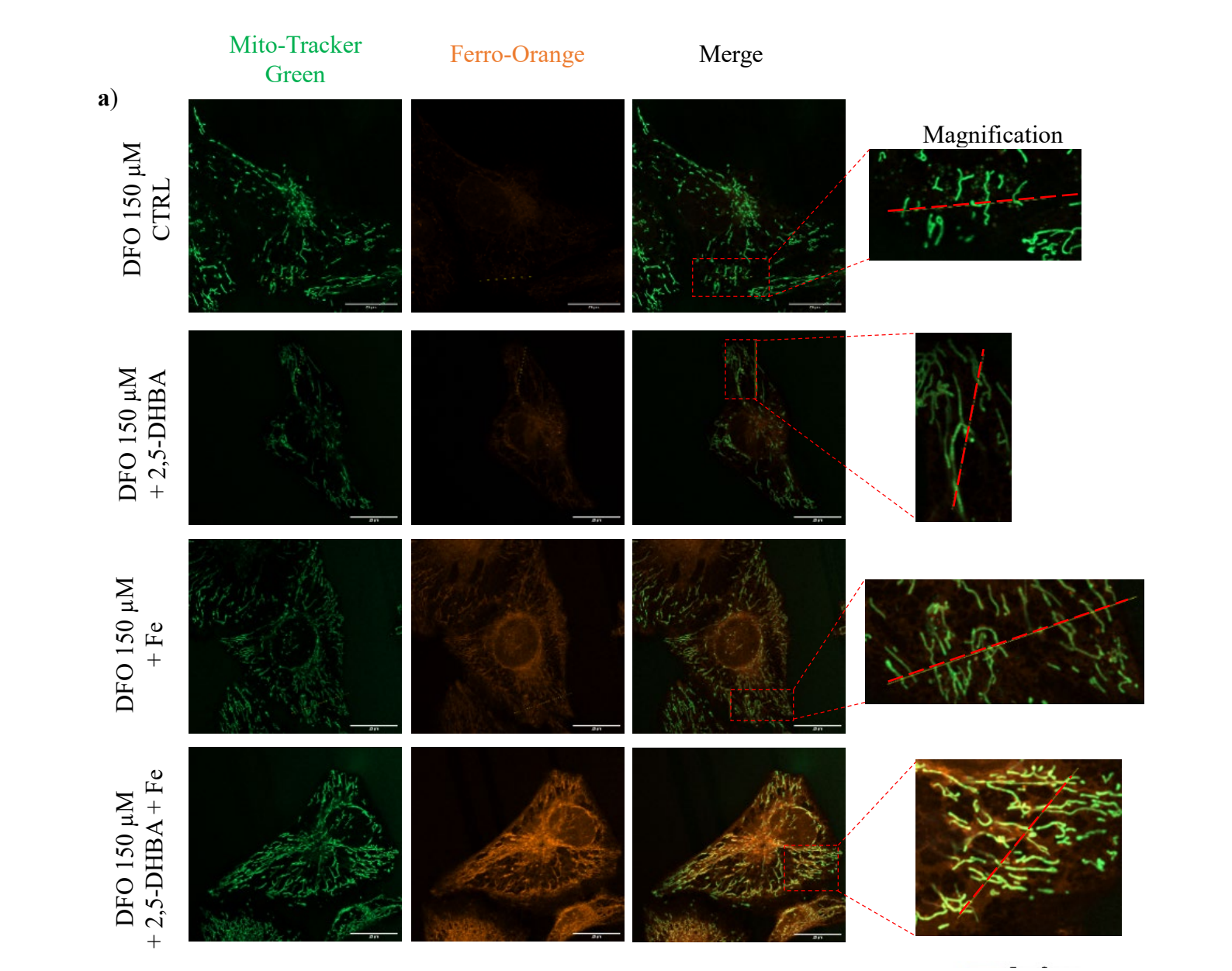
Mito-Tracker Green
Ferro-Orange
Merge
a)
DFO 150 µM CTRL
DFO 150 µM + 2,5-DHBA
DFO 150 µM + Fe
DFO 150 µM + 2,5-DHBA + Fe
Magnification

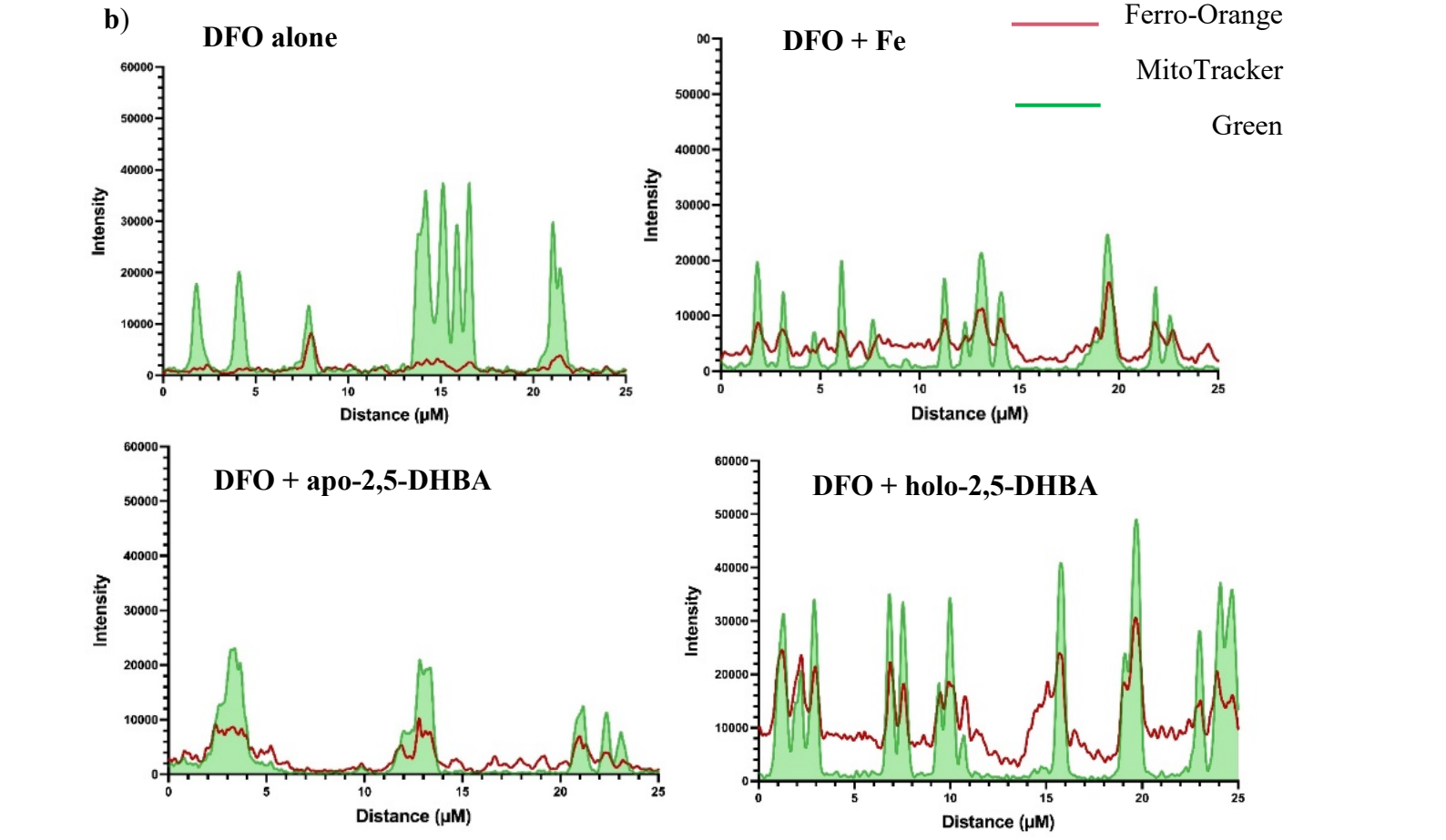
b)
DFO alone
DFO + Fe
DFO + apo-2,5-DHBA
DFO + holo-2,5-DHBA
Ferro-Orange
MitoTracker Green
Intensity
Distance (µM)

Figure 30: Effect 2,5-DHBA and/or iron treatment on iron concentrations in the mitochondria.

a) Live cell imaging of the mitochondrial network and the labile iron pool in HeLa cells stained with Mito-Tracker Green and Ferro-Orange fluorescent probes, respectively (scales bars = 25 µm). The cells were first iron-starved for 24h with 150 µM DFO treatment before the addition of either 500 µM of iron chloride tetrahydrate (Fe), 2,5-dihydroxibenzoic acid (apo-2,5-DHBA) or a combination of both molecules (holo-2,5-DHBA) for an additional 24 h. Cells were then observed with a LSM 980 Airyscan 2 microscope. **b**) Transept analysis of Ferro-Orange (in red) and Mito-Tracker Green (in green) fluorescence intensities across a distance of 25 µm. The location of the transept is shown in the magnified micrographs which correspond to the areas delimited by the red boxes.

3.3.5. Involvement of 2,5-DHBA in mitochondrial iron import in HeLa cells.

Unfortunately, studies addressing 2,5-DHBA are scarce and come mainly from the same group[246,247,278–280] so it was important to confirm whether 2,5-DHBA could be involved in mitochondrial iron loading. We took advantage of a fluorescent probe able to detect free Fe^{2+} (the LIP) called Ferro-Orange[205] to compare the ability of iron (Fe), 2,5-DHBA alone (apo-2,5-DHBA) or DHBA that was pre-incubated with Fe (holo-2,5-DHBA) to increase mitochondrial LIP in naïve HeLa cells. In order to mimic the putative iron depletion induced by *B. abortus* infection, cells were first starved of iron with 150 µM DFO for 24 h. We next added 500 µM of either one of the compounds to compare their respective ability to restore iron levels in the mitochondria. Staining of the mitochondrial population was performed with the "Mito-Tracker Green" fluorescent probe allowing us to visualise the co-localisation between free iron detected by the "Ferro-Orange" fluorescent probe with the mitochondrial network. The fluorescence intensities on transept sections in the cells were then plotted and analysed (**Figure 30**).

Strikingly, the addition of apo-2,5-DHBA was sufficient to induce a small increase in Ferro-Orange staining inside the mitochondria but not in the surrounding cytosol demonstrating that 2,5-DHBA role in iron metabolism is specific to the mitochondria (**Figure 30**). Furthermore, holo-2,5-DHBA was much more potent at increasing global, and especially mitochondrial, iron levels than a Fe-treatment alone indicating that 2,5-DHBA increases the bioavailability of iron. Notably, the Fe treatment was also able to substantially increase mitochondrial iron concentrations, that can probably be attributed to endogenous levels of 2,5-DHBA and/or, possibly, by the existence of other mitochondrial iron import mechanisms. If our hypothesis is right, this effect would be much more limited in *B. abortus*-infected cells due to the depletion of intracellular 2,5-DHBA pools.

Collectively, these different observations confirmed that 2,5-DHBA is an important molecular effector in iron uptake by the mitochondria that could thus be relevant to *Brucella* infection. As a 2,5-DHBA deficit linked to a defective synthesis (in a *bdh2* zebrafish mutant) has already been linked with mitochondrial stress and induction of mitophagy[281], we thus hypothetised that a deficit in 2,5-DHBA induced by *Brucella* could be responsible for the mitochondrial phenotypes observed in infected HeLa cells.

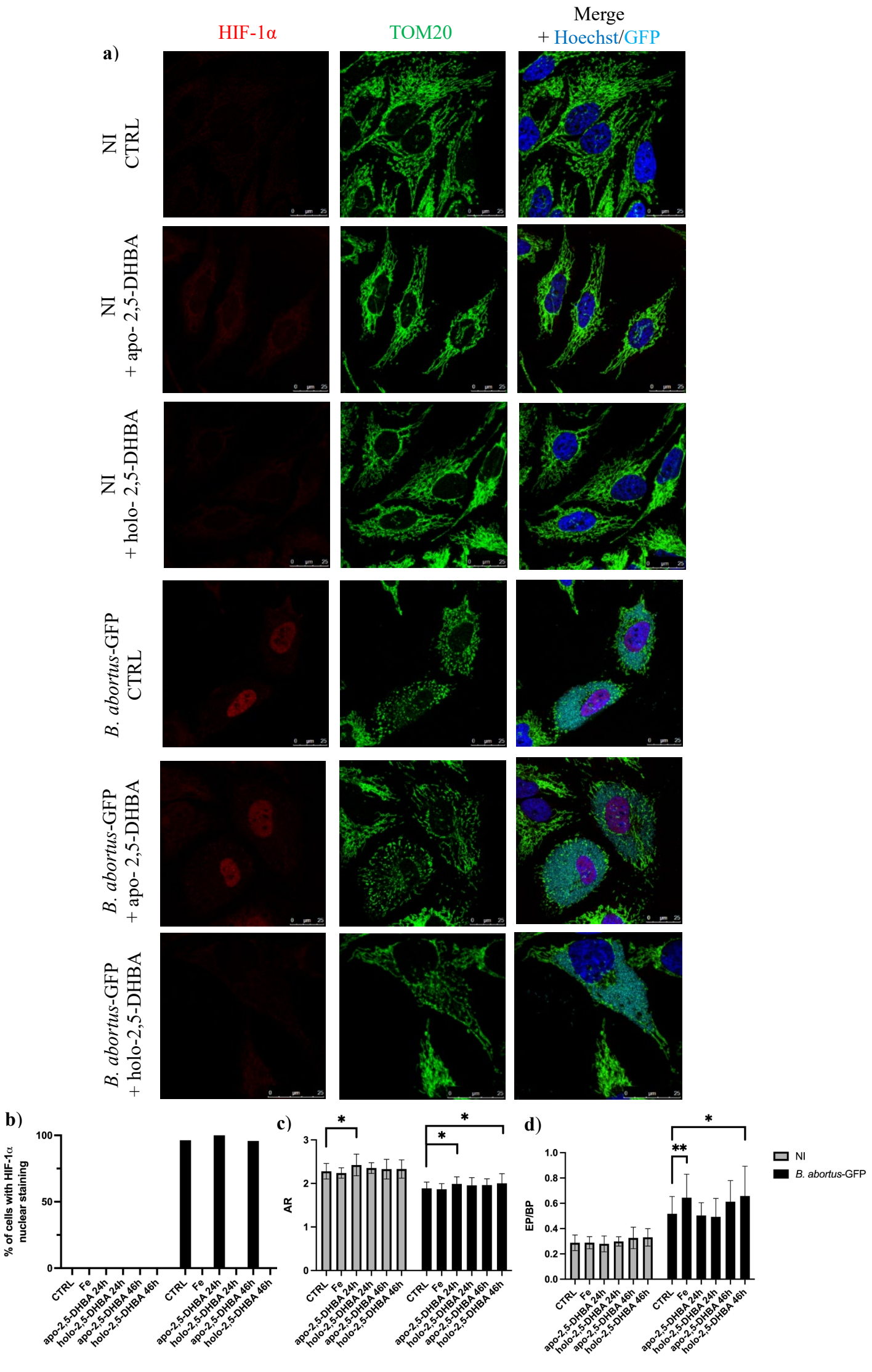
a)
HIF-1α
TOM20
Merge
+ Hoechst/GFP
NI
CTRL
NI
+ apo- 2,5-DHBA
NI
+ holo- 2,5-DHBA
B. abortus-GFP
CTRL
B. abortus-GFP
+ apo- 2,5-DHBA
B. abortus-GFP
+ holo-2,5-DHBA
b)
% of cells with HIF-1α nuclear staining
100
50
0
c)
AR
3
2
1
0
d)
EP/BP
1.0
0.8
0.6
0.4
0.2
0.0
NI
B. abortus-GFP
CTRL
Fe
apo-2,5-DHBA 24h
holo-2,5-DHBA 24h
apo-2,5-DHBA 46h
holo-2,5-DHBA 46h
*
**

Figure 31: Comparison of 500 µM iron, apo- or holo-2,5-DHBA treatment effects on *B. abortus*-induced HIF-1α stabilisation and mitochondrial fragmentation.

a) Co-immunostaining of TOM20 and HIF-1α in HeLa cells infected or not (CTRL) with *B. abortus*-GFP- for 48 h and then observed by confocal microscopy. When indicated, cells were treated with 500 µM iron (Fe) at 2 h post-infection. In addition, 2,5-dihydroxibenzoic acid (DHBA) alone (apo-2,5-DHBA) or pre-incubated with Fe in a 1:1 concentration ratio (holo-DHBA) were added at 24 h p.i. (scale bars = 25 µm) **b**) Quantification of the percentages (%) of cells that display a nuclear HIF-1α staining calculated on an average of n = 25 cells/condition (for 1 experiment) upon treatment of cells with Fe (at 2 h p.i.), apo-2,5-DHBA or holo-2,5-DHBA (at either 2 h p.i., giving 46 h of treatment, or 24 h p.i.). **c**) Quantification of the fragmentation of the mitochondrial population assessed by the aspect ratio (AR) and end-point branch-point ratio (EP/BP) in cells immunostained for TOM20 with upon treatment of cells with Fe (at 2 h p.i.), apo-2,5-DHBA or holo-2,5-DHBA (at either 2 h p.i., giving 46 h of treatment, or 24 h p.i.). Results are expressed as the means ± 1 SD calculated from an average of n = 25 cells/condition (for 1 experiment). Statistical analysis: rank sum test (Mann-Whitney's test, *: $p < 0.05$, **: $p < 0.01$).

3.3.6. Effect of 2,5-DHBA supplementation on B. abortus-induced HIF-1α stabilisation and mitochondrial fragmentation.

To test whether 2,5-DHBA was involved in the induction of mitochondrial fragmentation during *B. abortus* infection, infected HeLa cells were supplemented with 500 µM of either apo- or holo-2,5-DHBA. To avoid a potential bias caused by a putative effect of 2,5-DHBA treatment on early *Brucella* trafficking and/or replication, cells were either treated at 24h p.i. (**Figure 31.a**) or at 2h p.i. (Supplementary Figure 3), so after and before rBCV maturation, respectively[15]. Interestingly, apo-2,5-DHBA, in contrast to iron (Fe) or holo-2,5-DHBA, did not reduce the percentage of infected HeLa cells with a positive staining for nuclear HIF-1α (**Figure 31.b**). The quantification of the mitochondria fragmentation in cells incubated with 2,5-DHBA reveal a small but constant increase in the AR in comparison to control cells in both non-infected and *B. abortus*-infected HeLa cells. Such increase is not seen for cells exposed to Fe supplementation alone (**Figure 31.c**).

Some of these differences reached statistical significance such as for the apo-2,5-DHBA supplementation at 24h p.i. in both NI and *B. abortus*-infected background or following holo-2,5-DHBA supplementation at 2h p.i., but only in *B. abortus*-infected cells. Unfortunately, these observations are not observed for the EP/BP ratio. Strikingly, when *B. abortus*-infected cells are incubated with either 500 µM iron or holo-2,5-DHBA added at 2 h p.i., but not 24h p.i., an increase in the EP/BP ratio is observed at 48 h p.i (**Figure 31.d**). These results suggest an increase in mitochondrial network fragmentation. These surprising observations indicate that treating the cells at 2 h p.i. with iron and/or 2,5-DHBA induce aspecific effects. Notably, iron overload, induced by similar concentrations of iron as used in this study, was shown to induce endolysosomal dysfunction in a cultured cell line (HEK293T) translating in a decrease in the autophagic flux[282]. We can thus hypothesise that the supplementation of *B. abortus*-infected cells with iron decrease the rate of mitophagic turnover leading to a modest, but measurable, accumulation of fragmented piece of mitochondria.

Collectively, these results suggest that 2,5-DHBA treatment, at a concentration able to induce a strong mitochondrial iron loading in HeLa cells (**Figure 13**), has no, or a very weak, effect on *B. abortus*-induced mitochondrial fragmentation.

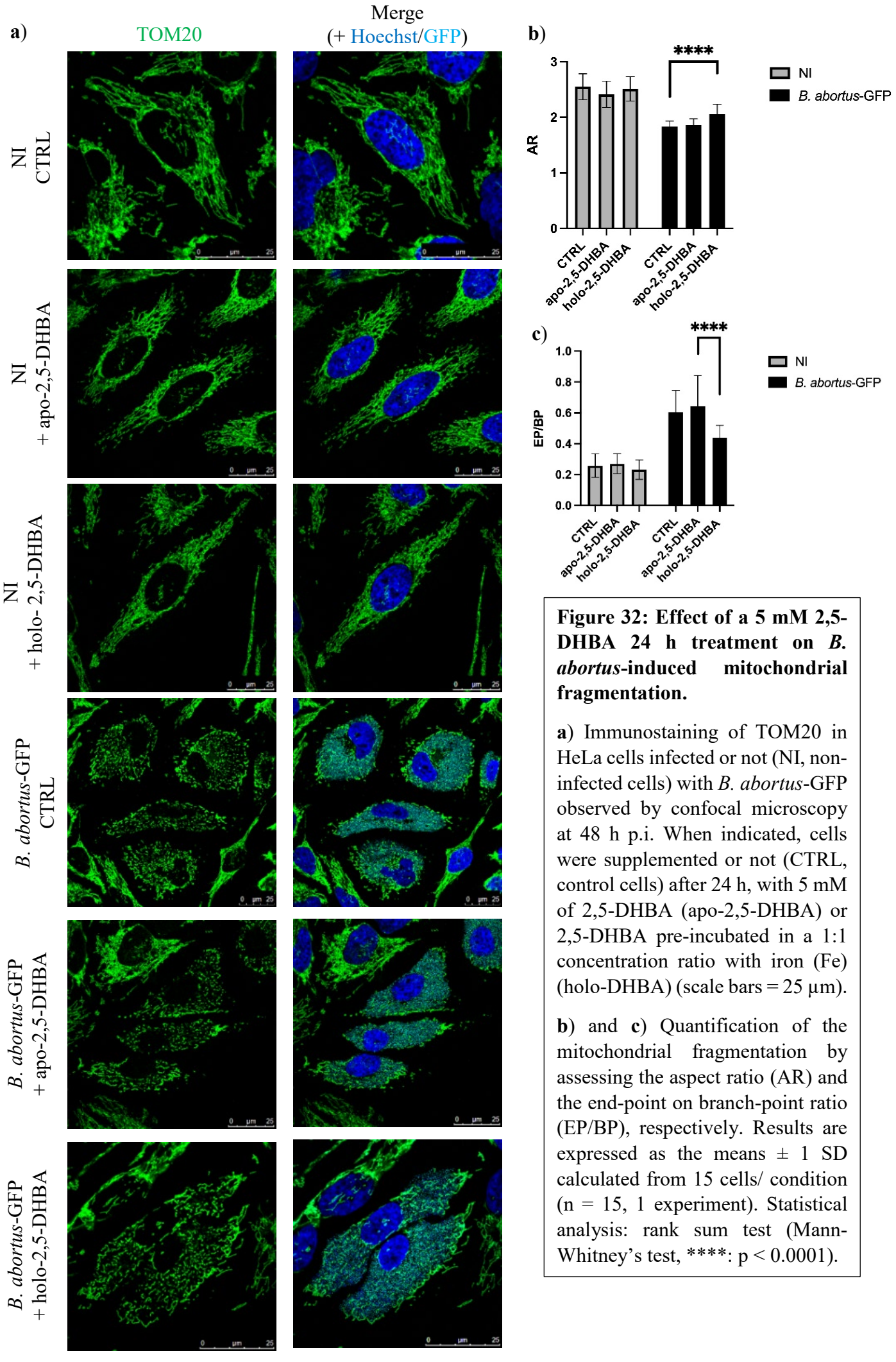

Figure 32: Effect of a 5 mM 2,5-DHBA 24 h treatment on *B. abortus*-induced mitochondrial fragmentation.

a) Immunostaining of TOM20 in HeLa cells infected or not (NI, non-infected cells) with *B. abortus*-GFP observed by confocal microscopy at 48 h p.i. When indicated, cells were supplemented or not (CTRL, control cells) after 24 h, with 5 mM of 2,5-DHBA (apo-2,5-DHBA) or 2,5-DHBA pre-incubated in a 1:1 concentration ratio with iron (Fe) (holo-DHBA) (scale bars = 25 µm).

b) and **c**) Quantification of the mitochondrial fragmentation by assessing the aspect ratio (AR) and the end-point on branch-point ratio (EP/BP), respectively. Results are expressed as the means ± 1 SD calculated from 15 cells/ condition (n = 15, 1 experiment). Statistical analysis: rank sum test (Mann-Whitney's test, ****: $p < 0.0001$).

However, following the hypothesis that *B. abortus* is able to consume 2,5-DHBA during its massive intracellular replication, we hypothesised that the amount of 2,5-DHBA needed to allow sufficient mitochondrial iron loading is much higher in *B. abortus*-infected cells than in non-infected control cells. Indeed, whereas in non-infected cells the majority of the extra 2,5-DHBA is available for the mitochondria, a proportion of the molecule could be redirected to the growing bacterium in *B. abortus*-infected cells. According to this hypothesis, a higher concentration of 2,5-DHBA would be required in *Brucella*-infected cells to observe the same effect than in non-infected control cells.

We thus tested whether a very high concentration of 2,5-DHBA (5 mM) added at 24 h p.i. (to avoid any putative non-specific effect on early infection events and time point) would be more potent at inhibiting *B. abortus*-induced mitochondrial fragmentation. Interestingly, 5 mM, holo-, but not apo-, 2,5-DHBA partially reduces/prevents *B. abortus*-induced mitochondrial fragmentation regarding both the length of mitochondrial fragments (AR) and the connectivity between these fragments (EP/BP) monitored at 48 h p.i. (**Figure 32**). While we need to be cautious with these preliminary results, the inability of apo-2,5-DHBA to prevent *B. abortus*-induced mitochondrial fragmentation strongly indicates that the holo-2,5-DHBA acts by a mechanism that involves an increase in mitochondrial iron import. Importantly, a holo-2,5-DHBA treatment induces an intermediary phenotype between non-infected and *B. abortus*-infected cells indicating that the concentrations we used might still be too low to completely recover/prevent the fragmentation or that 2,5-DHBA depletion and mitochondrial iron loading are only partly responsible for *B. abortus*-induced mitochondrial fragmentation. Nevertheless, these preliminary results suggest that a specific impairment of mitochondrial iron import at the level of the mammalian siderophore 2,5-DHBA could be at the origin of *B. abortus*-induced mitochondrial fragmentation and the putative downstream mitophagy events.

4. Conclusions and perspectives

In the last decade, the mitochondria emerged as a central regulator of the cellular immune response with modulation of the fusion/fission balance involved in the proper functioning of several immune cells types, including macrophages[77,283]. Unsurprisingly, this organelle was found to constitute a target of choice for a wide range of bacterial pathogens that modulate, among others, metabolic, apoptotic or innate immune pathways in order to get replicative and/or survival advantages[69,70,76,77].

B. abortus is a bacterial pathogen that invade the macrophages where it replicates massively inside the ER of the host cell in a remarkably stealthy way[15]. However, the studies addressing the relationship between *Brucella* and the mitochondria are scarce[10,67,68,178,284]. Smooth virulent *B. melitensis* 16M strain was shown to induce a down-regulation of nuclear-encoded mitochondrial genes such as apoptosis-related genes in infected macrophages[67], while the rough attenuated *B. abortus* strain RB51 was shown to induce macrophage cell death involving the caspase 2-dependent permeabilisation of the OMM, the release of cytochrome c[285] and also mtDNA that is associated with the activation of the NLRP3 inflammasome and IL-1β production[171,286]. The mitochondria-localised enzyme ACOD1 has been involved in anti-*Brucella* immunity in alveolar macrophages (AM), a process mediated by the production of the immune-metabolite itaconate[10]. Itaconate was proposed to inhibit bacterial multiplication by targeting the bacterial enzyme isocitrate lyase[10]. *B. abortus* infection does also disrupt mitochondrial metabolic functions and promote a switch towards aerobic glycolysis[68]. Finally, previous published work from our team discovered that BCVs are associated with mitochondria and that an important fragmentation of the mitochondrial network is observed in both HeLa œlls and BMDMs infected with *B. abortus*[178].

Unfortunately, the function and the mechanism(s) by which *B. abortus* induces the fragmentation of the mitochondrial population remain(s) elusive. Mitochondrial fragmentation is linked to the induction of the co-localisation between LC3 and the mitochondria in *B. abortus*-infected cells, indicative of mitophagy, without concomitant widespread reduction of MMP or Parkin recruitment on the mitochondria (Jérémy Verbeke, ongoing PhD thesis, unpublished data). Importantly, the abundance of the Parkin-independent mitophagy receptor BNIP-3L is dramatically increased at 48 and 72 h after *B. abortus* infection and localised on the fragmented mitochondria (**see introduction Figure 10.a**) (Jérémy Verbeke, ongoing PhD thesis, unpublished data). Furthermore, this phenotype is associated with a strong nuclear localisation of the HIF-1α transcription factor starting at 24 h p.i. (**see introduction Figure 10.g**) (Verbeke J., ongoing PhD thesis unpublished data), the canonical positive regulator of BNIP-3L transcription[179,180] suggesting an HIF-1α-dependent induction of mitochondrial fragmentation and, possibly, mitophagy during *B. abortus* infection of HeLa and RAW264.7 cells.

In consequence, the main objectives of this master thesis, centred on HIF-1α regulation, were (i) to identify the molecular actors responsible for HIF-1α stabilisation in response to *B. abortus* infection by focusing on known regulators of PHD activity such as oxygen, ROS and iron, (ii) to determine whether HIF-1α stabilisation is involved in the mitochondrial phenotypes associated with *B. abortus* infection or not and (iii) to better characterize the putative role of *Brucella* and/or the host cells in these events.

During this master thesis, *B. abortus*-induced HIF-1α stabilisation was found to be an iron-dependent process (**Figure 22** and **23**) with no (or little) involvement of hypoxia (**Figure 18**) and ROS production (**Figure 20** and Supplementary Figure 2) at least in HeLa cells. Our

results does also not apparently support an involvement of HIF-1α and BNIP-3L in *B. abortus* replication (**Figure 25**) nor in *B. abortus*-induced mitochondrial fragmentation during infection of HeLa cells. These data are in apparent contradiction with other results generated by Lisa Martin that showed an involvement of BNIP-3L in *B. abortus*-induced mitochondrial fragmentation (**Figure 29**, master thesis, 2022). However, preliminary results suggest that a deficiency in the mammalian siderophore 2,5-DHBA might induce a stress due to an iron deficit in the mitochondria responsible for *B. abortus*-induced mitochondrial fragmentation. This would constitute, to our knowledge and after confirmation, an original report for a pathogen-induced mitophagy, not already described in the literature.

4.1. Mechanisms of *B. abortus*-induced HIF-1α stabilisation.

Even if a drop in oxygen tension is the canonical stimulus described for HIF-1α stabilisation, the PHD-dependent mechanism of regulation of HIF-1α accumulation was subsequently associated with the sensing of many other parameters molecules such as ROS and NO production, levels of Krebs cycle metabolites (such as fumarate or succinate) and intracellular concentrations of iron[198]. We were not able to demonstrate the presence of a substantial hypoxia in *B. abortus*-infected cells using the hypoxia marker EF-5 (**Figure 18** and Supplementary Figure 1), or at least to levels compatible with HIF-1α stabilisation.

During the course of the study, a paper reported that succinate-dependent mtROS in response to STING stimulation production is responsible for *B. abortus*-induced HIF-1α stabilisation in primary BMDM[203]. However, in our experimental conditions this possibility can be most likely ruled out due to the total inability of mitochondria-targeted antioxidant (**Figure 20**) or general anti-oxidants (Supplementary Figure 1) to reduce *B. abortus*-induced HIF-1α stabilisation in HeLa cells. HIF-1α stabilisation following *B. abortus* infection can thus apparently not simply be explained by an inflammatory HIF-1α stabilisation as a general response to bacterial infections[287]. This assumption is supported by the lack of effect of the inhibition of HIF-1α through iron treatment on *B. abortus* proliferation as assessed by CFU numbers (**Figure 25**). This would nevertheless need to be confirmed in BMDM.

In consequence, our current hypothesis to explain *B. abortus*-induced HIF-1α stabilisation is a putative reduction in intracellular free iron concentrations. The direct monitoring of intracellular Fe is complicated in our experimental conditions as the microscope resolution available for live microscopy in biosafety level 3 conditions (Eclipse Ti2, Nikon, see **Figure 19**) is too low to obtain exploitable micrographies with Ferro-Orange staining (data not shown). Alternatively, an increase in IRP1/2 stability[288] (the master regulators of the iron starvation response), a decrease in ferritin levels or an increase in surface expression of the TfR1 would indirectly demonstrate that the host cells face an iron starvation stress during *B. abortus* infection (see **Figure 14** in the introduction)[216]. The next step would thus be to determine whether this is a host or a bacteria induced phenomenon or, even more probably, a combination of both. Indeed, it is perfectly conceivable that the massive intracellular proliferation of *B. abortus* would lead at a moment to the depletion of intracellular iron stores.

In addition, in response to intracellular bacterial infection, the host reduces intracellular iron levels to limit bacterial growth[206,213]. Accordingly, RAW 264.7 macrophage-like cells up-regulates ferroportin mRNA levels at 24 h p.i. in response to *B. abortus* infection leading to increased protein levels at 48 h p.i. leading to reduced intracellular iron concentrations[231]. A proteomic study done on samples extracted from *B. abortus*-infected J774 macrophages at 48 h p.i. also revealed that *Brucella* face an iron starvation stress and upregulates its iron import mechanisms[234], a response correlated with ferroportin expression[231]. Even if data on earlier time

point is lacking, the bacteria does apparently not face an iron starvation stress before 48 h p.i., or, at least, not to a sufficient extent to prevent the important proliferation observed inside HeLa cells. It might nevertheless be interesting to monitor ferroportin protein abundance in *B. abortus*-infected HeLa cells to determine whether the host immune response could be implicated in HIF-1α stabilisation in our experimental conditions.

4.2. Relationship between *B. abortus*-induced HIF-1α stabilisation, BNIP-3L abundance and mitochondrial fragmentation/mitophagy

Currently, we suppose that the mitochondrial fragmentation serve as a prerequisite step for mitophagy as the mitochondria colocalises with LC3B in *B. abortus*-infected cells (see introduction **Figure 10.e**) (Jeremy Verbeke, ongoing PhD thesis, unpublished data). However, this evidence is quite indirect, so the induction of mitophagy in *B. abortus*-infected cells will be confirmed by using a Fis1-GFP-mCherry construct[249]. This construct allow to discriminate the mitochondria fragments (as Fis1 is an OMM protein) being degraded in the lysosomes from the rest of mitochondrial network because GFP fluorescence is quenched by acidic conditions[249]. If the intensity of red fluorescence is stronger in *B. abortus*-infected cells, it would confirm the induction of mitophagy in infected-cells.

In addition to induce HIF-1α stabilisation and BNIP-3L expression[189,195], iron chelators including DFO were also reported to induce Parkin-independent mitophagy[249–251,256] which led us to hypothetise that both events could be mechanistically linked during *B. abortus* infection. Strikingly however, iron supplementation-mediated inhibition of *B. abortus*-induced HIF-1α stabilisation (**Figure 22**) and BNIP-3L expression (**Figure 28**) did not negatively affect *B. abortus*-induced mitochondrial fragmentation (**Figure 26**) and LC3-mitochondria co-localisation (**Figure 27**). This is in apparent contradiction with the fact that the silencing of BNIP-3L expression by the siRNA approach significantly prevents *B. abortus*-induced mitochondrial fragmentation (**Figure 29**, Lisa Martin, master thesis, 2022). To add another layer of complexity, encouraging preliminary data indicate that supplementation of *B. abortus*-infected HeLa cells with the iron-loaded form of the mammalian siderophore 2,5-DHBA partially prevents *B. abortus*-induced mitochondrial fragmentation, this time supporting a causal role of mitochondrial iron levels in the induction of a putative mitophagy.

Unfortunately, we do not have currently a full comprehensive hypothesis to explain these discrepancies. For the reasons exposed in the section 3.3.4., an aspecific effect linked to iron supplementation might, as it might not, be responsible for the opposite effects obtained on *B. abortus*-induced mitochondrial fragmentation between iron-mediated and siRNA-mediated BNIP-3L suppression. Importantly, both BNIP-3L deficiency and holo-2,5-DHBA supplementation induce a partial restoration of mitochondrial network morphology possibly indicating that both mechanisms are involved in independent pathways leading to mitophagy. These two different mechanisms might be a consequence of two overlapping stress induced by *B. abortus*-induced infection: namely a generalised iron stress, which induce HIF-1α-dependent BNIP-3L expression, and a mitochondria-specific iron stress that induces a still unidentified mitochondrial fragmentation/mitophagy pathway.

We can then postulate that the reduction of BNIP-3L expression following iron supplementation was inefficient to prevent mitochondrial fragmentation and/or mitophagy because, even if this was able to restore *B. abortus*-induced general iron deficit, it could not recover the mitochondria-specific iron deficit, possibly due to impaired mitochondrial iron import through the 2,5-DHBA pathway. In that case, BNIP-3L absence would be compensated by the other, unidentified, mitochondrial fragmentation mechanism induced by the

mitochondrial iron stress. However, this should also be observed after siRNA-mediated BNIP-3L silencing.

Importantly, the major difference between these two approaches is that, with the siRNA approach, HIF-1α stabilisation is probably maintained while HIF-1α is not stabilised anymore in response to iron supplementation situation. As previously suggested (see section 3.3.4.), it would be interesting to determine whether specific siRNA-mediated depletion of HIF-1α in *B. abortus*-infected cells does phenocopy BNIP-3L deficiency on mitochondrial network morphology. This would allow us to determine whether the conservation of *B. abortus*-induced mitochondrial fragmentation and increase in LC3-mitochondria colocalisation following iron supplementation is due to non-specific effect(s) of the treatment.

In addition, it would be interesting to follow the non-infected cells in close proximity to *B. abortus*-infected cells that present a nuclear HIF-1α staining to determine if it is associated with an increase in BNIP-3L expression. If that's the case, we could determine if BNIP-3L expression is sufficient to induce mitochondrial fragmentation and/or mitophagy on its own or if BNIP-3L action required a specific micro-environment only present in *B. abortus*-infected cells.

Strikingly, the possibility of two mitochondrial fragmentation pathways co-existing during *B. abortus* infection was already proposed based on data generated previously by our team [178]. Indeed, even if *Brucella* was able to induce mitochondrial fragmentation in DRP1 KO cells, it is to a lesser extent than in WT cells, at least for the AR. These results suggest that both a DRP1-independent and a DRP1-dependent pathway seems to be induced by *Brucella*[178]. Furthermore, in the case of chemical hypoxia-induced mitophagy (by treating HeLa cells with $CoCl_2$), it was reported that the double KO of BNIP3 and BNIP-3L only partially prevents mitophagy induction[180]. These results nicely show that a several different mitophagy pathways can be activated at the same time and that BNIP3/BNIP-3L are only contributors in addition to other, BNIP3 and BNIP-3L-independent, mitophagy receptors such as FUNDC1[117] and FKBP8[289].

Indeed, based on the literature, BNIP-3L might not be the only effector of *B. abortus*-induced mitochondrial fragmentation as it been shown to be dependent on DRP1 in muscles cells and keratinocytes[126,290]. Mechanistically, ER-located BNIP-3L was shown to induce calcium (Ca) release from ER stores leading to the dephosphorylation and activation of DRP1 by the calcium-dependent phosphatase PPP3CA[290]. Importantly, in HeLa cells, calcium-dependent activation of DRP1 is also present and was associated with Ca^{2+}/calmodulin-dependent protein kinase 1α (CaMK1α)[291]. It would thus maybe be interesting to monitor whether the siRNA-mediated depletion of BNIP-3L is still able to prevent *B. abortus*-induced mitochondrial fragmentation in DRP1 KO cells.

In addition, different other mechanisms have been identified in the case of iron chelation-induced mitophagy. A very interesting candidate to constitute the potential effector of *B. abortus*-induced DRP1 independent mitochondrial fragmentation is FKBP8. FKBP8 was effectively shown to induce mitochondrial fragmentation (and mitophagy) following iron chelator treatment (DFP) in HeLa cells independently of DRP1[131]. In contrast, in DFO-treated HeLa cells, mitophagy was completely dependent on FUNDC1[251]. DFO triggered an impairment of Fe-S cluster synthesis leading to an IRP1 response. IRP1 mRNA-binding activity was shown to be essential for the activation FUNDC1, mediated by the phosphatase PGAM5[251]. Importantly, FUNDC1-mediated mitophagy is dependent on DRP1-mediated mitochondrial fission[129,292,293]. Interestingly, some parallels can be made between BNIP-3L and FUNDC1 as the latter was also shown to promote Ca release from the ER upon overexpression in

cardiomyocytes[294]. FUNDC1 was also reported to be important for MAM integrity[294]. However, they seem to be involved in separate independent pathways as the overexpression of either FUNDC1 or BNIP-3L rescue hypoxia-induced mitophagy in FUNDC1 + BNIP-3L double KD HeLa cells[295].

In addition to a deficit in Fe-S cluster synthesis[251], mitochondrial fragmentation could be induced by a deficit in heme synthesis, as it was recently reported for yeast cells treated with an inhibitor of ALAS enzymes (see introduction Figure 13)[296]. We might thus hypothetise that *B. abortus*-induced mitochondrial fragmentation is partly linked to an impairment of heme synthesis due to altered mitochondrial iron import, an hypothesis that could easily be tested by supplementing *B. abortus*-infected HeLa cells with hemin before monitoring mitochondrial morphology.

Interestingly, PGAM5 mediated activation of FUNDC1 in HeLa cells relies on particularly interesting actor called Syntaxin 17 (STX17, an ER-resident SNARE protein)[297]. STX17 was also associated with a new mitophagy pathway as its overexpression inducing a BNIP-3L/Parkin/FUNDC1-independent mitophagy in HeLa cells invalidated for Fis1[298]. An important observation is that the mitophagy induced by STX17 overexpression in Fis1 KO[298] or DFP-induced mitophagy[249] are both linked to a decrease in OXPHOS activity. Importantly, the extent of mitophagy induction is strongly reduced when the cells are forced to rely on OXPHOS for energy generation in galactose-containing media[249,298]. Furthermore, 2,5-DHBA deficiency in a zebrafish embryo mutated for the enzyme responsible for its synthesis (Bdh2) also results in a decreased respiratory activity and the induction of mitophagy[281].

As the reduction in OXPHOS activity seem to be a common point between these different form of mitophagy, we will test in the near future whether incubating *B. abortus*-infected cells in galactose-containing media might reduce the induction of mitophagy (monitored by the Fis1-GFP-mCherry construct) to potentially link *B. abortus*-induced mitophagy with DFP-induced mitophagy[249]. Depending on the results, that kind of experiments could also indicate a putative involvement STX17 in *B. abortus*-induced mitophagy that could be further tested.

4.3. *B. abortus* and the mitochondria: a battle for iron acquisition

This work ended on the encouraging observation that the supplementation of *B. abortus*-infected HeLa cells with the mammalian siderophore 2,5-DHBA prevents, at least partly, the fragmentation of the mitochondrial network (**Figure 32**). The presence of 2,5-DHBA has been causally related with mitochondrial iron import[246], an observation that we confirmed by using the LIP-sensitive fluorescent probe Ferro-Orange (**Figure 30**). If 2,5-DHBA effect is confirmed, the next step would naturally be to determine the respective contribution of the host and the pathogen in the depletion of intracellular concentrations of 2,5-DHBA. Naturally, it is tempting to speculate that *B. abortus* is generating a 2,5-DHBA deficit resulting from its consumption as it has been observed during *E. Coli* infection of mice[247].

This exciting discovery would be another argument in support of the endosymbiotic theory, emphasizing the mitochondria and *Brucella* as distant relatives. The importance of these monocatecols for iron metabolism is also exemplified in the remarkable functional conservation of the enzymes responsible for 2,3-DHBA and 2,5-DHBA, the bacterial enzyme EntA and its mammalian homolog Bdh2, respectively[246]. Indeed, in a nice demonstration, Devireddy and colleagues showed that Bdh2 is able to synthesise, in addition to 2,5-DHBA, the bacterial siderophore 2,3-DHBA[246]. In addition, due to their high structural similarity, the 2,3-DHBA transporter in *E. Coli* was able to mediate 2,5-DHBA import during *in vitro* culture[247]. 2,3-

DHBA was the first siderophore identified for *B. abortus*[299] but 2,3-DHBA is more likely to be acting as a precursor in the synthesis of a more complex siderophore: brucebactin (**see Figure 15.a in the introduction**)[228]. This supports the hypothesis that *B. abortus* might consume host-derived 2,5-DHBA during infection thanks to the transporter initially dedicated to 2,3-DHBA transport. This kind of siderophore "piracy" could constitute an evolutive advantage for *B. abortus* as it would spare the energetic cost associated with the *de novo* synthesis of 2,3-DHBA[227]. One single paper has explored the mechanisms of 2,3-DHBA transport in *B. abortus* in which the authors identified the ABC transporter DstC, also called fatC (**see Figure 15.b in the introduction**)[228], as important for 2,3-DHBA import[236]. In the future, it will be important to determine whether 2,5-DHBA supplementation could promote the growth of *B. abortus* and a *fatC* mutant not only *in vitro* under iron deficient conditions but also during intracellular infection. If the *fatC* mutant has a reduced ability to use 2,5-DHBA as a nutrient source, it should also limit the ability of *B. abortus* to cause mitochondrial fragmentation in infected cells.

Unfortunately, the function of 2,3-DHBA and/or brucebactin production for *B. abortus* virulence is ambiguous as a mutant unable to synthesise 2,3-DHBA has a reduced ability to cause abortion in pregnant ruminants[228,300] but has a similar ability to cause chronic infection in mice[301]. Interestingly, these mutants would probably still be able to import 2,3-DHBA or, as we suspect, 2,5-DHBA present in the host cells. It would then be interesting to monitor whether a 2,5-DHBA import mutant is attenuated during chronic infection of mice. However, a *fatC* mutant, that is supposedly deficient 2,5-DHBA import, was not attenuated during mice infection[236]. This finding could be explained by the hypothesis that 2,5-DHBA can promote, but is not necessary for *B. abortus* growth. Indeed, *Brucella* was found to use other iron sources such as heme[239] or Fe^{2+} [240] that have been shown to be required for the establishment of chronic infection in the spleens of mice contrary to 2,3-DHBA. We could then envisage *B. abortus* as an opportunistic bacteria that could consume 2,5-DHBA if it is present but mainly rely on other iron sources in its absence.

Perhaps, 2,5-DHBA might not even constitute an available iron source for *B. abortus* as it was shown that 2,5-DHBA production was also subjected to the nutritional immunity imposed by the host during bacterial infection[247]. Indeed, TLR stimulation, including the TLR2, 9 and 4, that have been linked with *Brucella* infection[31,33,34,36], induce a downregulation of *bhd2* expression, the gene encoding the Bdh2 enzyme, inducing a reduction of 2,5-DHBA levels in the liver of *E. Coli* and *S. aureus*-infected mice [247]. Furthermore, induction of ER stress, by the chemical inhibitor of protein glycosylation tunicamycin, led to a reduction in *bdh2* expression in THP-1 human macrophages-like cells[280]. This could provide an interesting link between *Brucella* infection and 2,5-DHBA deficiency. Indeed, *Brucella* is known to induce an ER-UPR during intracellular infection of both HeLa cells and macrophages at least for the IRE1 branch of the ER-UPR[64,65,172,302], that has also been observed in our model of infection of HeLa cells with *B. abortus* (Lisa Martin, unpublished data, master thesis, 2022). The putative 2,5-DHBA deficiency present during *B. abor*tus infection might thus also be linked to the host nutritional immunity or involve both host and bacteria-derived components.

To decipher between these two possibilities, it might be informative to monitor Bdh2 expression levels in *B. abortus*-infected cells to uncover a potential involvement of host nutritional immunity mechanisms causing Bdh2 down-expression. In addition, the reduction of the ER-UPR by the use of tauroursodeoxycholic acid (TUDCA), a chemical chaperone that downregulates the UPR[65,172], might allow to determine if *B. abortus*-induced UPR could diminish Bdh2 abundance and thus, possibly, mitochondrial fragmentation and/or mitophagy. We could also impair the host TLR-mediated signalling responsible for Bdh2 by targeting the transcriptional repressor B lymphocyte-induced maturation protein-1 (BLIMP) that has been reported to be responsible for LPS-induced 2,5-DHBA depletion[247]. Finally, it will be important

to confirm those finding *in vivo* by determining whether supplementation of mice with 2,5-DHBA increases susceptibility to *B. abortus* infection as it was previously demonstrated for *E. coli*[247].

4.4. Putative functions of *B. abortus*-induced mitochondrial fragmentation and mitophagy

Determining the functional impact that the *B. abortus*-induced mitochondrial fragmentation and mitophagy could have during intracellular infection will be a fundamental part of the future of the project. Different hypothesises can be proposed: (i) mitophagy could limit the induction of inflammatory pathways, (ii) mitophagy might constitute a quality control mechanism to increase the host cell survival upon infection and thus bacterial survival.

4.4.1. Downregulation of inflammatory responses

As exposed in the introduction (see section 1.4.4.3.), the induction of mitochondrial fragmentation and mitophagy were both associated with a reduced activation of the inflammasome and subsequent reduced IL-1β secretion by macrophages [170,174,176,303]. As IL-1β was demonstrated to be a protective cytokine for the host during *B. abortus* infection, the possibility remain that *B. abortus*-induced mitophagy might downregulate the innate immune response and contribute to the "stealthy" behaviour of the pathogen. Accordingly, a paper reported that *B. abortus*-induced LC3B and general autophagy was associated with the inhibition of M1 polarisation and secretion of pro-inflammatory cytokines (IL-1β, TNF-α) in primary macrophages[304]. Furthermore, BNIP-3L-dependent mitophagy was shown to reduce IFN-β production through the MAVS pathway[305].

4.4.2. Protective mechanism against the mitochondrial dysfunction induced by iron depletion stress.

Several studies showed that iron chelators treatment induce a progressive decrease in OXPHOS activity in different cell types[249,250]. This was associated with a minor increase in the number of depolarised mitochondria in mammalian cells[249,250]. However, in the yeast *C. glabrata*, the inhibition of mitophagy upon iron starvation strongly decreased the polarisation state of the mitochondrial population suggesting that induction of mitophagy is a quality control mechanism in response to the mitochondrial stress induced by iron starvation[306]. Accordingly, a small increase in mtROS production is observed after iron chelator treatment[249,251] that is increased upon interference with the FUNDC1-dependent mitophagy in HeLa cells leading to an increase in protein carbonylation, indicative of an oxidative stress[251]. We thus propose that the putative mitophagy mechanism(s) involved in *B. abortus*-induced mitochondrial fragmentation and/or mitophagy is a quality control mechanism that counteracts the mitochondrial iron stress observed during infection. In that way, mitophagy would favour the survival of the *B. abortus*-infected host cell. If this assumption is true, the interference with mitochondrial fragmentation and/or mitophagy by depleting BNIP-3L should lead to an increase in mtROS production that could be monitored with mito-SOX (**Figure 19**). Subsequently, we could use siRNA-mediated depletion of BNIP-3L to uncover a potential role of the mitophagy in the host cell survival by monitoring apoptosis induction[307,308].

In addition, a putative reduction of oxidative stress mediated by mitophagy induction might also contribute to intracellular *Brucella* survival. As exposed in the introduction (see section 1.4.4.), mitochondria emerged as important contributor to the anti-microbial defences

of macrophages against invading pathogens[153,154]. Importantly, anti-bacterial mtROS during bacterial infection relies on the activation of the IRE1 pathway of the UPR in infected macrophages[154]. As already mentioned, *Brucella* is well known to induce IRE1 signaling in both HeLa cells and macrophages[64,172,302]. However, the exact role of IRE1 activation is still controversial, as some authors reported that IRE1 inhibition totally impairs *B. abortus* and *B. melitensis* replication in both HeLa and macrophages cells[109,172,302,309] while IRE1 absence does not modulate *B. abortus* replication in similar cell types[64,310] including in our experimental conditions (Lisa Martin, master thesis, 2022). Mechanistically, the *B. abortus*-promoting promoting effect of IRE1 is linked to the activation of host AMPK [108] and ULK1[109]. Host AMPK was reported to increase bacterial replication by decreasing NOX-derived ROS production in HeLa cells[108] while ULK1 activity was reported to be essential for the intracellular multiplication of *Brucella* inside macrophages[109]. However, over-activation of IRE1 by a rough attenuated *Brucella* mutant is also associated with the induction of macrophage cell death[155] suggesting a dual role of IRE1 during *Brucella* infection.

In consequence, it seems that IRE1 activation must be tightly modulated by *B. abortus* to promote the parasitism of infected host cells with the downside that IRE1 activation might probably lead to an increase in inflammatory gene expression and mtROS production[154,171] that, if exaggerated, could be detrimental to *B. abortus* long term infection by increasing the immune system response[171,311,312] and contributing to the induction of cell death[155,307] of the host cell. Indeed, *Brucella* was found to inhibit apoptosis induction by several ways [67,308,313–315] showing the importance of the preservation of its replication niche. We therefore propose that *B. abortus*-induced mitophagy is a contributing factor to *B. abortus*-infected cell resistance to apoptosis by acting as a pro-survival mechanism to preserve mitochondrial function during infection. This mechanism could be important for the establishment of a chronic infection in mice by preserving its replication niche and limiting anti-*Brucella* immune response. To test the relevance of this hypothesis, we might compare the ability of rough attenuated *Brucella* strains (such as *B. abortus* RB51) and smooth virulent *Brucella* strains (such as the *B. abortus* 544, used here) to induce mitophagy. Indeed, rough strains were shown to induce the death of infected macrophages to a much greater extent than smooth strains[285] that, we hypothetise, might be linked to a diminished ability of rough strains to induce mitophagy.

In addition, *B. abortus*-induced iron stress might also be linked to apoptosis resistance in infected cells independently of mitophagy, as it will be discussed in the next section.

4.4.3. Preservation of the bacterial replicative niche by the induction of a pro-survival/anti-apoptotic program.

An interesting observation that can be made with *B. abortus*-infected cells, is that a small proportion (about 25%) develops enlarged mitochondria (Supplementary Figure 4) (Jeremy Verbeke, unpublished data, ongoing PhD thesis). Importantly, such enlarged and abnormal mitochondria were already described in the literature when transformed cell lines (including HeLa cells) were exposed to hypoxia[316]. The formation of these enlarged mitochondria are dependent on HIF-1 and its downstream target genes such as BNIP-3 and BNIP-3L[316] which could thus be involved in *B. abortus*-induced formation of enlarged mitochondria. Strikingly, these mitochondria stay polarised, functional and protects the cell from apoptosis induction[316]. The formation of these enlarged mitochondria can be induced by down-regulating the different components of the iron-sulfure cluster (ISC) machinery (ISCU or NFS1 see introduction **Figure 13**) and also by repressing the mitochondrial iron importer MFR2[317]. Furthermore, hypoxia is likely to induce mitochondrial enlargement by downregulating the expression of the genes encoding several components of the ISC machinery

such as ISCU, cysteine desulfurase NFS1 and frataxin (FXN) in a manner dependent on HIF-1 activity[317]. These observations raise the following attractive idea: *B. abortus*-induced mitochondrial iron stress in infected HeLa cells might be responsible for the formation of enlarged mitochondria (**see Supplementary Figure 4**). These enlarged mitochondria are quite rare at 48 h p.i. in infected-HeLa cells but this number increase by 72 h p.i. (Jeremy Verbeke, unpublished data, ongoing PhD thesis) so we could assume that the number of *B. abortus*-infected HeLa cells presenting enlarged mitochondria should increase as the infection proceeds.

Importantly, these enlarged mitochondria are associated with apoptosis resistance and might thus favour the conservation of the replication niche of *Brucella* during intracellular infection, thereby promoting chronic and lasting infection in mice[25]. As BNIP3/BNIP-3L function is associated with the apparition of the enlarged mitochondria[316], we could determine if BNIP-3L expression is also involved in the apparition of this phenotype in the case *B. abortus* intracellular infection. Furthermore, it would be interesting to determine if enlarged mitochondria can be observed in the spleen of infected mice during chronic infection.

The link between ISC machinery down-regulation and the appareance of the enlarged mitochondria was shown to rely on a Fe_2-S_2 cluster protein called CDGSH iron-sulfur domain protein 2 (CISD2)[317]. This protein, also called NAF-1 or Miner1, is an ER-resident protein localised at the MAM[318] that is necessary for normal mitochondrial function[319] and that is causing the disease Wolfram syndrome when mutated[320]. It is part of a larger group of Fe-S protein, the NEET proteins, that also comprises CISD1 (also called mitoNEET) and the less studied CISD3 (also called miNT)[321,322]. NEET proteins attracted much attention lately because they were found to play a central role in ROS, calcium and iron metabolism[321,322]. They have been proposed to act as iron sensors inside cells, especially CISD1 whose Fe-S cluster is very labile and sensitive to iron depletion, such as following a DFO treatment[323]. Importantly, the destabilisation of CISD1 Fe-S cluster was shown to induce a fragmentation of the mitochondrial network[324]. Ultrastructure observation by transmission electron microscopy revealed that the effect of CISD1 destabilisation on mitochondrial network morphology was not linked to a modification of the fusion/fission balance but rather due to a disruption of close sites of apposition between adjacent mitochondria called intermitochondrial junctions (IMJ)[324]. We could therefore hypothesise that *B. abortus*-induced iron depletion negatively affects Fe-S cluster synthesis leading to CISD1 destabilisation that could be involved in the fragmentation of the mitochondrial network observed during infection of HeLa cells. Destabilisation of CISD1 by 50 µM DFO was observed to induce a sharp downregulation of CISD1 protein levels within 24 h of treatment[323], so we would be able to see a down-regulation of CISD1 protein levels in *B. abortus*-infected HeLa cells after 48 h of infection. Subsequently, by overexpressing a mutant form of CISD1 unable to lose its Fe-S cluster[324], we could determine whether this protein is involved in *B. abortus*-induced mitochondrial fragmentation or not.

Finally, exploring the role of NEET proteins during intracellular *B. abortus* infection might establish the missing link between iron metabolism, the induction of a mitochondrial stress, and calcium metabolism that was reported to be tightly linked with BNIP-3L ability to induce mitochondrial fragmentation[290]. Especially, CISD2, that localises at the MAM, was found to form a macromolecular complex with the inositol-triphosphate receptor channel (IP3R)[325], a calcium channel essential for Ca signalling at the ER-mitochondria contact sites[322]. CISD2 KD was effectively shown to induce an increase in cytosolic calcium concentrations that can induce calcium-activated signalling[326]. As BNIP-3L-mediated mitochondrial fragmentation was linked with its ER localisation, IP3R function, Ca release and DRP1 activation by a calcium-activated phosphatase[290], the CISD2 pathway might be relevant to BNIP-3L function in *B. abortus*-infected cells.

4.5. General conclusion

At the end, this master thesis increased our understanding of the intracellular events associated with intracellular *B. abortus* infection and especially its effect on the host cell. Indeed, this work highlighted the critical role of iron in the induction of a major signalling pathway of the host, i.e. the stabilisation of HIF-1α. Furthermore, encouraging preliminary results indicate that *Brucella* might trigger dysfunction of host's mitochondria by disrupting mitochondrial iron import through the mammalian siderophore 2,5-DHBA. If these results are confirmed, it could constitute an original finding in the context of *Brucella* infection that would, once again, highlight the remarkable evolutionary conservation of some molecular pathways between old relatives that are *Brucella* and the mitochondria. Due to the importance of this siderophore in the mice susceptibility to other bacterial infections[247], this work could constitute a first step towards the understanding of a new virulence mechanism of *Brucella*. Indeed, as the intracellular lifestyle of this pathogen is thought to be tightly linked with its virulence, a greater knowledge of the molecular actors linked to the ability of *B. abortus* to establish and maintain over time its replicative niche might contribute to the design of new and innovative therapies for this highly debilitating and long lasting disease.

5. References

1. Pappas, G., Papadimitriou, P., Akritidis, N., Christou, L. & Tsianos, E. V. The new global map of human brucellosis. *Lancet Infect Dis* **6**, 91–99 (2006).

2. Byndloss, M. X. & Tsolis, R. M. Brucella spp. Virulence Factors and Immunity. *Annual Review of Animal Biosciences* **4**, 111–127 (2016).

3. Dean, A. S. *et al.* Clinical Manifestations of Human Brucellosis: A Systematic Review and Meta-Analysis. *PLOS Neglected Tropical Diseases* **6**, e1929 (2012).

4. Nejad, R. B., Krecek, R. C., Khalaf, O. H., Hailat, N. & Arenas-Gamboa, A. M. Brucellosis in the Middle East: Current situation and a pathway forward. *PLOS Neglected Tropical Diseases* **14**, e0008071 (2020).

5. Dadar, M., Shahali, Y. & Whatmore, A. M. Human brucellosis caused by raw dairy products: A review on the occurrence, major risk factors and prevention. *Int J Food Microbiol* **292**, 39–47 (2019).

6. Khurana, S. K. *et al.* Bovine brucellosis – a comprehensive review. *Veterinary Quarterly* **41**, 61–88 (2021).

7. Suárez-Esquivel, M., Chaves-Olarte, E., Moreno, E. & Guzmán-Verri, C. Brucella Genomics: Macro and Micro Evolution. *International Journal of Molecular Sciences* **21**, 7749 (2020).

8. Olsen, S. C. & Palmer, M. V. Advancement of Knowledge of Brucella Over the Past 50 Years. *Vet Pathol* **51**, 1076–1089 (2014).

9. Archambaud, C. *et al.* Contrasting roles of macrophages and dendritic cells in controlling initial pulmonary Brucella infection. *Eur J Immunol* **40**, 3458–3471 (2010).

10. Demars, A. *et al.* Aconitate decarboxylase 1 participates in the control of pulmonary Brucella infection in mice. *PLoS Pathog* **17**, e1009887 (2021).

11. de Figueiredo, P., Ficht, T. A., Rice-Ficht, A., Rossetti, C. A. & Adams, L. G. Pathogenesis and Immunobiology of Brucellosis: Review of Brucella–Host Interactions. *The American Journal of Pathology* **185**, 1505–1517 (2015).

12. Anderson, T. D. & Cheville, N. F. Ultrastructural morphometric analysis of Brucella abortus-infected trophoblasts in experimental placentitis. Bacterial replication occurs in rough endoplasmic reticulum. *Am J Pathol* **124**, 226–237 (1986).

13. Salcedo, S. P. *et al.* Pathogenic Brucellae Replicate in Human Trophoblasts. *The Journal of Infectious Diseases* **207**, 1075–1083 (2013).

14. Roop, R. M., Gaines, J. M., Anderson, E. S., Caswell, C. C. & Martin, D. W. Survival of the fittest: how Brucella strains adapt to their intracellular niche in the host. *Med Microbiol Immunol* **198**, 221–238 (2009).

15. Celli, J. The Intracellular Life Cycle of Brucella spp. in *Bacteria and Intracellularity* 101–111 (John Wiley & Sons, Ltd, 2019). doi:10.1128/9781683670261.ch7.

16. Price, J. V. & Vance, R. E. The Macrophage Paradox. *Immunity* **41**, 685–693 (2014).

17. Murray, P. J. & Wynn, T. A. Protective and pathogenic functions of macrophage subsets. *Nat Rev Immunol* **11**, 723–737 (2011).

18. Kawai, T. & Akira, S. Toll-like Receptors and Their Crosstalk with Other Innate Receptors in Infection and Immunity. *Immunity* **34**, 637–650 (2011).

19. Blander, J. M. & Sander, L. E. Beyond pattern recognition: five immune checkpoints for scaling the microbial threat. *Nat Rev Immunol* **12**, 215–225 (2012).

20. Smith, J. A. STING, the Endoplasmic Reticulum, and Mitochondria: Is Three a Crowd or a Conversation? *Frontiers in Immunology* **11**, 3556 (2021).

21. Kaufmann, S. H. E. & Dorhoi, A. Molecular Determinants in Phagocyte-Bacteria Interactions. *Immunity* **44**, 476–491 (2016).

22. Weiss, G. & Schaible, U. E. Macrophage defense mechanisms against intracellular bacteria. *Immunological Reviews* **264**, 182–203 (2015).

23. Ortega-Gómez, A., Mauro, P. & Soehnlein, O. Resolution of inflammation: an integrated view. *EMBO Molecular Medicine* **5**, 661–674 (2013).

24. Shapouri-Moghaddam, A. *et al.* Macrophage plasticity, polarization, and function in health and disease. *Journal of Cellular Physiology* **233**, 6425–6440 (2018).

25. Köhler, S., Michaux-Charachon, S., Porte, F., Ramuz, M. & Liautard, J.-P. What is the nature of the replicative niche of a stealthy bug named Brucella? *Trends in Microbiology* **11**, 215–219 (2003).

26. Jiménez de Bagüés, M. P., Gross, A., Terraza, A. & Dornand, J. Regulation of the Mitogen-Activated Protein Kinases by Brucella spp. Expressing a Smooth and Rough Phenotype: Relationship to Pathogen Invasiveness. *Infection and Immunity* **73**, 3178–3183 (2005).

27. Barquero-Calvo, E. *et al.* Brucella abortus Uses a Stealthy Strategy to Avoid Activation of the Innate Immune System during the Onset of Infection. *PLOS ONE* **2**, e631 (2007).

28. Ko, J., Gendron-Fitzpatrick, A. & Splitter, G. A. Susceptibility of IFN regulatory factor-1 and IFN consensus sequence binding protein-deficient mice to brucellosis. *J Immunol* **168**, 2433–2440 (2002).

29. Murphy, E. A., Sathiyaseelan, J., Parent, M. A., Zou, B. & Baldwin, C. L. Interferon-gamma is crucial for surviving a Brucella abortus infection in both resistant C57BL/6 and susceptible BALB/c mice. *Immunology* **103**, 511–518 (2001).

30. Wang, M., Qureshi, N., Soeurt, N. & Splitter, G. High levels of nitric oxide production decrease early but increase late survival of Brucella abortus in macrophages. *Microbial Pathogenesis* **31**, 221–230 (2001).

31. Gomes, M. T. *et al.* TLR9 is required for MAPK/NF-κB activation but does not cooperate with TLR2 or TLR6 to induce host resistance to Brucella abortus. *Journal of Leukocyte Biology* **99**, 771–780 (2016).

32. Macedo, G. C. *et al.* Central role of MyD88-dependent dendritic cell maturation and proinflammatory cytokine production to control Brucella abortus infection. *J Immunol* **180**, 1080–1087 (2008).

33. Copin, R., De Baetselier, P., Carlier, Y., Letesson, J.-J. & Muraille, E. MyD88-dependent activation of B220-CD11b+LY-6C+ dendritic cells during Brucella melitensis infection. *J Immunol* **178**, 5182–5191 (2007).

34. Campos, M. A. *et al.* Role of Toll-Like Receptor 4 in Induction of Cell-Mediated Immunity and Resistance to Brucella abortus Infection in Mice. *Infection and Immunity* **72**, 176–186 (2004).

35. Weiss, D. S., Takeda, K., Akira, S., Zychlinsky, A. & Moreno, E. MyD88, but Not Toll-Like Receptors 4 and 2, Is Required for Efficient Clearance of Brucella abortus. *Infection and Immunity* **73**, 5137–5143 (2005).

36. Giambartolomei, G. H. *et al.* Lipoproteins, Not Lipopolysaccharide, Are the Key Mediators of the Proinflammatory Response Elicited by Heat-Killed Brucella abortus. *The Journal of Immunology* **173**, 4635–4642 (2004).

37. Gomes, M. T. R. *et al.* Critical Role of ASC Inflammasomes and Bacterial Type IV Secretion System in Caspase-1 Activation and Host Innate Resistance to Brucella abortus Infection. *The Journal of Immunology* **190**, 3629–3638 (2013).

38. Terwagne, M. *et al.* Innate immune recognition of flagellin limits systemic persistence of Brucella. *Cellular Microbiology* **15**, 942–960 (2012).

39. Bouhet, S., Lafont, V., Billard, E., Gross, A. & Dornand, J. The IFNγ-induced STAT1-CBP/P300 association, required for a normal response to the cytokine, is disrupted in Brucella-infected macrophages. *Microbial Pathogenesis* **46**, 88–97 (2009).

40. Khan, M. *et al.* Brucella suppress STING expression via miR-24 to enhance infection. *PLOS Pathogens* **16**, e1009020 (2020).

41. Salcedo, S. *et al.* BtpB, a novel Brucella TIR-containing effector protein with immune modulatory functions. *Frontiers in Cellular and Infection Microbiology* **3**, 28 (2013).

42. Salcedo, S. P. *et al.* Brucella Control of Dendritic Cell Maturation Is Dependent on the TIR-Containing Protein Btp1. *PLOS Pathogens* **4**, e21 (2008).

43. Bialer, M. G. *et al.* Adhesins of Brucella: Their Roles in the Interaction with the Host. *Pathogens* **9**, 942 (2020).

44. Czibener, C. *et al.* BigA is a novel adhesin of Brucella that mediates adhesion to epithelial cells. *Cellular Microbiology* **18**, 500–513 (2016).

45. Watarai, M., Makino, S., Fujii, Y., Okamoto, K. & Shirahata, T. Modulation of Brucella-induced macropinocytosis by lipid rafts mediates intracellular replication. *Cellular Microbiology* **4**, 341–355 (2002).

46. Porte, F., Naroeni, A., Ouahrani-Bettache, S. & Liautard, J.-P. Role of the Brucella suis Lipopolysaccharide O Antigen in Phagosomal Genesis and in Inhibition of Phagosome-Lysosome Fusion in Murine Macrophages. *Infection and Immunity* **71**, 1481–1490 (2003).

47. Starr, T., Ng, T. W., Wehrly, T. D., Knodler, L. A. & Celli, J. Brucella intracellular replication requires trafficking through the late endosomal/lysosomal compartment. *Traffic* **9**, 678–694 (2008).

48. Celli, J. *et al.* Brucella Evades Macrophage Killing via VirB-dependent Sustained Interactions with the Endoplasmic Reticulum. *Journal of Experimental Medicine* **198**, 545–556 (2003).

49. Sedzicki, J. *et al.* 3D correlative electron microscopy reveals continuity of Brucella-containing vacuoles with the endoplasmic reticulum. *J Cell Sci* **131**, (2018).

50. Miller, C. N. *et al.* A Brucella Type IV Effector Targets the COG Tethering Complex to Remodel Host Secretory Traffic and Promote Intracellular Replication. *Cell Host & Microbe* **22**, 317-329.e7 (2017).

51. de Barsy, M. *et al.* Identification of a Brucella spp. secreted effector specifically interacting with human small GTPase Rab2. *Cellular Microbiology* **13**, 1044–1058 (2011).

52. de Jong, M. F., Sun, Y.-H., den Hartigh, A. B., van Dijl, J. M. & Tsolis, R. M. Identification of VceA and VceC, two members of the VjbR regulon that are translocated into macrophages by the Brucella type IV secretion system. *Mol Microbiol* **70**, 1378–1396 (2008).

53. Marchesini, M. I., Herrmann, C. K., Salcedo, S. P., Gorvel, J.-P. & Comerci, D. J. In search of Brucella abortus type IV secretion substrates: screening and identification of four proteins translocated into host cells through VirB system. *Cellular Microbiology* **13**, 1261–1274 (2011).

54. Myeni, S. *et al.* Brucella Modulates Secretory Trafficking via Multiple Type IV Secretion Effector Proteins. *PLOS Pathogens* **9**, e1003556 (2013).

55. Arriola Benitez, P. C. *et al.* The Effector Protein BPE005 from Brucella abortus Induces Collagen Deposition and Matrix Metalloproteinase 9 Downmodulation via Transforming Growth Factor β1 in Hepatic Stellate Cells. *Infection and Immunity* **84**, 598–606.

56. Borghesan, E. *et al.* A Brucella effector modulates the Arf6-Rab8a GTPase cascade to promote intravacuolar replication. *EMBO J* **40**, e107664 (2021).

57. Luizet, J.-B. *et al.* The Brucella effector BspL targets the ER-associated degradation (ERAD) pathway and delays bacterial egress from infected cells. *PNAS* **118**, (2021).

58. Marchesini, M. I., Morrone Seijo, S. M., Guaimas, F. F. & Comerci, D. J. A T4SS Effector Targets Host Cell Alpha-Enolase Contributing to Brucella abortus Intracellular Lifestyle. *Front. Cell. Infect. Microbiol.* **6**, (2016).

59. Zhang, J. *et al.* Deletion of the Type IV Secretion System Effector VceA Promotes Autophagy and Inhibits Apoptosis in Brucella-Infected Human Trophoblast Cells. *Curr Microbiol* **76**, 510–519 (2019).

60. Coronas-Serna, J. M. *et al.* The TIR-domain containing effectors BtpA and BtpB from Brucella abortus impact NAD metabolism. *PLOS Pathogens* **16**, e1007979 (2020).

61. Porte, F., Liautard, J. P. & Köhler, S. Early acidification of phagosomes containing Brucella suis is essential for intracellular survival in murine macrophages. *Infect Immun* **67**, 4041–4047 (1999).

62. Boschiroli, M. L. *et al.* The Brucella suis virB operon is induced intracellularly in macrophages. *PNAS* **99**, 1544–1549 (2002).

63. Altamirano-Silva, P. *et al.* Brucella abortus Senses the Intracellular Environment through the BvrR/BvrS Two-Component System, Which Allows B. abortus To Adapt to Its Replicative Niche. *Infection and Immunity* **86**, e00713-17 (2018).

64. de Jong, M. F. *et al.* Sensing of bacterial type IV secretion via the unfolded protein response. *mBio* **4**, e00418-00412 (2013).

65. Smith, J. A. *et al.* Brucella induces an unfolded protein response via TcpB that supports intracellular replication in macrophages. *PLoS Pathog* **9**, e1003785 (2013).

66. Smith, E. P., Miller, C. N., Child, R., Cundiff, J. A. & Celli, J. Postreplication Roles of the Brucella VirB Type IV Secretion System Uncovered via Conditional Expression of the VirB11 ATPase. *mBio* **7**, e01730-16 (2016).

67. He, Y. *et al.* Brucella melitensis Triggers Time-Dependent Modulation of Apoptosis and Down-Regulation of Mitochondrion-Associated Gene Expression in Mouse Macrophages. *Infection and Immunity* **74**, 5035–5046 (2006).

68. Czyż, D. M., Willett, J. W. & Crosson, S. Brucella abortus Induces a Warburg Shift in Host Metabolism That Is Linked to Enhanced Intracellular Survival of the Pathogen. *Journal of Bacteriology* **199**, (2017).

69. Fielden, L. F., Kang, Y., Newton, H. J. & Stojanovski, D. Targeting mitochondria: how intravacuolar bacterial pathogens manipulate mitochondria. *Cell Tissue Res* **367**, 141–154 (2017).

70. Lobet, E., Letesson, J.-J. & Arnould, T. Mitochondria: a target for bacteria. *Biochem Pharmacol* **94**, 173–185 (2015).

71. Senft, D. & Ronai, Z. A. UPR, autophagy, and mitochondria crosstalk underlies the ER stress response. *Trends in Biochemical Sciences* **40**, 141–148 (2015).

72. Chakrabarty, R. P. & Chandel, N. S. Mitochondria as Signaling Organelles Control Mammalian Stem Cell Fate. *Cell Stem Cell* **28**, 394–408 (2021).

73. Grasso, D., Zampieri, L. X., Capelôa, T., Velde, J. A. V. de & Sonveaux, P. Mitochondria in cancer. *Cell Stress* **4**, 114–146 (2020).

74. Roger, A. J., Muñoz-Gómez, S. A. & Kamikawa, R. The Origin and Diversification of Mitochondria. *Current Biology* **27**, R1177–R1192 (2017).

75. Pallen, M. J. Time to recognise that mitochondria are bacteria? *Trends in Microbiology* **19**, 58–64 (2011).

76. Khan, S., Raj, D., Jaiswal, K. & Lahiri, A. Modulation of host mitochondrial dynamics during bacterial infection. *Mitochondrion* **53**, 140–149 (2020).

77. Tiku, V., Tan, M.-W. & Dikic, I. Mitochondrial Functions in Infection and Immunity. *Trends in Cell Biology* **30**, 263–275 (2020).

78. Ryan, D. G. & O'Neill, L. A. J. Krebs Cycle Reborn in Macrophage Immunometabolism. *Annual Review of Immunology* **38**, 289–313 (2020).

79. Liesa, M. & Shirihai, O. S. Mitochondrial Dynamics in the Regulation of Nutrient Utilization and Energy Expenditure. *Cell Metabolism* **17**, 491–506 (2013).

80. Kadenbach, B., Ramzan, R., Moosdorf, R. & Vogt, S. The role of mitochondrial membrane potential in ischemic heart failure. *Mitochondrion* **11**, 700–706 (2011).

81. Azzu, V. & Brand, M. D. The on-off switches of the mitochondrial uncoupling proteins. *Trends in Biochemical Sciences* **35**, 298–307 (2010).

82. Heytler, P. G. [58] Uncouplers of oxidative phosphorylation. in *Methods in Enzymology* vol. 55 462–472 (Academic Press, 1979).

83. Brand, M. D. Mitochondrial generation of superoxide and hydrogen peroxide as the source of mitochondrial redox signaling. *Free Radical Biology and Medicine* **100**, 14–31 (2016).

84. Mills, E. L. *et al.* Succinate Dehydrogenase Supports Metabolic Repurposing of Mitochondria to Drive Inflammatory Macrophages. *Cell* **167**, 457-470.e13 (2016).

85. Zorova, L. D. *et al.* Mitochondrial membrane potential. *Analytical Biochemistry* **552**, 50–59 (2018).

86. Schieber, M. & Chandel, N. S. ROS Function in Redox Signaling and Oxidative Stress. *Current Biology* **24**, R453–R462 (2014).

87. Mishra, P. & Chan, D. C. Mitochondrial dynamics and inheritance during cell division, development and disease. *Nat Rev Mol Cell Biol* **15**, 634–646 (2014).

88. Dorn, G. W. Evolving Concepts of Mitochondrial Dynamics. *Annual Review of Physiology* **81**, 1–17 (2019).

89. Kraus, F. & Ryan, M. T. The constriction and scission machineries involved in mitochondrial fission. *Journal of Cell Science* **130**, 2953–2960 (2017).

90. Friedman, J. R. *et al.* ER Tubules Mark Sites of Mitochondrial Division. *Science* **334**, 358–362 (2011).

91. Wong, Y. C., Ysselstein, D. & Krainc, D. Mitochondria–lysosome contacts regulate mitochondrial fission via RAB7 GTP hydrolysis. *Nature* **554**, 382–386 (2018).

92. Escobar-Henriques, M. & Joaquim, M. Mitofusins: Disease Gatekeepers and Hubs in Mitochondrial Quality Control by E3 Ligases. *Front Physiol* **10**, 517 (2019).

93. Ishihara, N., Eura, Y. & Mihara, K. Mitofusin 1 and 2 play distinct roles in mitochondrial fusion reactions via GTPase activity. *Journal of Cell Science* **117**, 6535–6546 (2004).

94. Rambold, A. S., Kostelecky, B., Elia, N. & Lippincott-Schwartz, J. Tubular network formation protects mitochondria from autophagosomal degradation during nutrient starvation. *PNAS* **108**, 10190–10195 (2011).

95. de Brito, O. M. & Scorrano, L. Mitofusin 2 tethers endoplasmic reticulum to mitochondria. *Nature* **456**, 605–610 (2008).

96. Naon, D. *et al.* Critical reappraisal confirms that Mitofusin 2 is an endoplasmic reticulum–mitochondria tether. *PNAS* **113**, 11249–11254 (2016).

97. Sugiura, A. *et al.* MITOL Regulates Endoplasmic Reticulum-Mitochondria Contacts via Mitofusin2. *Molecular Cell* **51**, 20–34 (2013).

98. Chen, H., Chomyn, A. & Chan, D. C. Disruption of Fusion Results in Mitochondrial Heterogeneity and Dysfunction *. *Journal of Biological Chemistry* **280**, 26185–26192 (2005).

99. Mishra, P., Carelli, V., Manfredi, G. & Chan, D. C. Proteolytic Cleavage of Opa1 Stimulates Mitochondrial Inner Membrane Fusion and Couples Fusion to Oxidative Phosphorylation. *Cell Metabolism* **19**, 630–641 (2014).

100. Giacomello, M., Pyakurel, A., Glytsou, C. & Scorrano, L. The cell biology of mitochondrial membrane dynamics. *Nature Reviews Molecular Cell Biology* **21**, 204–224 (2020).

101. Onoue, K. *et al.* Fis1 acts as a mitochondrial recruitment factor for TBC1D15 that is involved in regulation of mitochondrial morphology. *Journal of Cell Science* **126**, 176–185 (2013).

102. Yu, R., Jin, S.-B., Lendahl, U., Nistér, M. & Zhao, J. Human Fis1 regulates mitochondrial dynamics through inhibition of the fusion machinery. *EMBO J* **38**, e99748 (2019).

103. Palikaras, K., Lionaki, E. & Tavernarakis, N. Mechanisms of mitophagy in cellular homeostasis, physiology and pathology. *Nature Cell Biology* **20**, 1013–1022 (2018).

104. Levine, B., Mizushima, N. & Virgin, H. W. Autophagy in immunity and inflammation. *Nature* **469**, 323–335 (2011).

105. Russell, R. C., Yuan, H.-X. & Guan, K.-L. Autophagy regulation by nutrient signaling. *Cell Res* **24**, 42–57 (2014).

106. Egan, D. F. *et al.* Phosphorylation of ULK1 (hATG1) by AMP-Activated Protein Kinase Connects Energy Sensing to Mitophagy. *Science* **331**, 456–461 (2011).

107. Kim, J., Kundu, M., Viollet, B. & Guan, K.-L. AMPK and mTOR regulate autophagy through direct phosphorylation of Ulk1. *Nat Cell Biol* **13**, 132–141 (2011).

108. Liu, N. *et al.* Inositol-Requiring Enzyme 1-Dependent Activation of AMPK Promotes Brucella abortus Intracellular Growth. *J Bacteriol* **198**, 986–993 (2016).

109. Pandey, A. *et al.* Activation of Host IRE1α-Dependent Signaling Axis Contributes the Intracellular Parasitism of Brucella melitensis. *Front Cell Infect Microbiol* **8**, 103 (2018).

110. Hamasaki, M. *et al.* Autophagosomes form at ER–mitochondria contact sites. *Nature* **495**, 389–393 (2013).

111. Hailey, D. W. *et al.* Mitochondria Supply Membranes for Autophagosome Biogenesis during Starvation. *Cell* **141**, 656–667 (2010).

112. Nishimura, T. & Tooze, S. A. Emerging roles of ATG proteins and membrane lipids in autophagosome formation. *Cell Discov* **6**, 1–18 (2020).

113. Mizushima, N., Yoshimori, T. & Ohsumi, Y. The Role of Atg Proteins in Autophagosome Formation. *Annual Review of Cell and Developmental Biology* **27**, 107–132 (2011).

114. Zachari, M. & Ktistakis, N. T. Mammalian Mitophagosome Formation: A Focus on the Early Signals and Steps. *Frontiers in Cell and Developmental Biology* **8**, 171 (2020).

115. Rogov, V. V. *et al.* Phosphorylation of the mitochondrial autophagy receptor Nix enhances its interaction with LC3 proteins. *Scientific Reports* **7**, 1131 (2017).

116. Zhu, Y. *et al.* Modulation of Serines 17 and 24 in the LC3-interacting Region of Bnip3 Determines Pro-survival Mitophagy versus Apoptosis *. *Journal of Biological Chemistry* **288**, 1099–1113 (2013).

117. Liu, L. *et al.* Mitochondrial outer-membrane protein FUNDC1 mediates hypoxia-induced mitophagy in mammalian cells. *Nature Cell Biology* **14**, 177–185 (2012).

118. Nguyen, T. N. *et al.* Atg8 family LC3/GABARAP proteins are crucial for autophagosome–lysosome fusion but not autophagosome formation during PINK1/Parkin mitophagy and starvation. *Journal of Cell Biology* **215**, 857–874 (2016).

119. Vargas, J. N. S. *et al.* Spatiotemporal Control of ULK1 Activation by NDP52 and TBK1 during Selective Autophagy. *Molecular Cell* **74**, 347-362.e6 (2019).

120. Murakawa, T. *et al.* A Mammalian Mitophagy Receptor, Bcl2-L-13, Recruits the ULK1 Complex to Induce Mitophagy. *Cell Rep* **26**, 338-345.e6 (2019).

121. Wu, W. *et al.* ULK1 translocates to mitochondria and phosphorylates FUNDC1 to regulate mitophagy. *EMBO Rep* **15**, 566–575 (2014).

122. Gomes, L. C., Benedetto, G. D. & Scorrano, L. During autophagy mitochondria elongate, are spared from degradation and sustain cell viability. *Nat Cell Biol* **13**, 589–598 (2011).

123. Ikeda, Y. *et al.* Endogenous Drp1 Mediates Mitochondrial Autophagy and Protects the Heart Against Energy Stress. *Circulation Research* **116**, 264–278 (2015).

124. Tanaka, A. *et al.* Proteasome and p97 mediate mitophagy and degradation of mitofusins induced by Parkin. *Journal of Cell Biology* **191**, 1367–1380 (2010).

125. da Silva Rosa, S. C. *et al.* BNIP3L/Nix-induced mitochondrial fission, mitophagy, and impaired myocyte glucose uptake are abrogated by PRKA/PKA phosphorylation. *Autophagy* **0**, 1–16 (2020).

126. Simpson, C. L. *et al.* NIX initiates mitochondrial fragmentation via DRP1 to drive epidermal differentiation. *Cell Reports* **34**, 108689 (2021).

127. Lee, Y., Lee, H.-Y., Hanna, R. A. & Gustafsson, Å. B. Mitochondrial autophagy by Bnip3 involves Drp1-mediated mitochondrial fission and recruitment of Parkin in cardiac myocytes. *American Journal of Physiology-Heart and Circulatory Physiology* **301**, H1924–H1931 (2011).

128. Tol, M. J. *et al.* A PPARγ-Bnip3 Axis Couples Adipose Mitochondrial Fusion-Fission Balance to Systemic Insulin Sensitivity. *Diabetes* **65**, 2591–2605 (2016).

129. Wu, W. *et al.* FUNDC1 regulates mitochondrial dynamics at the ER–mitochondrial contact site under hypoxic conditions. *The EMBO Journal* **35**, 1368–1384 (2016).

130. Wu, W. *et al.* FUNDC1 is a novel mitochondrial-associated-membrane (MAM) protein required for hypoxia-induced mitochondrial fission and mitophagy. *Autophagy* **12**, 1675–1676 (2016).

131. Yoo, S.-M. *et al.* FKBP8 LIRL-dependent mitochondrial fragmentation facilitates mitophagy under stress conditions. *The FASEB Journal* **34**, 2944–2957 (2020).

132. Murakawa, T. *et al.* Bcl-2-like protein 13 is a mammalian Atg32 homologue that mediates mitophagy and mitochondrial fragmentation. *Nat Commun* **6**, 7527 (2015).

133. Youle, R. J. & van der Bliek, A. M. Mitochondrial Fission, Fusion, and Stress. *Science* **337**, 1062–1065 (2012).

134. Xian, H. & Liou, Y.-C. Functions of outer mitochondrial membrane proteins: mediating the crosstalk between mitochondrial dynamics and mitophagy. *Cell Death Differ* **28**, 827–842 (2021).

135. Yamashita, S. *et al.* Mitochondrial division occurs concurrently with autophagosome formation but independently of Drp1 during mitophagy. *Journal of Cell Biology* **215**, 649–665 (2016).

136. Escoll, P. & Buchrieser, C. Metabolic reprogramming of host cells upon bacterial infection: Why shift to a Warburg-like metabolism? *The FEBS Journal* **285**, 2146–2160 (2018).

137. Heiden, M. G. V., Cantley, L. C. & Thompson, C. B. Understanding the Warburg Effect: The Metabolic Requirements of Cell Proliferation. *Science* **324**, 1029–1033 (2009).

138. Mirzaei, R. *et al.* Immunometabolism in human brucellosis: An emerging field of investigation. *Microbial Pathogenesis* **158**, 105115 (2021).

139. Xavier, M. N. *et al.* PPARγ-Mediated Increase in Glucose Availability Sustains Chronic Brucella abortus Infection in Alternatively Activated Macrophages. *Cell Host & Microbe* **14**, 159–170 (2013).

140. Kerrinnes, T. *et al.* Utilization of Host Polyamines in Alternatively Activated Macrophages Promotes Chronic Infection by Brucella abortus. *Infect Immun* **86**, e00458-17 (2018).

141. Gao, Z. *et al.* Mitochondrial dynamics controls anti-tumour innate immunity by regulating CHIP-IRF1 axis stability. *Nat Commun* **8**, 1805 (2017).

142. Zhang, Y. *et al.* Mitoguardin Regulates Mitochondrial Fusion through MitoPLD and Is Required for Neuronal Homeostasis. *Molecular Cell* **61**, 111–124 (2016).

143. Buck, M. D. *et al.* Mitochondrial Dynamics Controls T Cell Fate through Metabolic Programming. *Cell* **166**, 63–76 (2016).

144. Kapetanovic, R. *et al.* Lipopolysaccharide promotes Drp1-dependent mitochondrial fission and associated inflammatory responses in macrophages. *Immunology & Cell Biology* **98**, 528–539 (2020).

145. Mohasin, M. *et al.* Macrophages utilize mitochondrial fission to enhance mROS production during responses to Streptococcus pneumoniae. *bioRxiv* 722603 (2019) doi:10.1101/722603.

146. Campos, P. C. *et al.* Brucella abortus nitric oxide metabolite regulates inflammasome activation and IL-1β secretion in murine macrophages. *European Journal of Immunology* **49**, 1023–1037 (2019).

147. Chowdhury, S. R. *et al.* Chlamydia preserves the mitochondrial network necessary for replication via microRNA-dependent inhibition of fission. *Journal of Cell Biology* **216**, 1071–1089 (2017).

148. Kurihara, Y. *et al.* Chlamydia trachomatis targets mitochondrial dynamics to promote intracellular survival and proliferation. *Cellular Microbiology* **21**, e12962 (2019).

149. Escoll, P. *et al.* Legionella pneumophila Modulates Mitochondrial Dynamics to Trigger Metabolic Repurposing of Infected Macrophages. *Cell Host & Microbe* **22**, 302-316.e7 (2017).

150. Guido, C. *et al.* Mitochondrial Fission Induces Glycolytic Reprogramming in Cancer-Associated Myofibroblasts, Driving Stromal Lactate Production, and Early Tumor Growth. *Oncotarget* **3**, 798–810 (2012).

151. Nair, S. *et al.* Lipopolysaccharide-induced alteration of mitochondrial morphology induces a metabolic shift in microglia modulating the inflammatory response in vitro and in vivo. *Glia* **67**, 1047–1061 (2019).

152. Zhang, L. *et al.* Lipopolysaccharide-induced proliferation and glycolysis in airway smooth muscle cells via activation of Drp1. *Journal of Cellular Physiology* **234**, 9255–9263 (2019).

153. West, A. P. *et al.* TLR signalling augments macrophage bactericidal activity through mitochondrial ROS. *Nature* **472**, 476–480 (2011).

154. Abuaita, B. H., Schultz, T. L. & O'Riordan, M. X. Mitochondria-Derived Vesicles Deliver Antimicrobial Reactive Oxygen Species to Control Phagosome-Localized Staphylococcus aureus. *Cell Host & Microbe* **24**, 625-636.e5 (2018).

155. Li, P. *et al.* Brucella Rough Mutant Induce Macrophage Death via Activating IRE1α Pathway of Endoplasmic Reticulum Stress by Enhanced T4SS Secretion. *Front Cell Infect Microbiol* **7**, 422 (2017).

156. Wiese, M. *et al.* Hypoxia-Mediated Impairment of the Mitochondrial Respiratory Chain Inhibits the Bactericidal Activity of Macrophages. *Infection and Immunity* **80**, 1455–1466 (2012).

157. Oliva-Ramírez, J., Moreno-Altamirano, M. M. B., Pineda-Olvera, B., Cauich-Sánchez, P. & Sánchez-García, F. J. Crosstalk between circadian rhythmicity, mitochondrial dynamics and macrophage bactericidal activity. *Immunology* **143**, 490–497 (2014).

158. Zhang, Y. *et al.* Listeria hijacks host mitophagy through a novel mitophagy receptor to evade killing. *Nature Immunology* **20**, 433–446 (2019).

159. Hu, H. *et al.* Brucella infection regulates peroxiredoxin-5 protein expression to facilitate intracellular survival by reducing the production of nitric oxide and reactive oxygen species. *Biochemical and Biophysical Research Communications* **516**, 82–88 (2019).

160. Franco, M. M. C. *et al.* Brucella abortus Triggers a cGAS-Independent STING Pathway To Induce Host Protection That Involves Guanylate-Binding Proteins and Inflammasome Activation. *The Journal of Immunology* **200**, 607–622 (2018).

161. Kwon, D., Park, E. & Kang, S.-J. Stimulator of IFN genes–mediated DNA-sensing pathway is suppressed by NLRP3 agonists and regulated by mitofusin 1 and TBC1D15, mitochondrial dynamics mediators. *The FASEB Journal* **31**, 4866–4878 (2017).

162. Buß, C. *et al.* Essential Role of Mitochondrial Antiviral Signaling, IFN Regulatory Factor (IRF)3, and IRF7 in Chlamydophila pneumoniae-Mediated IFN-β Response and Control of Bacterial Replication in Human Endothelial Cells. *The Journal of Immunology* **184**, 3072–3078 (2010).

163. Cheng, Y. & Schorey, J. S. Extracellular vesicles deliver Mycobacterium RNA to promote host immunity and bacterial killing. *EMBO Rep* **20**, e46613 (2019).

164. Hagmann, C. A. *et al.* RIG-I Detects Triphosphorylated RNA of Listeria monocytogenes during Infection in Non-Immune Cells. *PLOS ONE* **8**, e62872 (2013).

165. Monroe, K. M., McWhirter, S. M. & Vance, R. E. Identification of Host Cytosolic Sensors and Bacterial Factors Regulating the Type I Interferon Response to Legionella pneumophila. *PLOS Pathogens* **5**, e1000665 (2009).

166. Gurung, P., Lukens, J. R. & Kanneganti, T.-D. Mitochondria: diversity in the regulation of the NLRP3 inflammasome. *Trends in Molecular Medicine* **21**, 193–201 (2015).

167. Zhou, R., Yazdi, A. S., Menu, P. & Tschopp, J. A role for mitochondria in NLRP3 inflammasome activation. *Nature* **469**, 221–225 (2011).

168. Iyer, S. S. *et al.* Mitochondrial Cardiolipin Is Required for Nlrp3 Inflammasome Activation. *Immunity* **39**, 311–323 (2013).

169. Shimada, K. *et al.* Oxidized Mitochondrial DNA Activates the NLRP3 Inflammasome during Apoptosis. *Immunity* **36**, 401–414 (2012).

170. Nakahira, K. *et al.* Autophagy proteins regulate innate immune responses by inhibiting the release of mitochondrial DNA mediated by the NALP3 inflammasome. *Nat Immunol* **12**, 222–230 (2011).

171. Bronner, D. N. *et al.* Endoplasmic Reticulum Stress Activates the Inflammasome via NLRP3- and Caspase-2-Driven Mitochondrial Damage. *Immunity* **43**, 451–462 (2015).

172. Guimarães, E. S. *et al.* Brucella abortus Cyclic Dinucleotides Trigger STING-Dependent Unfolded Protein Response That Favors Bacterial Replication. *The Journal of Immunology* **202**, 2671–2681 (2019).

173. Park, S. *et al.* Defective mitochondrial fission augments NLRP3 inflammasome activation. *Scientific Reports* **5**, 15489 (2015).

174. Li, W. *et al.* FUN14 Domain-Containing 1–Mediated Mitophagy Suppresses Hepatocarcinogenesis by Inhibition of Inflammasome Activation in Mice. *Hepatology* **69**, 604–621 (2019).

175. Lupfer, C. *et al.* Receptor interacting protein kinase 2–mediated mitophagy regulates inflammasome activation during virus infection. *Nat Immunol* **14**, 480–488 (2013).

176. Sanchez-Lopez, E. *et al.* Choline Uptake and Metabolism Modulate Macrophage IL-1β and IL-18 Production. *Cell Metabolism* **29**, 1350-1362.e7 (2019).

177. Xu, Y., Wang, J., Xu, W., Ding, F. & Ding, W. Prohibitin 2-mediated mitophagy attenuates renal tubular epithelial cells injury by regulating mitochondrial dysfunction and NLRP3 inflammasome activation. *American Journal of Physiology-Renal Physiology* **316**, F396–F407 (2019).

178. Lobet, E. *et al.* Mitochondrial fragmentation affects neither the sensitivity to TNFα-induced apoptosis of Brucella -infected cells nor the intracellular replication of the bacteria. *Scientific Reports* **8**, 5173 (2018).

179. Sowter, H. M., Ratcliffe, P. J., Watson, P., Greenberg, A. H. & Harris, A. L. HIF-1-dependent Regulation of Hypoxic Induction of the Cell Death Factors BNIP3 and NIX in Human Tumors. *Cancer Res* **61**, 6669–6673 (2001).

180. Sulkshane, P. *et al.* Ubiquitination and receptor-mediated mitophagy converge to eliminate oxidation-damaged mitochondria during hypoxia. *Redox Biology* **45**, 102047 (2021).

181. Lee, P., Chandel, N. S. & Simon, M. C. Cellular adaptation to hypoxia through hypoxia inducible factors and beyond. *Nature Reviews Molecular Cell Biology* **21**, 268–283 (2020).

182. Schödel, J. & Ratcliffe, P. J. Mechanisms of hypoxia signalling: new implications for nephrology. *Nature Reviews Nephrology* **15**, 641–659 (2019).

183. Albadari, N., Deng, S. & Li, W. The transcriptional factors HIF-1 and HIF-2 and their novel inhibitors in cancer therapy. *Expert Opinion on Drug Discovery* **14**, 667–682 (2019).

184. Semenza, G. L. Hypoxia-Inducible Factors in Physiology and Medicine. *Cell* **148**, 399–408 (2012).

185. Zhang, H. *et al.* Mitochondrial autophagy is an HIF-1-dependent adaptive metabolic response to hypoxia. *J Biol Chem* **283**, 10892–10903 (2008).

186. Berra, E. *et al.* HIF prolyl-hydroxylase 2 is the key oxygen sensor setting low steady-state levels of HIF-1alpha in normoxia. *EMBO J* **22**, 4082–4090 (2003).

187. Schofield, C. J. & Ratcliffe, P. J. Oxygen sensing by HIF hydroxylases. *Nature Reviews Molecular Cell Biology* **5**, 343–354 (2004).

188. Bell, E. L. *et al.* The Qo site of the mitochondrial complex III is required for the transduction of hypoxic signaling via reactive oxygen species production. *Journal of Cell Biology* **177**, 1029–1036 (2007).

189. Knowles, H. J., Raval, R. R., Harris, A. L. & Ratcliffe, P. J. Effect of Ascorbate on the Activity of Hypoxia-inducible Factor in Cancer Cells. *Cancer Res* **63**, 1764–1768 (2003).

190. Schroedl, C., McClintock, D. S., Budinger, G. R. S. & Chandel, N. S. Hypoxic but not anoxic stabilization of HIF-1α requires mitochondrial reactive oxygen species. *American Journal of Physiology-Lung Cellular and Molecular Physiology* **283**, L922–L931 (2002).

191. Chua, Y. L. *et al.* Stabilization of Hypoxia-inducible Factor-1α Protein in Hypoxia Occurs Independently of Mitochondrial Reactive Oxygen Species Production*,. *Journal of Biological Chemistry* **285**, 31277–31284 (2010).

192. Haase, V. H. The sweet side of HIF. *Kidney International* **78**, 10–13 (2010).

193. Blouin, C. C., Pagé, E. L., Soucy, G. M. & Richard, D. E. Hypoxic gene activation by lipopolysaccharide in macrophages: implication of hypoxia-inducible factor 1α. *Blood* **103**, 1124–1130 (2004).

194. Cramer, T. *et al.* HIF-1α Is Essential for Myeloid Cell-Mediated Inflammation. *Cell* **112**, 645–657 (2003).

195. Esteban-Martínez, L. *et al.* Programmed mitophagy is essential for the glycolytic switch during cell differentiation. *EMBO J* **36**, 1688–1706 (2017).

196. Tannahill, G. M. *et al.* Succinate is an inflammatory signal that induces IL-1β through HIF-1α. *Nature* **496**, 238–242 (2013).

197. Gleeson, L. E. *et al.* Cutting Edge: Mycobacterium tuberculosis Induces Aerobic Glycolysis in Human Alveolar Macrophages That Is Required for Control of Intracellular Bacillary Replication. *The Journal of Immunology* **196**, 2444–2449 (2016).

198. Devraj, G., Beerlage, C., Brüne, B. & Kempf, V. A. J. Hypoxia and HIF-1 activation in bacterial infections. *Microbes and Infection* **19**, 144–156 (2017).

199. Jantsch, J. *et al.* Toll-like receptor activation and hypoxia use distinct signaling pathways to stabilize hypoxia-inducible factor 1α (HIF1A) and result in differential HIF1A-dependent gene expression. *Journal of Leukocyte Biology* **90**, 551–562 (2011).

200. Lachmandas, E. *et al.* Microbial stimulation of different Toll-like receptor signalling pathways induces diverse metabolic programmes in human monocytes. *Nat Microbiol* **2**, 1–10 (2016).

201. Lee, G. *et al.* Oxidative Dimerization of PHD2 is Responsible for its Inactivation and Contributes to Metabolic Reprogramming via HIF-1α Activation. *Sci Rep* **6**, 18928 (2016).

202. Lampropoulou, V. *et al.* Itaconate Links Inhibition of Succinate Dehydrogenase with Macrophage Metabolic Remodeling and Regulation of Inflammation. *Cell Metabolism* **24**, 158–166 (2016).

203. Gomes, M. T. R. *et al.* STING regulates metabolic reprogramming in macrophages via HIF-1α during Brucella infection. *PLOS Pathogens* **17**, e1009597 (2021).

204. Li, C. *et al.* PINK1 and PARK2 Suppress Pancreatic Tumorigenesis through Control of Mitochondrial Iron-Mediated Immunometabolism. *Developmental Cell* **46**, 441-455.e8 (2018).

205. Weber, R. A. *et al.* Maintaining Iron Homeostasis Is the Key Role of Lysosomal Acidity for Cell Proliferation. *Molecular Cell* **77**, 645-655.e7 (2020).

206. Siegert, I. *et al.* Ferritin-Mediated Iron Sequestration Stabilizes Hypoxia-Inducible Factor-1α upon LPS Activation in the Presence of Ample Oxygen. *Cell Reports* **13**, 2048–2055 (2015).

207. Gerald, D. *et al.* JunD Reduces Tumor Angiogenesis by Protecting Cells from Oxidative Stress. *Cell* **118**, 781–794 (2004).

208. Li, Y.-N. *et al.* NADPH oxidase-mitochondria axis-derived ROS mediate arsenite-induced HIF-1α stabilization by inhibiting prolyl hydroxylases activity. *Toxicology Letters* **224**, 165–174 (2014).

209. Lu, H. *et al.* Reversible Inactivation of HIF-1 Prolyl Hydroxylases Allows Cell Metabolism to Control Basal HIF-1 *. *Journal of Biological Chemistry* **280**, 41928–41939 (2005).

210. Nytko, K. J. *et al.* Vitamin C is dispensable for oxygen sensing in vivo. *Blood* **117**, 5485–5493 (2011).

211. Hartmann, H. *et al.* Hypoxia-Independent Activation of HIF-1 by Enterobacteriaceae and Their Siderophores. *Gastroenterology* **134**, 756-767.e6 (2008).

212. Telser, J. *et al.* Metabolic reprogramming of Salmonella infected macrophages and its modulation by iron availability and the mTOR pathway. *Microb Cell* **6**, 531–543 (2019).

213. Nairz, M. & Weiss, G. Iron in infection and immunity. *Molecular Aspects of Medicine* **75**, 100864 (2020).

214. Soares, M. P. & Weiss, G. The Iron age of host–microbe interactions. *EMBO reports* **16**, 1482–1500 (2015).

215. Muckenthaler, M. U., Rivella, S., Hentze, M. W. & Galy, B. A Red Carpet for Iron Metabolism. *Cell* **168**, 344–361 (2017).

216. Hentze, M. W., Muckenthaler, M. U., Galy, B. & Camaschella, C. Two to Tango: Regulation of Mammalian Iron Metabolism. *Cell* **142**, 24–38 (2010).

217. Patel, S. J. *et al.* A PCBP1–BolA2 chaperone complex delivers iron for cytosolic [2Fe–2S] cluster assembly. *Nat Chem Biol* **15**, 872–881 (2019).

218. Paul, B. T., Manz, D. H., Torti, F. M. & Torti, S. V. Mitochondria and Iron: current questions. *Expert Review of Hematology* **10**, 65–79 (2017).

219. Eid, R., Arab, N. T. T. & Greenwood, M. T. Iron mediated toxicity and programmed cell death: A review and a re-examination of existing paradigms. *Biochimica et Biophysica Acta (BBA) - Molecular Cell Research* **1864**, 399–430 (2017).

220. Finazzi, D. & Arosio, P. Biology of ferritin in mammals: an update on iron storage, oxidative damage and neurodegeneration. *Arch Toxicol* **88**, 1787–1802 (2014).

221. Biasiotto, G., Di Lorenzo, D., Archetti, S. & Zanella, I. Iron and Neurodegeneration: Is Ferritinophagy the Link? *Mol Neurobiol* **53**, 5542–5574 (2016).

222. Bogdan, A. R., Miyazawa, M., Hashimoto, K. & Tsuji, Y. Regulators of Iron Homeostasis: New Players in Metabolism, Cell Death, and Disease. *Trends in Biochemical Sciences* **41**, 274–286 (2016).

223. Meyron-Holtz, E. G. *et al.* Genetic ablations of iron regulatory proteins 1 and 2 reveal why iron regulatory protein 2 dominates iron homeostasis. *The EMBO Journal* **23**, 386 (2004).

224. Peyssonnaux, C., Nizet, V. & Johnson, R. S. Role of the hypoxia inducible factors HIF in iron metabolism. *Cell Cycle* **7**, 28–32 (2008).

225. Li, X. *et al.* NCOA4 is regulated by HIF and mediates mobilization of murine hepatic iron stores after blood loss. *Blood* **136**, 2691–2702 (2020).

226. Yang, A., Wang, L., Jiang, K., Lei, L. & Li, H. Nuclear receptor coactivator 4-mediated ferritinophagy drives proliferation of dental pulp stem cells in hypoxia. *Biochemical and Biophysical Research Communications* **554**, 123–130 (2021).

227. Palmer, L. D. & Skaar, E. P. Transition Metals and Virulence in Bacteria. *Annual Review of Genetics* **50**, 67–91 (2016).

228. Roop II, R. M., Elhassanny, A. E., Almirón, M. A., Anderson, E. S. & Atkinson, X. J. Iron. in *Metals and the Biology and Virulence of Brucella* (eds. Roop II, R. M. & Caswell, C. C.) 9–39 (Springer International Publishing, 2017). doi:10.1007/978-3-319-53622-4_2.

229. Nairz, M. *et al.* Iron Regulatory Proteins Mediate Host Resistance to Salmonella Infection. *Cell Host & Microbe* **18**, 254–261 (2015).

230. Nairz, M. *et al.* Nitric oxide-mediated regulation of ferroportin-1 controls macrophage iron homeostasis and immune function in Salmonella infection. *J Exp Med* **210**, 855–873 (2013).

231. Hop, H. T. *et al.* Lipocalin 2 (Lcn2) interferes with iron uptake by Brucella abortus and dampens immunoregulation during infection of RAW 264.7 macrophages. *Cellular Microbiology* **20**, e12813 (2018).

232. Wang, Q. *et al.* Lipocalin 2 Protects Against Escherichia coli Infection by Modulating Neutrophil and Macrophage Function. *Frontiers in Immunology* **10**, 2594 (2019).

233. Fischbach, M. A. *et al.* The pathogen-associated iroA gene cluster mediates bacterial evasion of lipocalin 2. *PNAS* **103**, 16502–16507 (2006).

234. Roset, M. S., Alefantis, T. G., DelVecchio, V. G. & Briones, G. Iron-dependent reconfiguration of the proteome underlies the intracellular lifestyle of Brucella abortus. *Scientific Reports* **7**, 10637 (2017).

235. Leonard, B. a. (b a.), Lopez-Goñi, I. (Ignacio) & Baldwin, C. L. (c L.). Brucella abortus siderophore 2,3-dihydroxybenzoic acid protects brucellae from killing by macrophages. (1997).

236. Danese, I. *et al.* The Ton System, an ABC Transporter, and a Universally Conserved GTPase Are Involved in Iron Utilization by Brucella melitensis 16M. *Infection and Immunity* **72**, 5783–5790 (2004).

237. Michelle A., P. *et al.* Brucella abortus siderophore2,3-dihydroxybenzoic acid (DHBA) facilitatesintracellular survival of the bacteria. *Microbial Pathogenesis* **32**, 239–248 (2002).

238. Jain, N. *et al.* Effect of entF deletion on iron acquisition and erythritol metabolism by Brucella abortus 2308. *FEMS Microbiology Letters* **316**, 1–6 (2011).

239. Paulley, J. T., Anderson, E. S. & Roop, R. M. Brucella abortus Requires the Heme Transporter BhuA for Maintenance of Chronic Infection in BALB/c Mice. *Infection and Immunity* **75**, 5248–5254 (2007).

240. Elhassanny, A. E. M., Anderson, E. S., Menscher, E. A. & Roop, R. M. The ferrous iron transporter FtrABCD is required for the virulence of Brucella abortus 2308 in mice. *Molecular Microbiology* **88**, 1070–1082 (2013).

241. Hughes, C. E. *et al.* Cysteine Toxicity Drives Age-Related Mitochondrial Decline by Altering Iron Homeostasis. *Cell* **180**, 296-310.e18 (2020).

242. Das, A., Nag, S., Mason, A. B. & Barroso, M. M. Endosome–mitochondria interactions are modulated by iron release from transferrin. *Journal of Cell Biology* **214**, 831–845 (2016).

243. Shvartsman, M., Kikkeri, R., Shanzer, A. & Cabantchik, Z. I. Non-transferrin-bound iron reaches mitochondria by a chelator-inaccessible mechanism: biological and clinical implications. *Am J Physiol Cell Physiol* **293**, C1383-1394 (2007).

244. Wolff, N. A. *et al.* A role for divalent metal transporter (DMT1) in mitochondrial uptake of iron and manganese. *Sci Rep* **8**, 211 (2018).

245. Paradkar, P. N., Zumbrennen, K. B., Paw, B. H., Ward, D. M. & Kaplan, J. Regulation of Mitochondrial Iron Import through Differential Turnover of Mitoferrin 1 and Mitoferrin 2. *Molecular and Cellular Biology* **29**, 1007–1016 (2009).

246. Devireddy, L. R., Hart, D. O., Goetz, D. H. & Green, M. R. A Mammalian Siderophore Synthesized by an Enzyme with a Bacterial Homolog Involved in Enterobactin Production. *Cell* **141**, 1006–1017 (2010).

247. Liu, Z. *et al.* Regulation of mammalian siderophore 2,5-DHBA in the innate immune response to infection. *Journal of Experimental Medicine* **211**, 1197–1213 (2014).

248. Delpino, M. V. *et al.* Macrophage-elicited osteoclastogenesis in response to Brucella abortus infection requires TLR2/MyD88-dependent TNF-α production. *J Leukoc Biol* **91**, 285–298 (2012).

249. Allen, G. F. G., Toth, R., James, J. & Ganley, I. G. Loss of iron triggers PINK1/Parkin-independent mitophagy. *EMBO reports* **14**, 1127–1135 (2013).

250. Hara, Y. *et al.* Iron loss triggers mitophagy through induction of mitochondrial ferritin. *EMBO reports* **21**, e50202 (2020).

251. Wu, H. *et al.* Defective mitochondrial ISCs biogenesis switches on IRP1 to fine tune selective mitophagy. *Redox Biology* **36**, 101661 (2020).

252. Shapiro, J. S. *et al.* Abstract 19082: Cellular Iron Regulates Mitochondrial Dynamics and Mitophagy Through the RNA-Binding Protein Tristetraprolin. *Circulation* **136**, A19082–A19082 (2017).

253. Shapiro, J. S. *et al.* Abstract 13202: Cellular Iron Regulates Mitochondrial Dynamics Through the RNA-Binding Protein Tristetraprolin (TTP). *Circulation* **134**, A13202–A13202 (2016).

254. Kang, D., Kirienko, D. R., Webster, P., Fisher, A. L. & Kirienko, N. V. Pyoverdine, a siderophore from Pseudomonas aeruginosa, translocates into C. elegans, removes iron, and activates a distinct host response. *Virulence* **9**, 804–817 (2018).

255. Kirienko, N. V., Ausubel, F. M. & Ruvkun, G. Mitophagy confers resistance to siderophore-mediated killing by Pseudomonas aeruginosa. *PNAS* **112**, 1821–1826 (2015).

256. Schiavi, A. *et al.* Iron-Starvation-Induced Mitophagy Mediates Lifespan Extension upon Mitochondrial Stress in C. elegans. *Current Biology* **25**, 1810–1822 (2015).

257. Lucey, B. P., Nelson-Rees, W. A. & Hutchins, G. M. Henrietta Lacks, HeLa cells, and cell culture contamination. *Arch Pathol Lab Med* **133**, 1463–1467 (2009).

258. Koch, C. Measurement of absolute oxygen levels in cells and tissues using oxygen sensors and 2-nitroimidazole EF5. *Methods in enzymology* **352**, (2002).

259. De Vos, K. J. & Sheetz, M. P. Visualization and Quantification of Mitochondrial Dynamics in Living Animal Cells. in *Methods in Cell Biology* vol. 80 627–682 (Academic Press, 2007).

260. Rest, R. F. & Robertson, D. C. Characterization of the electron transport system in Brucella abortus. *Journal of Bacteriology* **122**, 139–144 (1975).

261. Bagüés, M. P. J. de, Loisel-Meyer, S., Liautard, J.-P. & Jubier-Maurin, V. Different Roles of the Two High-Oxygen-Affinity Terminal Oxidases of Brucella suis: Cytochrome c Oxidase, but Not Ubiquinol Oxidase, Is Required for Persistence in Mice. *Infection and Immunity* **75**, 531–535 (2007).

262. James, P. E., Grinberg, O. Y., Michaels, G. & Swartz, H. M. Intraphagosomal oxygen in stimulated macrophages. *Journal of Cellular Physiology* **163**, 241–247 (1995).

263. Loisel-Meyer, S., Bagüés, M. P. J. de, Köhler, S., Liautard, J.-P. & Jubier-Maurin, V. Differential Use of the Two High-Oxygen-Affinity Terminal Oxidases of Brucella suis for In Vitro and Intramacrophagic Multiplication. *Infection and Immunity* **73**, 7768–7771 (2005).

264. Kempf Volkhard A.J. *et al.* Activation of Hypoxia-Inducible Factor-1 in Bacillary Angiomatosis. *Circulation* **111**, 1054–1062 (2005).

265. Werth, N. *et al.* Activation of Hypoxia Inducible Factor 1 Is a General Phenomenon in Infections with Human Pathogens. *PLOS ONE* **5**, e11576 (2010).

266. Kizaka-Kondoh, S. & Konse-Nagasawa, H. Significance of nitroimidazole compounds and hypoxia-inducible factor-1 for imaging tumor hypoxia. *Cancer Science* **100**, 1366–1373 (2009).

267. Stothers, C. L., Luan, L., Fensterheim, B. A. & Bohannon, J. K. Hypoxia-inducible factor-1α regulation of myeloid cells. *J Mol Med* **96**, 1293–1306 (2018).

268. Yang, S.-G. *et al.* Mito-TEMPO improves development competence by reducing superoxide in preimplantation porcine embryos. *Sci Rep* **8**, 10130 (2018).

269. Trnka, J., Blaikie, F. H., Smith, R. A. J. & Murphy, M. P. A mitochondria-targeted nitroxide is reduced to its hydroxylamine by ubiquinol in mitochondria. *Free Radic Biol Med* **44**, 1406–1419 (2008).

270. Nicholas, S. A. & Sumbayev, V. V. The role of redox-dependent mechanisms in the downregulation of ligand-induced Toll-like receptors 7, 8 and 4-mediated HIF-1α prolyl hydroxylation. *Immunology & Cell Biology* **88**, 180–186 (2010).

271. Nishi, K. *et al.* LPS Induces Hypoxia-Inducible Factor 1 Activation in Macrophage-Differentiated Cells in a Reactive Oxygen Species–Dependent Manner. *Antioxidants & Redox Signaling* **10**, 983–996 (2008).

272. Hu, H. *et al.* Brucella Infection Regulates Thioredoxin-Interacting Protein Expression to Facilitate Intracellular Survival by Reducing the Production of Nitric Oxide and Reactive Oxygen Species. *The Journal of Immunology* **204**, 632–643 (2020).

273. Dalmasso, G. *et al.* Yersiniabactin siderophore of Crohn's disease-associated adherent-invasive escherichia coli is involved in autophagy activation in host cells. *International Journal of Molecular Sciences* **22**, (2021).

274. Vincent, G. *et al.* Nix-Mediated Mitophagy Modulates Mitochondrial Damage During Intestinal Inflammation. *Antioxidants & Redox Signaling* **33**, 1–19 (2020).

275. Huang, X. T. *et al.* Iron-induced energy supply deficiency and mitochondrial fragmentation in neurons. *Journal of Neurochemistry* **147**, 816–830 (2018).

276. Lee, D. G., Kam, M. K., Lee, S.-R., Lee, H. J. & Lee, D.-S. Peroxiredoxin 5 deficiency exacerbates iron overload-induced neuronal death via ER-mediated mitochondrial fission in mouse hippocampus. *Cell Death Dis* **11**, 204 (2020).

277. Wang, L.-L. *et al.* Host Prdx6 contributing to the intracellular survival of Brucella suis S2 strain. *BMC Veterinary Research* **15**, 304 (2019).

278. Liu, Z., Ciocea, A. & Devireddy, L. Endogenous Siderophore 2,5-Dihydroxybenzoic Acid Deficiency Promotes Anemia and Splenic Iron Overload in Mice. *Molecular and Cellular Biology* **34**, 2533–2546 (2014).

279. Liu, Z. *et al.* Siderophore-mediated iron trafficking in humans is regulated by iron. *J Mol Med* **90**, 1209–1221 (2012).

280. Zughaier, S. M., Stauffer, B. B. & McCarty, N. A. Inflammation and ER Stress Downregulate BDH2 Expression and Dysregulate Intracellular Iron in Macrophages. *Journal of Immunology Research* **2014**, e140728 (2014).

281. Davuluri, G. *et al.* Inactivation of 3-hydroxybutyrate dehydrogenase 2 delays zebrafish erythroid maturation by conferring premature mitophagy. *PNAS* **113**, E1460–E1469 (2016).

282. Fernández, B. *et al.* Iron overload causes endolysosomal deficits modulated by NAADP-regulated 2-pore channels and RAB7A. *Autophagy* **12**, 1487–1506 (2016).

283. Cervantes-Silva, M. P., Cox, S. L. & Curtis, A. M. Alterations in mitochondrial morphology as a key driver of immunity and host defence. *EMBO Rep* **22**, e53086 (2021).

284. Li, T. *et al.* Brucella Melitensis 16M Regulates the Effect of AIR Domain on Inflammatory Factors, Autophagy, and Apoptosis in Mouse Macrophage through the ROS Signaling Pathway. *PLOS ONE* **11**, e0167486 (2016).

285. Chen, F. & He, Y. Caspase-2 Mediated Apoptotic and Necrotic Murine Macrophage Cell Death Induced by Rough Brucella abortus. *PLOS ONE* **4**, e6830 (2009).

286. Bronner, D., O'Riordan, M. & He, Y. 'Oliver'. Caspase-2 mediates a Brucella abortus RB51-induced hybrid cell death having features of apoptosis and pyroptosis. *Frontiers in Cellular and Infection Microbiology* **3**, 83 (2013).

287. Peyssonnaux, C. *et al.* HIF-1α expression regulates the bactericidal capacity of phagocytes. *J Clin Invest* **115**, 1806–1815 (2005).

288. Johnson, N. B., Deck, K. M., Nizzi, C. P. & Eisenstein, R. S. A synergistic role of IRP1 and FBXL5 proteins in coordinating iron metabolism during cell proliferation. *J Biol Chem* **292**, 15976–15989 (2017).

289. Bhujabal, Z. *et al.* FKBP8 recruits LC3A to mediate Parkin-independent mitophagy. *EMBO Rep* **18**, 947–961 (2017).

290. Rosa, S. C. da S. *et al.* BNIP3L/Nix-induced mitochondrial fission, mitophagy, and impaired myocyte glucose uptake are abrogated by PRKA/PKA phosphorylation. *Autophagy* **0**, 1–16 (2020).

291. Han, X.-J. *et al.* CaM kinase Iα–induced phosphorylation of Drp1 regulates mitochondrial morphology. *Journal of Cell Biology* **182**, 573–585 (2008).

292. Chai, P. *et al.* USP19 promotes hypoxia-induced mitochondrial division via FUNDC1 at ER-mitochondria contact sites. *Journal of Cell Biology* **220**, (2021).

293. Chen, M. *et al.* Mitophagy receptor FUNDC1 regulates mitochondrial dynamics and mitophagy. *Autophagy* **12**, 689–702 (2016).

294. Wu, S. *et al.* Binding of FUN14 Domain Containing 1 With Inositol 1,4,5-Trisphosphate Receptor in Mitochondria-Associated Endoplasmic Reticulum Membranes Maintains Mitochondrial Dynamics and Function in Hearts in Vivo. *Circulation* **136**, 2248–2266 (2017).

295. Li, W. *et al.* MicroRNA-137 Is a Novel Hypoxia-responsive MicroRNA That Inhibits Mitophagy via Regulation of Two Mitophagy Receptors FUNDC1 and NIX*. *Journal of Biological Chemistry* **289**, 10691–10701 (2014).

296. Martinez-Guzman, O. *et al.* Mitochondrial–nuclear heme trafficking in budding yeast is regulated by GTPases that control mitochondrial dynamics and ER contact sites. *Journal of Cell Science* **133**, (2020).

297. Sugo, M. *et al.* Syntaxin 17 regulates the localization and function of PGAM5 in mitochondrial division and mitophagy. *EMBO J* **37**, e98899 (2018).

298. Xian, H., Yang, Q., Xiao, L., Shen, H.-M. & Liou, Y.-C. STX17 dynamically regulated by Fis1 induces mitophagy via hierarchical macroautophagic mechanism. *Nat Commun* **10**, 2059 (2019).

299. López-Goñi, I., Moriyón, I. & Neilands, J. B. Identification of 2,3-dihydroxybenzoic acid as a Brucella abortus siderophore. *Infect Immun* **60**, 4496–4503 (1992).

300. Bellaire, B. H. *et al.* Genetic Organization and Iron-Responsive Regulation of the Brucella abortus 2,3-Dihydroxybenzoic Acid Biosynthesis Operon, a Cluster of Genes Required for Wild-Type Virulence in Pregnant Cattle. *Infection and Immunity* **71**, 1794–1803 (2003).

301. Parent, M. A. *et al.* Brucella abortus siderophore 2,3-dihydroxybenzoic acid (DHBA) facilitates intracellular survival of the bacteria. *Microb Pathog* **32**, 239–248 (2002).

302. Taguchi, Y. *et al.* Yip1A, a Novel Host Factor for the Activation of the IRE1 Pathway of the Unfolded Protein Response during Brucella Infection. *PLOS Pathogens* **11**, e1004747 (2015).

303. Zhong, Z. *et al.* NF-κB Restricts Inflammasome Activation via Elimination of Damaged Mitochondria. *Cell* **164**, 896–910 (2016).

304. Wang, Y. *et al.* Brucella Dysregulates Monocytes and Inhibits Macrophage Polarization through LC3-Dependent Autophagy. *Frontiers in Immunology* **8**, 691 (2017).

305. Shi, Y. *et al.* Upstream ORFs Prevent MAVS Spontaneous Aggregation and Regulate Innate Immune Homeostasis. *iScience* **23**, 101059 (2020).

306. Nagi, M. *et al.* Iron-depletion promotes mitophagy to maintain mitochondrial integrity in pathogenic yeast Candida glabrata. *Autophagy* **12**, 1259–1271 (2016).

307. Byndloss, M. X. *et al.* Brucella abortus Infection of Placental Trophoblasts Triggers Endoplasmic Reticulum Stress-Mediated Cell Death and Fetal Loss via Type IV Secretion System-Dependent Activation of CHOP. *mBio* **10**, e01538-19 (2019).

308. Ma, Z. *et al.* Brucella abortus BspJ Is a Nucleomodulin That Inhibits Macrophage Apoptosis and Promotes Intracellular Survival of Brucella. *Front Microbiol* **11**, 599205 (2020).

309. Qin, Q.-M. *et al.* RNAi Screen of Endoplasmic Reticulum–Associated Host Factors Reveals a Role for IRE1α in Supporting Brucella Replication. *PLOS Pathogens* **4**, e1000110 (2008).

310. Starr, T. *et al.* Selective Subversion of Autophagy Complexes Facilitates Completion of the Brucella Intracellular Cycle. *Cell Host & Microbe* **11**, 33–45 (2012).

311. Keestra-Gounder, A. M. *et al.* NOD1 and NOD2 signalling links ER stress with inflammation. *Nature* **532**, 394–397 (2016).

312. Talty, A. *et al.* Inhibition of IRE1α RNase activity reduces NLRP3 inflammasome assembly and processing of pro-IL1β. *Cell Death Dis* **10**, 1–11 (2019).

313. Cui, G. *et al.* Brucella infection inhibits macrophages apoptosis via Nedd4-dependent degradation of calpain2. *Vet Microbiol* **174**, 195–205 (2014).

314. Gross, A., Terraza, A., Ouahrani-Bettache, S., Liautard, J.-P. & Dornand, J. In Vitro Brucella suis Infection Prevents the Programmed Cell Death of Human Monocytic Cells. *Infection and Immunity* **68**, 342–351 (2000).

315. Zhang, K. *et al.* OMP31 of Brucella melitensis 16M impairs the apoptosis of macrophages triggered by TNF-α. *Experimental and Therapeutic Medicine* **12**, 2783–2789 (2016).

316. Chiche, J. *et al.* Hypoxic enlarged mitochondria protect cancer cells from apoptotic stimuli. *Journal of Cellular Physiology* **222**, 648–657 (2010).

317. Ferecatu, I. *et al.* Dysfunction in the mitochondrial Fe-S assembly machinery leads to formation of the chemoresistant truncated VDAC1 isoform without HIF-1α activation. *PLOS ONE* **13**, e0194782 (2018).

318. Bian, C., Marchetti, A., Hammel, P. & Cosson, P. Intracellular targeting of Cisd2/Miner1 to the endoplasmic reticulum. *BMC Molecular and Cell Biology* **22**, 48 (2021).

319. Holt, S. H. *et al.* Activation of apoptosis in NAF-1-deficient human epithelial breast cancer cells. *Journal of Cell Science* **129**, 155–165 (2016).

320. Wiley, S. E. *et al.* Wolfram Syndrome protein, Miner1, regulates sulphydryl redox status, the unfolded protein response, and Ca2+ homeostasis. *EMBO Mol Med* **5**, 904–918 (2013).

321. Mittler, R. *et al.* NEET Proteins: A New Link Between Iron Metabolism, Reactive Oxygen Species, and Cancer. *Antioxidants & Redox Signaling* **30**, 1083–1095 (2019).

322. Nechushtai, R. *et al.* The balancing act of NEET proteins: Iron, ROS, calcium and metabolism. *Biochimica et Biophysica Acta (BBA) - Molecular Cell Research* **1867**, 118805 (2020).

323. Salameh, M. *et al.* New Insights of the NEET Protein CISD2 Reveals Distinct Features Compared to Its Close Mitochondrial Homolog mitoNEET. *Biomedicines* **9**, 384 (2021).

324. Vernay, A. *et al.* MitoNEET-dependent formation of intermitochondrial junctions. *PNAS* **114**, 8277–8282 (2017).

325. Chang, N. C., Nguyen, M., Germain, M. & Shore, G. C. Antagonism of Beclin 1-dependent autophagy by BCL-2 at the endoplasmic reticulum requires NAF-1. *EMBO J* **29**, 606–618 (2010).

326. Wang, C.-H. *et al.* Cisd2 modulates the differentiation and functioning of adipocytes by regulating intracellular Ca2+ homeostasis. *Hum Mol Genet* **23**, 4770–4785 (2014).

327. Wai, T. & Langer, T. Mitochondrial Dynamics and Metabolic Regulation. *Trends in Endocrinology & Metabolism* **27**, 105–117 (2016).

328. Louche, A. *et al.* The unique Brucella effectors NyxA and NyxB target SENP3 to modulate the subcellular localisation of nucleolar proteins. *bioRxiv* 2021.04.23.441069 (2021) doi:10.1101/2021.04.23.441069.

329. Yuan, Y. *et al.* BNIP3L/NIX-mediated mitophagy protects against ischemic brain injury independent of PARK2. *Autophagy* **13**, 1754–1766 (2017).

330. Khaminets, A., Behl, C. & Dikic, I. Ubiquitin-Dependent And Independent Signals In Selective Autophagy. *Trends Cell Biol* **26**, 6–16 (2016).

331. Marinho, F. V., Benmerzoug, S., Oliveira, S. C., Ryffel, B. & Quesniaux, V. F. J. The Emerging Roles of STING in Bacterial Infections. *Trends in Microbiology* **25**, 906–918 (2017).

332. Novak, I. *et al.* Nix is a selective autophagy receptor for mitochondrial clearance. *EMBO Rep* **11**, 45–51 (2010).

333. Zhu, Y. *et al.* Modulation of Serines 17 and 24 in the LC3-interacting Region of Bnip3 Determines Pro-survival Mitophagy versus Apoptosis *. *Journal of Biological Chemistry* **288**, 1099–1113 (2013).

334. Costa, T. R. D. *et al.* Secretion systems in Gram-negative bacteria: structural and mechanistic insights. *Nat Rev Microbiol* **13**, 343–359 (2015).

335. Takeuchi, O. & Akira, S. Pattern Recognition Receptors and Inflammation. *Cell* **140**, 805–820 (2010).

336. Araki, K. *et al.* Mitochondrial protein E2F3d, a distinctive E2F3 product, mediates hypoxia-induced mitophagy in cancer cells. *Commun Biol* **2**, 1–12 (2019).

337. Koentjoro, B., Park, J.-S. & Sue, C. M. Nix restores mitophagy and mitochondrial function to protect against PINK1/Parkin-related Parkinson's disease. *Sci Rep* **7**, 44373 (2017).

338. Döhmer, P. H., Valguarnera, E., Czibener, C. & Ugalde, J. E. Identification of a type IV secretion substrate of Brucella abortus that participates in the early stages of intracellular survival. *Cellular Microbiology* **16**, 396–410 (2014).

339. Roop, R. M., Barton, I. S., Hopersberger, D. & Martin, D. W. Uncovering the Hidden Credentials of Brucella Virulence. *Microbiol Mol Biol Rev* **85**, e00021-19 (2021).

340. Li, W. *et al.* Brucella TIR-like protein TcpB/Btp1 specifically targets the host adaptor protein MAL/TIRAP to promote infection. *Biochem Biophys Res Commun* **477**, 509–514 (2016).

341. Sengupta, D. *et al.* Subversion of innate immune responses by Brucella through the targeted degradation of the TLR signaling adapter, MAL. *J Immunol* **184**, 956–964 (2010).

6. Supplementary data

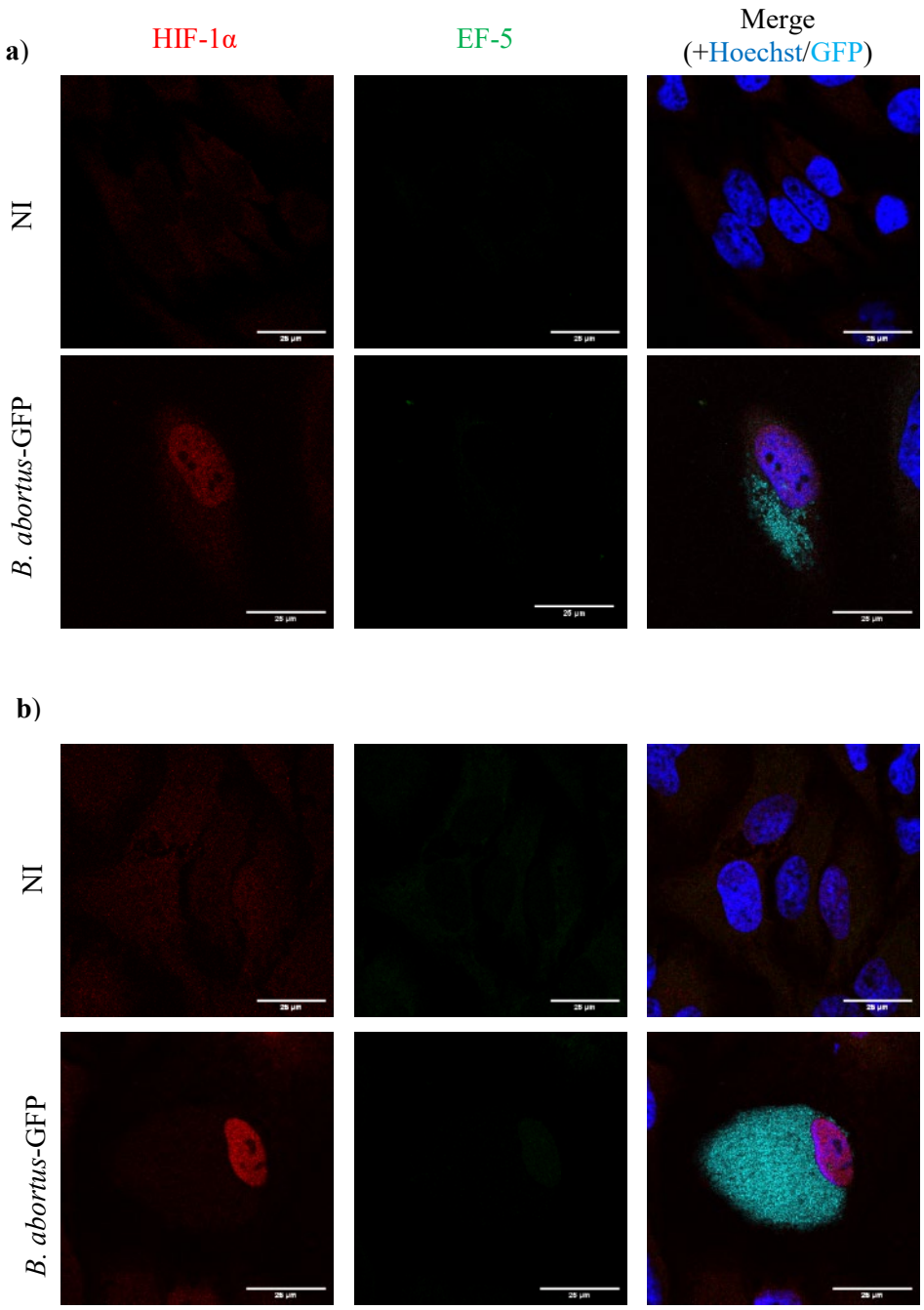

Supplementary Figure 1: *B. abortus* infection do not trigger a substantial hypoxia as monitored by EF-5 staining.

Co-immunostaining of EF-5 and HIF-1α in HeLa cells at 24h (in **a**) or 72h (in **b**) after infection with *B. abortus*-544-GFP (or not for non-infected controls, NI). Three hours before fixation, cells were incubated for 3h with 100 µM EF-5 in normoxic conditions to allow adduct formation that are subsequently detected with a monoclonal antibody conjugated with Cyanin-5. Micrographies were taken using confocal microscopy and are representative of 4 independent experiments (scale bars = 25 µm).

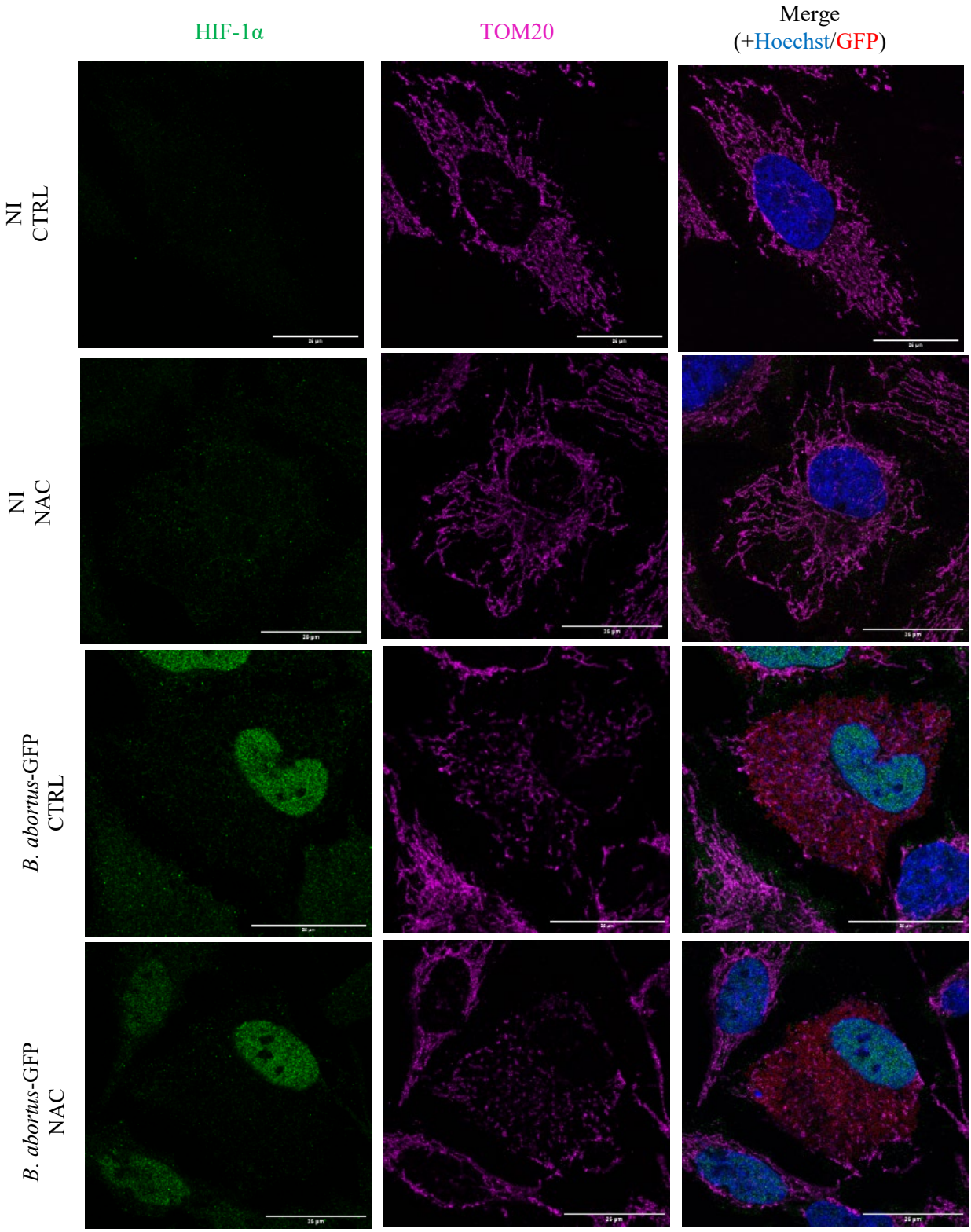

Supplementary Figure 2: Effect of NAC treatment on *B. abortus*-induced HIF-1α stabilisation and mitochondrial fragmentation.

Co-immunostaining of HIF-1α and TOM20 in HeLa cells infected or not (non-infected controls, NI) for 48 h with *B. abortus*-GFP visualised with a LSM 980 Airyscan 2 microscope. When indicated, cells were treated or not (controls, CTRL) with 5 mM of *N*-acetylcysteine (NAC) at 24 h p.i. (scale bars = 25 µm).

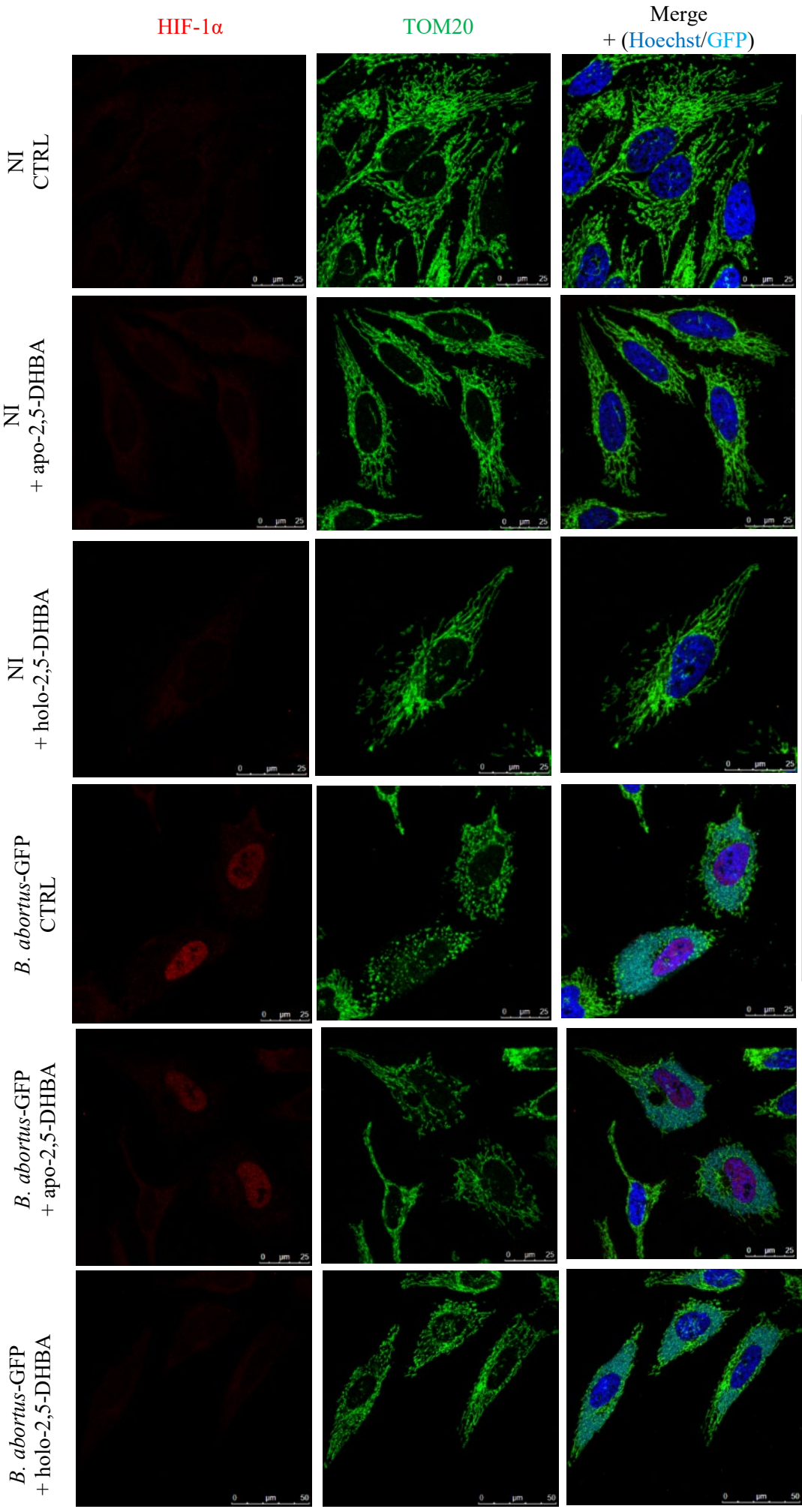

Supplementary Figure 3: Comparison of 500 µM iron, apo- or holo-2,5-DHBA 46 h treatment effects on *B. abortus*-induced HIF-1α stabilisation and mitochondrial fragmentation.

Co-immunostaining of TOM20 and HIF-1α in HeLa cells infected or not (NI non-infected controls) with *B. abortus*-GFP for 48 h and then observed by confocal microscopy. When indicated, cells were treated or not (CTRL, controls) with 500 µM of either 2,5-dihydroxibenzoic acid (DHBA) alone (apo-2,5-DHBA) or pre-incubated with Fe in a 1:1 concentration ratio (holo-DHBA) at 2 h post-infection (scale bars = 25 µm).

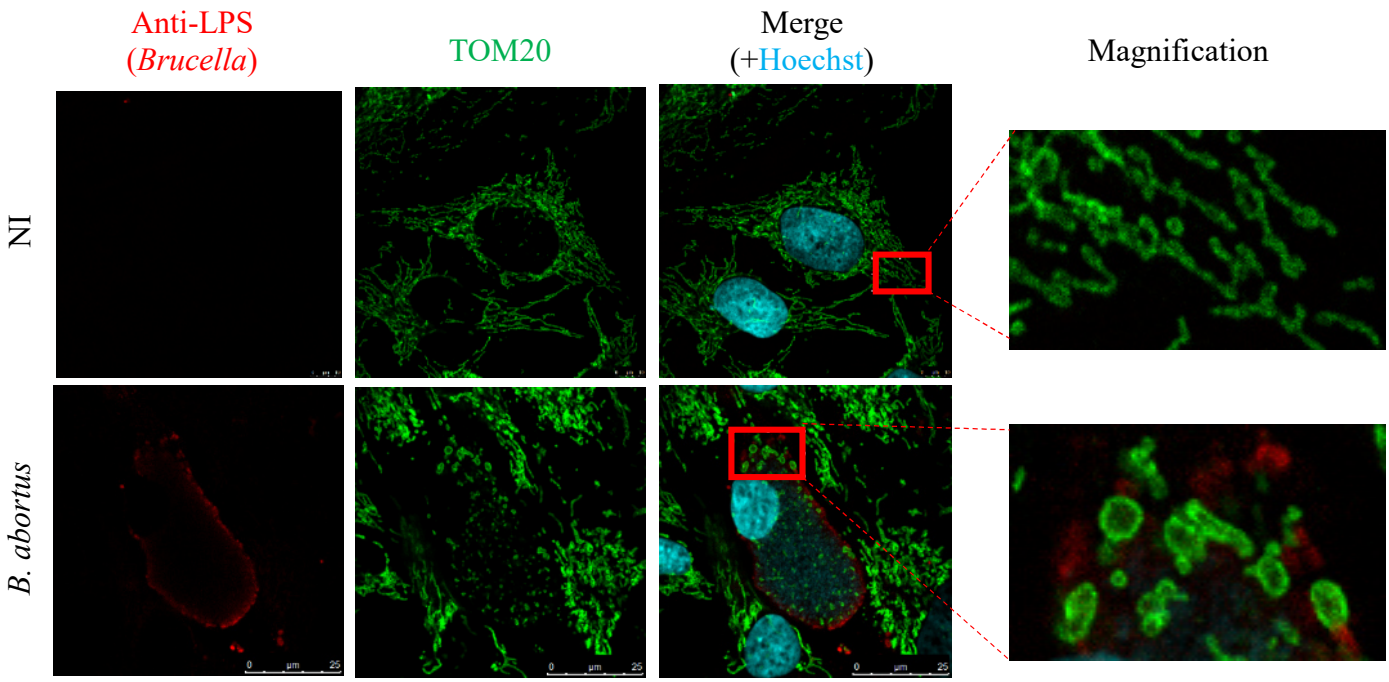

Supplementary Figure 4: Presence of enlarged mitochondria in *B. abortus*-infected cells

Immunostaining of TOM20 and LPS in *B. abortus*-infected HeLa cells 72 h after infection. Zoomed micrographs correspond to the areas surrounded to red boxes. (Scale bars = 25 µm). Jérémy Verbeke, ongoing PhD thesis, unpublished data.